NASA

Technical Memorandum 83827

ASSESSMENT OF THE FIRST RADIANCES RECEIVED FROM THE VISSR ATMOSPHERIC SOUNDER (VAS) INSTRUMENT

D. Chesters, L. W. Uccellini,
H. Montgomery, A. Mostek
and W. Robinson

August 1981

National Aeronautics and
Space Administration

Goddard Space Flight Center
Greenbelt, Maryland 20771

TM 83827

ASSESSMENT OF THE FIRST RADIANCES RECEIVED FROM THE VISSR ATMOSPHERIC SOUNDER (VAS) INSTRUMENT

Dennis Chesters, Louis W. Uccellini, Harry Montgomery
Goddard Laboratory for Atmospheric Sciences (GLAS)
Greenbelt, MD 20771

and

Anthony Mostek and Wayne Robinson
Computer Sciences Corporation
Silver Spring, MD 20910

August 10, 1981

ABSTRACT

The first orderly, calibrated radiances from the VAS-D instrument on the GOES-4 satellite (launched 9SEP80) were received at GSFC on 7NOV80, 1900-2100GMT. These VAS radiances are examined for: (a) image quality; (b) radiometric precision; (c) radiation transfer verification at clear air radiosonde sites; (d) regression retrieval accuracy; and (e) mesoscale analysis features. Several figures and tables of general interest are included in this paper for reference by future VAS users. Also, postlaunch problems involving calibration and data processing irregularities of scientific or operational significance are outlined for historical purposes.

The image and radiometric quality of the 7NOV80 VAS data meets the prelaunch specifications that were tested, although systematic biases comparable to the single sample detector noise were discovered. Calculated radiances, based upon line-by-line radiation transfer models for the conditions observed at 19 radiosonde sites in the clear air of the southeastern United States, disagree by several °K in brightness temperature in most channels. Some of the radiance discrepancy can be attributed to the normal mismatches in the nature of satellite and radiosonde data. However, the mid- and upper-tropospheric temperature sounding channels appear to be about 4° K colder than calculated with no plausible model adjustment to account for the disagreement. In order to remove unaccountable biases, clear air retrievals were made by empirical regression between VAS radiances and radiosondes taken 3 hours later. These empirical temperature and moisture retrievals, compared to the original radiosonde data, have the RMS residuals expected before launch (roughly ±2° C in temperature and ±25 percent in moisture). Temperature and moisture fields, analysed from a regular grid of VAS retrievals over the entire Southeast, show detailed spatial features that are not available in the conventional radiosonde analyses, especially in the data-void areas like the Gulf of Mexico. The lack of other "ground truth" data, colocated in space and time with the satellite radiances, makes it impossible to have a truly independent verification of these first VAS soundings.

Consequently, the first VAS radiances provide good visual and relative radiometric data for empirically conditioned retrievals of mesoscale temperature and moisture fields in clear air. Physically based retrieval models must await the resolution of the biases between calculated and observed VAS brightnesses. Retrievals in more interesting meteorological conditions must be demonstrated from other VAS observations.

CONTENTS

	Page
ABSTRACT	ii
SECTION 1 – OBJECTIVES AND OUTLINE	1
OBJECTIVES	1
OUTLINE	2
SUMMARY OF OBJECTIVES AND OUTLINE	3
SECTION 2 – DESCRIPTION OF VAS	4
BACKGROUND	4
THE VAS INSTRUMENT	6
VAS CHANNEL CHARACTERISTICS	7
SUMMARY DESCRIPTION OF VAS	8
SECTION 3 – PRELAUNCH ASSESSMENTS AT GSFC	9
VAS FILTER ASSESSMENT	9
VAS CHANNEL SENSITIVITY ESTIMATES	10
SIMULATED SOUNDING STUDIES	10
SECTION 4 – VAS-D OPERATIONS TO 7NOV80	14
THE VAS DATA TEAM	14
PRELAUNCH PROBLEMS	15
POSTLAUNCH CHECKOUT	15
Calibration Irregularities	15
Miscellaneous Postlaunch Irregularities	17
UNITED STATES APPEARANCE ON 7NOV80	17
SE UNITED STATES RADIOSONDES ON 7NOV80	18

OPERATIONS ON 7NOV80 19

SUMMARY OF VAS-D OPERATIONS TO 7NOV80 20

SECTION 5 – VAS-D IMAGE QUALITY 21

IMAGES IN ALL 12 VAS CHANNELS 21

IMAGE QUALITY DISCUSSION 23

Continuity 23
Registration 23
Navigation 24
Single Sample Noise 24
Line-by-Line Variation 25

IMAGE QUALITY SUMMARY 25

SECTION 6 VAS-D RADIOMETRIC QUALITY 27

PRELAUNCH RADIOMETRIC SPECIFICATIONS 27

OUTLINE OF THE VAS CALIBRATION CHAIN 27

Calibration on GOES 28
Calibration in the S/DB 28
Calibration in the VASPP 29
Calibration in the VASP 29

DISCUSSION OF UNAVERAGED VAS DWELL RADIANCES 29

Scattered Light 30
Noise 30
Relative Calibration 31
Absolute Calibration 31

AVERAGING VAS RADIANCES 32

Dwell Averaging 33
Averaging along a Line 33
Averaging Detectors 33
Averaging Lines 34

QUALITY ASSURANCE FOMs FOR VAS-D RADIOMETRY 34

Noise FOMs 35

Zero Point FOMs 35
Droop FOMs 36
Relative Stability FOMs 36

COMPARISON OF VAS RADIANCES TO HIRS2 ON TIROS-N 37

RADIANCE QUALITY SUMMARY 37

SECTION 7 – RADIATION TRANSFER VERIFICATION 39

RADIATION TRANSFER 39

RADIANCES COMPARED 41

Calculated Brightness 41
Brightness Differences 42
Window Channels 42
Shortwave Channels 43
Longwave Channels 43
Upper Air Moisture Channels 43

NUMERICAL ADJUSTMENTS 44

Radiation Transfer Model Adjustments 44
Ozone Absorption 44
Absorption Strength γ-Factor 45
Radiance Adjustments 46
Radiosonde Limitations for Radiation Transfer 46
Potential Radiation Transfer Model Adjustments 48

RADIATION TRANSFER VERIFICATION SUMMARY 48

SECTION 8 – VAS-D SOUNDING QUALITY 50

RETRIEVAL MATRICES USED 50

Conditioned Regression Retrievals 50
Simulated Retrievals using Prelaunch Studies 52
Empirical Retrievals using 7NOV80 Observations 53

INDEPENDENT VAS RADIANCES FOR RETRIEVAL TESTING 53

SAMPLE RETRIEVALS AT RADIOSONDE SITES 54

RESIDUAL ERRORS IN THE PROFILE RETRIEVALS 55

RMS Temperature Residuals 56
RMS Mixing Ratio Residuals 57
Profile Retrieval Error Assessment 58

RETRIEVAL SUMMARY 58

SECTION 9 MESOSCALE ANALYSIS OF EMPIRICAL VAS-D RETRIEVALS 60

MESOSCALE ANALYSIS 60

MESOSCALE ANALYSIS COMPARISONS 61

MESOSCALE ANALYSIS SUMMARY 63

SECTION 10 VAS-D ASSESSMENT SUMMARY 64

COLLECTION OF THE PREVIOUS SECTION SUMMARIES 64

Summary of Objectives and Outline 64
Summary Description of VAS 65
Summary of Prelaunch Assessments at GSFC 65
Summary of VAS-D Operations to 7NOV80 65
Image Quality Summary 66
Radiance Quality Summary 66
Radiation Transfer Verification Summary 67
Retrieval Summary 68
Mesoscale Analysis Summary 68

ASSESSMENT OF THE FIRST VAS-D Data 69

ACKNOWLEDGEMENTS 71

Page

REFERENCES 72

FIGURES 74

TABLES 110

LIST OF FIGURES

Figure		*Page*
1.	Measured and specified VAS-D spectral responses	74
2.	Weighting functions of VAS temperature sounding channels	75
3.	Weighting functions for VAS moisture and window channels	76
4	GOES-EAST VISSR picture of USA on 7NOV80	77
5.	VAS 12 page image sequence for SE USA on 7NOV80	78
6.	Image of "split window" contrast over SE USA	90
7.	Image of "two window" difference over SE USA	91
8.	Western VAS pixels for one spin of channel 8	92
9.	Western VAS pixels for one spin of channel 11	93
10.	Western VAS pixels for one dwell line of channel 11	94
11.	Quality assurance FOMs for VAS (A) noise, (B) zero point calibration, (C) droop, and (D) spin/spin stability	95
12.	Temperature and dewpoint profiles at 3 key sites	96
13.	VAS images in channels 12 and 10 with 19 sites shown	97
14.	Calculated radiance versus the absorption strength γ-factor for each VAS channel at Tampa Bay on 7NOV80	98
15.	Mean and RMS of (A) T*(calc) – T*(obs) and (B) absorption γ-factors for the VAS channels at 19 RAOB sites	99
16.	Fractional radiance accumulation functions for VAS (A) temperature sounding channels, and (B) moisture sounding and window channels	100
17.	Temperature and dewpoint retrievals at 3 sites: (A) Amarillo, Texas, (B) Tamp Bay, Fla., and (C) Jackson, Miss.	101
18.	RMS temperature residuals, using (▽) NOAA32, (⧖) NSSL210, (□) SEUSA19 regression, compared to the (*) preretrieval variance	102

19. RMS mixing ratio residuals, using (▽) NOAA32, (⧖) NSSL210, (□) SEUSA19 regression, compared to the (*) preretrieval variance 103

20. VAS image of SE USA, with 19 radiosonde and 75 retrieval sites 104

21. Conventional RAOB analyses of the (A) surface pressure and (B) 500 mb height field over the USA on the afternoon of 7NOV80 105

22. Analyzed mesoscale temperature fields at the surface, using 19 RAOBS or 75 VAS retrievals, and showing their differences 106

23. Analyzed mesoscale temperature fields at 850 mb 107

24. Analyzed mesoscale mixing ratio fields at 850 mb 108

25. Analyzed mesoscale temperature fields at 500 mb 109

LIST OF TABLES

Table		*Page*
1.	Specifications for the 12 VAS sounding channels	110
2.	Estimated transmission properties of 12 VAS channels	111
3.	Key radiance specifications for VAS channels	112
4.	VAS Plank radiances for 150°-350°K in 1°K steps	113
5.	19 radiosonde sites in SE USA, with VAS-viewed zenith angle	117
6.	Radiosonde temperature profiles at 19 sites	118
7.	Radiosonde dewpoint profiles at 19 sites	119
8.	Radiosonde dewpoint depression profiles at 19 sites	120
9.	VAS T*s observed at 19 sites in SE USA	121
10.	Calculated minus observed VAS ΔT^* at 19 sites	122
11.	VAS transmission γ-factor adjustments for 19 sites	123
12.	Observed and retrieved precipitable water at 3 sites	124

ASSESSMENT OF THE FIRST RADIANCES RECEIVED FROM THE VISSR ATMOSPHERIC SOUNDER (VAS) INSTRUMENT

SECTION 1
OBJECTIVES AND OUTLINE

This section justifies and outlines this status report on the first month of experience with the VISSR Atmospheric Sounder (VAS) sounding data at NASA/GSFC. This period culuminated with a successful dwell sounding.

1.1 OBJECTIVES

The VAS-D instrument is carried on GOES-4, which was launched on 9SEP80. After a month of checkout and software adjustments in the data processing chain, dwell sounding radiances suitable for processing were captured at the NASA/GSFC VAS Processor (VASP) on 7NOV80. The data frame covered North America during 1900-2100GMT.

These radiances are analyzed for internal quality and their consistency with radiosonde data taken from the southeastern (SE) United States a few hours later (0000GMT 8NOV80). These first VAS radiances are examined by the scientific users for:

1. Image quality.
2. Radiometric precision.
3. Radiation transfer verification.
4. Regression retrieval accuracy.
5. Mesoscale analysis features.

The initial data are compared to prelaunch specifications and to each other to establish confidence in their sounding quality.

In the absence of a "VAS Users Guide," this review will present technical details that are otherwise unpublished. As an initial status report, it is frank about operational problems and uncompleted work. Hopefully, the attempt to be comprehensive has not produced any oversimplifications or errors.

1.2 OUTLINE

This report is organized in chronological order with individual sections tracing prelaunch, postlaunch and postobservation analyses of VAS data characteristics.

- Section 1 states the report's objectives and outlines its contents.
- Section 2 is a programmatic and technical outline of VAS, focusing upon its role as a sounding instrument.
- Section 3 reviews GSFC's prelaunch assessment of the instrument's sounding capabilities.
- Section 4 reviews the postlaunch activity required to debug the VAS data processing chain and emphasizes the scientific implications of the problems encountered before the production of the first orderly dwell sounding radiances, which were taken at 1900-2100GMT on 7NOV80.
- Section 5 analyzes images from this data frame for their scientific quality.
- Section 6 compares radiances to prelaunch specifications of noise and calibration stability.
- Section 7 shows the calculation of radiances for clear air radiosonde sites in the SE USA, which reported 3 hours later. The synthesized radiances are compared to the VAS observations.
- Section 8 describes how temperature and dewpoint soundings are made from a simple radiance to radiosonde regression scheme, which is then used as a "radiosonde interpolator" to make a regular grid of retrievals over the SE USA.
- Section 9 analyzes the VAS soundings and the original radiosonde reports as temperature and mixing ratio contours on various pressure levels, then compares them to each other.
- Section 10 summarizes what has been learned from the first VAS radiances at GSFC and assesses their significance for future work with the VAS instrument.

This report can be "skimmed" by reading the abstract, summary section, and figures. Operational difficulties are largely found in the footnotes.

1.3 SUMMARY OF OBJECTIVES AND OUTLINE

The first orderly VAS dwell sounding radiances are examined by the scientific users for:

1. Image quality.
2. Radiometric precision.
3. Radiation transfer verification.
4. Regression retrieval accuracy.
5. Mesoscale analysis features.

The report is organized into the following sections:

1. Objectives and outline.
2. Description of VAS.
3. Prelaunch assessments at GSFC.
4. VAS-D operations to 7NOV80.
5. VAS-D image quality.
6. VAS-D radiometric quality.
7. Radiation transfer verification.
8. VAS-D sounding quality.
9. Mesoscale analyses from empirical retrievals.
10. VAS-D assessment summary.

SECTION 2
DESCRIPTION OF VAS

VAS is described in this section with increasing focus upon its role as a sounding instrument. This description proceeds from a programmatic view of the VAS Demonstration to a description of the VAS instrument's key features.

2.1 BACKGROUND

Present atmospheric soundings from operational satellites are designed to collect temperature and humidity data for global analysis and input to numerical models which simulate the large-scale general circulation. The soundings are performed from sun-synchronous polar orbiting satellites, which provide complete coverage of the globe with a spatial scale of several hundred kilometers twice per day per satellite. The entire system consists of the sounders on the satellites, the algorithms for reducing the data and retrieving the desired atmospheric variables, and the general circulation models and is aimed at improving the intermediate to long-range forecasts of the large-scale circulation patterns.

The need for understanding short-lived weather phenomena, such as severe local storms, and the growing requirements for more accurate local weather forecasts that require atmospheric data with a finer spatial scale and more frequent observations, points toward a different satellite system: one centered around soundings from a geosynchronous platform (Soumi, *et al.*, 1971). Severe local storm research and prediction require frequent observations at subsynoptic to mesoscale resolution to capture the relevant changes in the atmospheric mass and wind fields. The incorporation of ancillary data (e.g., conventional surface and radiosonde reports) from the meteorologically active areas is expected to become an important aid to the satellite sounding process. Likewise, an understanding of the physics of the phenomenon under observation should be helpful in modeling the radiation transfer for the retrieval algorithms.

The VISSR Atmospheric Sounder (VAS), which is now operating as an integral part of the Geostationary Operational Environmental Satellite (GOES) system, was designed to meet the requirements of observing subsynoptic to mesoscale temperature and moisture distributions. Ultimately, the goal is to observe, understand and predict the development of severe storms.

The geosynchronous VAS will watch the development of mesoscale weather systems, typically surveying the United States with 12 spectral bands once per hour at 15 km (nadir view) resolution. Satellite soundings derived from such multispectral scenes will have 30 to 90 km effective resolution, since several pixels must be used to average radiometric noise and deal with broken cloud cover in the net sounding field of view (SFOV).

At this time, the polar orbiting satellite sounders are operationally useful over the data-sparse oceans where both the underlying uniformity of the ocean surface and the passive microwave data are important data processing aids for synoptic scale retrievals. These soundings show some systematic error patterns, such as larger errors near the surface and tropopause, biased performance in partly cloudy areas, and low sensitivity to horizontal gradients (Phillips, *et al.*, 1979). Operational satellite soundings over land have similar errors: the subsynoptic gradients are underestimated, and there are significant errors where the underlying topography is unusual or persistently cloudy (Schlatter, 1981).

Operational satellite soundings are usually ignored in favor of the conventional radiosonde network despite the inadequate space-time resolution of the conventional synoptic data for mesoscale developments. Case studies over mesoscale networks with satellite radiances from the Vertical Temperature Profile Radiometer (VTPR) have been encouraging. VTPR retrievals at 70 km resolution over the Atmospheric Variability Experiment (AVE) produce temperature fields and precipitable water estimates comparable to the AVE data (Hillger and Vonder Haar, 1977). VTPR radiance correlations over the National Severe Storms Laboratory (NSSL) network showed a spatial structure comparable to the meteorological correlations in the NSSL analyses, although the retrieved moisture information was not well determined (Hillger and Vonder Haar, 1979).

Polar orbiting sounder studies are hampered by the lack of unambiguous, independent, co-located "ground truth" data taken with space-time resolution as good as the satellite observations. A prelaunch VAS simulation study (Chesters, *et al.*, 1981) avoided these problems by declaring that selected mesoscale profile analyses are "ground truth," and then retrieving profiles from corresponding synthetic radiance fields, so that unambiguous estimates of retrieval accuracy could be made. The quantitative results, which will be described in a following section, provide a benchmark for mesoscale retrieval accuracy available from the VAS sounder, for optimal sounding conditions without help from ancillary data or from physically modeled retrieval algorithms.

2.2 THE VAS INSTRUMENT

During the 1970s, the Visible Infrared Spin-Scan Radiometer (VISSR) was carried on the SMS/GOES series of geosynchronous satellites. VISSR infrared images in the 11 micron window are formed by stepping the scan line each spin by its own width (7 km resolution at nadir). During the 1980s, the GOES satellites will carry an upgraded instrument called the VISSR Atmospheric Sounder. The VAS instrument has programmable features which allow a ground-based operator to interact with the satellite by using the most recent observations to command when, where and how VAS will acquire data. The user will be limited only by the available time, filter/detector combinations and radiometric constraints (see Table 1). The geosynchronous location can be exploited to observe the development of mesoscale weather systems. For example, VAS can take sounding quality (low-noise) radiances at 15 km (nadir view) resolution along a full earth east-west swath with a north to south extent large enough to cover Oklahoma every 20 minutes or with a north to south extent large enough to cover the conterminous United States every hour.

VAS has 12 thermal infrared channels between 4 and 15 microns. The channels are chosen to distinguish the effects of tropospheric temperature, moisture and cloud cover upon the upwelling radiances. All 12 channels can be operated at 15 km resolution (instantaneous geometrical field of view at nadir), and channels, 4, 5, 7, 8, 9 and 10 can be operated at 7 km resolution (the other channels are too noise- or diffraction-limited to be operated at higher resolution).

Considerable effort has gone into prelaunch development of VAS radiometry (Malinowski and Ruiz, 1980; Menzel, 1980). The VISSR radiometer has been upgraded to yield high precision values (10 bits) from six detectors, and has been carefully calibrated with outer space (3°K) and an internal hot target (320°K). Radiometric noise is reduced by "dwell averaging" several spins on the same line and channel; the number of spins allocated to the channels is termed the "spin budget." Noise can also be reduced after data collection by judicious averaging of the clear adjacent fields of view.

Table 1 summarizes key design features of the 12 VAS channels: central wavelength, wavenumber and bandpass; purpose for sounding; main absorbing gasses and other important influences; single sample noise; radiometric noise requirements for sounding; and a nominal spin budget for dwell averaging each channel. Lower spin budgets can be used to trade radiometric accuracy for speed and latitude coverage. In that case, pixel averaging of the 15 km (nadir view) instantaneous geometrical fields of view (IGFOVs) into, say, a 60 km sounding field of view (SFOV) are possible to regain radiometric accuracy at the expense of detailed resolution. Nominal calibration specifications are ±1.5° K absolute and ±0.5° K relative brightness temperature in all channels for a typical earth scene. For comparison, the previous VISSR instrument had calibration errors of roughly ±3° K.

2.3 VAS CHANNEL CHARACTERISTICS

VAS transmission functions, $\tau(\nu,p)$, are computed for each channel (designated with wavenumber ν) down to 40 pressure levels p, from .2 to 1000 mb. The transmissions are done for CO_2, N_2, N_2O, NO, CH_4, O_2, plus H_2O, using line-by-line absorption coefficients (McClatchey, *et al.*, 1973) and important molecular continuum absorption cross sections (Burch, *et al.*, 1970-71; Roberts, 1976).

Corresponding weighting functions, $d\tau/d\ln P$, are shown for the U.S. Standard Atmosphere in Figure 2 for the temperature-sounding channels and in Figure 3 for the moisture and window

channels. The short wave channels are indicated with dashed lines. The redundancy between the long and short wave channels will be used to detect cloud contamination by exploiting the differential sensitivity of the Planck function to cloud top temperature. The sharp peaks of the moisture channels in Figure 3 are related to the exponential average distribution of water vapor, although their altitude is not very predictable for individual SFOVs, because they represent the radiance accumulation from the top few millimeters of the total water burden.

Figures 2 and 3 also show that the lower troposphere (500 to 1000 mb) is not well resolved by any one of the VAS channels. The radiation from the temperature and moisture structures just above the boundary layer (700 to 900 mb) is mixed with both surface and mid-tropospheric radiances in all key VAS channels (5, 6, 7, 8 and 12). The "man in the loop" concept will be an important factor to successful sounding with VAS (Smith, *et al.*, 1978) in cases where radiances will be confused by low clouds, topography and irregular surface emission. Also, the inclusion of surface temperature and moisture information into the retrieval scheme can be of great value in properly determining the atmospheric boundary conditions (Hayden, 1980).

2.4 SUMMARY DESCRIPTION OF VAS

The VAS instrument is an improved version of the VISSR device used operationally on the GOES satellites. It was designed to provide multispectral infrared sounding data and exploits the geosynchronous station to give frequent coverage of mesoscale weather developments. VAS has 12 calibrated thermal infrared channels between 4 and 15 microns, which are chosen to distinguish the effects of tropospheric temperature, moisture and cloud cover upon the upwelling radiances. The VAS channels cover the troposphere with roughly 5 km vertical and 15 km horizontal resolution, and they suffer the usual passive infrared limitations on determining the state of the lowest atmospheric layers without ancillary surface data.

SECTION 3
PRELAUNCH ASSESSMENTS AT GSFC

This section summarizes some of the prelaunch scientific studies of the radiation transfer and mesoscale retrieval capabilities of the VAS instrument. These studies were done at GSFC.

3.1 VAS FILTER ASSESSMENT

The prelaunch measurements of VAS-D filter/detector spectral responses were convolved with the foreoptics spectral characteristics, and the resultant spectral sensitivity at scores of points within each bandpass were reported to GSFC.[1] Figure 1 shows these measured bandpasses and compares them to the central and half-width wavenumbers in the prelaunch specifications of Table 1.

These measured bandpasses allow one to compute mean wavenumbers, listed in Table 3, which differ from the specifications listed in Table 1 by less than 1 percent for all channels. Compared to the specified bandpasses, the manufactured bandpasses result in only slight differences in the channels' line-by-line transmission functions (generally <1 percent) and the simulated brightness temperatures (generally $<1^\circ$ K) done with each set.

The weighting functions shown in Figures 2 and 3 are based upon the measured bandpasses. Noticeable disagreement with corresponding weighting functions for the specifications (not shown) occur only for the water vapor channels 9 and 10 where the actual bandpasses result in standard weighting functions that peak slightly deeper in the atmosphere (about 50 mb at 500 mb, a more desirable situation for severe weather analysis).

Table 4 lists Planck radiances calculated for every significant degree of brightness temperature using the effective VAS wavenumbers listed in Table 3. This radiance table is very convenient for quick verification of the magnitude and mutual consistency of actual VAS radiances from a sounding field of view (SFOV). Section 7 describes the GSFC method used for computing brightness temperature $T^*(\nu,R)$ for the effective wavenumber ν and observed radiance R.

[1]Personal communication, P. Menzel, University of Wisconsin, August 1980.

3.2 VAS CHANNEL SENSITIVITY ESTIMATES

Table 2 summarizes some calculated responses of the VAS channels to the clear atmosphere: the pressure level of the peak of each standard weighting function; the pressure range over which the middle 80 percent of the radiance accumulates; the net sensitivity of the brightness temperature to a 1° C increase in the entire air temperature profile or in the dewpoint profile or in the surface temperature alone; mean and standard deviations of VAS-simulated brightness temperatures for a set of 32 radiosondes distributed over North America; and "signal"/noise estimates made by comparing these variances to the single sample noise listed in Table 1. Roughly speaking, the "signal" (variance) in the tropospheric channels is 5 percent of the total brightness, and the noise is 0.5 percent, giving a "signal"/noise of about 10/1.

The net sensitivity estimates in Table 2 suggest simple channel combinations for special environments. One promising combination is VAS channels 7 and 8. These form a "split window" for water vapor determination in the lower troposphere, since the two channels have different sensitivity to moisture variations at nearly the same wavelength (Prabhakara, *et al.*, 1974). For instance, a SFOV with 5° C higher dewpoint than the U.S. Standard will appear 1.8° K colder at 12 microns, due to the increased absorption by water vapor, but only 1.0° K colder at 11 microns. Consequently, this "split window" should be able to directly display horizontal moisture gradients, such as pre-thunderstorm "dryline" environments with warm dry air next to cool moist air. Such interesting speculations have been examined more thoroughly by GSFC in prelaunch sounding studies of simulated VAS retrievals for realistic mesoscale situations, and the results are summarized in the following paragraph.

3.3 SIMULATED SOUNDING STUDIES

To prepare the GSFC personnel and computers for VAS data, radiances were synthesized and soundings were made and analyzed for severe storm conditions (Chesters, *et al.*, 1981). This report describes a prelaunch sounding simulation experiment to demonstrate:

1. The visibility of lower tropospheric moisture gradients in the VAS radiances.
2. The detectability of a potential convective instability in a pre-thunderstorm environment, using optimal soundings from the VAS channels.
3. The sensitivity of residual errors in VAS regression retrievals to "local" statistical conditioning for the kind of mesoscale phenomenon under investigation.

In order to estimate the accuracy of the three-dimensional VAS soundings within severe local storm systems, 12 channel radiance fields are simulated for thunderstorm environments observed in Oklahoma. Temperature and moisture profiles for 10 time frames (Mostele, *et al.*, 1980) are drawn from the radiosonde network operated by the NSSL in 1976. The profiles are gridded using a Barnes analysis (Barnes, *et al.*, 1981), covering Oklahoma with a grid at 20 km horizontal resolution and the troposphere at 1 km vertical resolution. Radiances are simulated for SFOVs in each frame, using line-by-line transmission functions for the temperature and moisture profiles.

Simulated VAS images of partly cloudy pre-storm conditions are shown for one of the NSSL frames where a corresponding SMS 11 micron picture is available. Radiances are computed at full VAS resolution (20 km projected view per SFOV). Grey level images in the "split window" channels at 11 and 12 microns show that realistic cloud cover does not seriously mask the underlying precursor storm conditions. Moisture gradients are visible in the clear areas with contrast greater than the expected VAS noise levels.

Temperature and moisture profile retrievals are done at the expected SFOV resolution by using a coarser (50 km) SFOV subset drawn from the finer (20 km) grid. These simulated radiances are separated into two sets: a "local" dependent training set used to determine clear air to radiance correlations and an independent test set used to determine the retrievability of atmospheric information from clear SFOVs. The impact of detailed statistical conditioning upon a regression retrieval scheme is demonstrated by comparing these "locally" conditioned retrievals to soundings done

with two other dependent training sets: a "global" set derived from 32 North American radiosondes and a wet/dry subset of the "local" dependent NSSL frames. For the latter comparison, the fields are partitioned into a "wet set" and a "dry set," using a threshold mixing ratio of 8 gm kg^{-1} at 850 mb.

Results from the simulated retrievals include:

1. Temperature profile residual errors in the troposphere are ±2° C across a 3° C gradient, and corresponding mixing ratio residuals are ±2 gm kg^{-1} across an 8 gm kg^{-1} gradient.
2. Horizontal and vertical temperature and moisture structures are retrieved in the lower troposphere, and potentially unstable air is recovered from simulated VAS radiances having the resolution and noise limits expected from the instrument. The absolute magnitude of the retrieved potential instability is significantly underestimated by the remote sounding process, which reflects the lack of vertical resolution in the 12 VAS channels. Relative temperature and moisture patterns are retrieved, although the magnitudes of the gradients are likewise underestimated.
3. Retrievals done with regression matrices conditioned with "local" weather statistics have smaller residual errors than those conditioned with "global" data. These results are due to the better resolution of ambiguities in vertical structure in favor of the most probable structure derived from a "local" statistical database. A further subdivision of the dependent NSSL6 dataset into "wet" and "dry" subsets did not make any statistically significant improvement in the "local" retrievals.
4. VAS should be capable of retrieving vertically integrated meteorological parameters. The main moisture and airmass features are captured in the form of retrieved fields of precipitable water and geopotential thickness. These simulations had only ±0.2 gm cm^{-2} error (less than 25 percent) in precipitable water and only ±3.3 meter error in the 500 to 920 mb thickness, using "locally" conditioned regression coefficients. The inadequacies of the "globally" conditioned retrievals are most dramatically displayed in retrieved thickness fields.

This prelaunch study of VAS retrievability gives promising results for pre-thunderstorm environments. Profile errors are comparable to those claimed for polar orbiting sounding instruments. Strong gradients are discernible in realistic partly cloudy conditions, although their magnitudes are underestimated like those observed with operational sounders. While not all of the complex factors in satellite data have been simulated in this study (such as multiple cloud structures, surface irregularities, reflected sunlight, and radiometric errors), these results still imply that VAS radiances will produce the best sounding when a human being classifies the scene, picks relatively clear areas for retrieval, and applies a "local" statistical database. The VAS simulated soundings show the same limitations in absolute accuracy and vertical resolution that are suffered by other passive infrared satellite instruments, especially in the lower tropospheric moisture retrievals. This weakness, even in these optimally simulated soundings, indicates that timely incorporation of conventional surface data will have to become part of VAS data processing to make the lower tropospheric retrievals more accurate. Nevertheless, VAS' spatial and temporal resolution should permit us to locate and effectively monitor the relative changes within potentially unstable mesoscale structures, and thus significantly improve upon the synoptic-scale, ground-based and polar orbiting data networks. The analysis of real VAS data will determine if this potential for monitoring mesoscale atmospheric changes can be realized with geosynchronous satellite sounding data.

The measured spectral responsivity of the VAS-D channels meets prelaunch specifications. The calculated sensitivity of the brightness temperature (°K) to the VAS channels' variations in temperature and moisture (°C) indicate a typical "variance/noise" ratio of 10° C/1° K over North America throughout the year. A sounding study of thunderstorm environments, using VAS radiances synthesized from NSSL radiosondes, yielded profile and gradient retrievals with acceptable error levels, provided that the algorithm was statistically conditioned to resolve ambiguities in favor of the most probable local conditions. However, there was a serious underestimate of the moisture content of the lower troposphere, which suggests that ancillary data is needed in order to retrieve this parameter accurately.

SECTION 4
VAS-D OPERATIONS TO 7NOV80

This section describes some of the problems with VAS-D which affected the acquisition of the first good dwell radiances or which could affect future users.

4.1 THE VAS DATA TEAM

Responsibility for the prelaunch checkout of VAS is given to the builder, Santa Barbara Research Center (SBRC) (Malinowski and Ruiz, 1980), and to the operational developer, the University of Wisconsin (UW) (Menzel, 1980). General management is by NASA's Operational Satellite Improvement Program (OSIP) via the VAS Demonstration Experiment at Goddard Space Flight Center (GSFC) (Montgomery, 1980).

GSFC also maintains a computer system capable of handling VAS data. This system, known as the VAS Processor (VASP), is expected to perform detailed sounding and mesoscale weather research on case studies, in contrast to the development of a prototype operational system at UW. Before the GSFC VASP receives the VAS data, it is processed by three other programmable computers: one on the GOES spacecraft, one at the central ground station at Wallops, Virginia, and one at GFSC.

The GSFC VASP has a front-end computer called the VAS PreProcessor (VASPP), which performs archiving, zero point calibration, dwell averaging, data unpacking and some documentation functions. The computer at the front end of the UW and GSFC computers is the Synchronizer/DataBuffer (S/DB), located at the ground station run by NOAA at Wallops, Virginia. Both the S/DB and the VASPP are being developed under contract by the Westinghouse Corporation (W). The computer onboard the GOES satellite, which performs the initial sampling and calibration steps, was developed by SBRC. It requires considerable technical coordination and software debugging to manage this data chain well enough to deliver orderly VAS radiances to the scientific user.

4.2 PRELAUNCH PROBLEMS

Before launch on 9SEP80, one of VAS-D's two large (15 km subsatellite resolution), long wave (6 to 15 micron sensitivity) detectors was unusable, probably due to a loose wire attached to the detector. The impact of this on sounding is to reduce the latitude coverage rates from design specifications by a factor of 2. In order to recover reasonable latitude coverage, the spin budget for dwell sounding was drastically reduced in the fainter stratospheric channels (see Table 1). GOES-D was launched despite this loss, because this detector is not used for operational VISSR data, and the VAS instrument is still only an experiment with VISSR compatibility.

In the testing prior to launch, SBRC accidentally fouled and then cleaned the primary telescope mirror, leaving a noticeable film known as the "green haze." Analysis of the residue determined that the "green haze" did not significantly degrade infrared performance of the optics (less than 10 percent absorption at VAS wavelengths, and GOES-4 was permitted to launch.[2]

4.3 POSTLAUNCH CHECKOUT

In any large project, the operational methodology is forged in the first days when procedures are adjusted to make the data chain actually work. For historical purposes, some of the important decisions that led to calibrated, documented, orderly VAS radiances suitable for dwell sounding are reviewed here.[3]

4.3.1 Calibration Irregularities

One adjustment of potential scientific importance involved the preliminary calibration step, an analog-to-digital (A/D) conversion of the detectors' raw positive voltage to a binary number for transmission to earth. VAS-D now uses a "constant" lookup table with enough leeway in each

---

[2] The situation is described in a memo for the record, dated September 24, 1980, and titled GOES-D VAS Contamination," by Dr. Harry Montgomery, VAS Demonstration Manager, NASA/GSFC, Greenbelt, MD 20771.

[3] A more detailed record can be found in the minutes of the meetings held by Dr. Harry Montgomery, VAS Demonstration Manager, NASA/GSFC, Greenbelt, MD 20771.

channel for the largest *conceivable* observation[4] to fit into 10 bits, rather than by using the originally planned "dynamic" scaling of each line of data with leeway for the largest *actual* observation within each line.

The original scheme provided a minimum of digital truncation errors, but the "dynamic jitter" in the data by factors of 2 from spin to spin was not manageable by the "dwell averaging" algorithms in the minicomputers at UW and GSFC. These minicomputers are not fast enough to do this much arithmetic with the VAS data streaming in at 1.75 megabits per second. Consequently, the adopted scheme, with 1 to 2 bits of leeway in the 10-bit word, yields roughly 8 significant bits of radiance information for a typical earth scene, making truncation noise comparable to radiometer noise in the brighter channels. For instance, if 8 significant bits (2^8=256) represents 100 ergs/etc in the 11 micron window (VAS channel 8), then the truncation error is 100/256=.4 ergs/etc, which is larger than the single sample radiometric noise (±.2 ergs/etc) specified in Table 1. This small error is not serious for basic sounding work, and the "constant" lookup tables on the satellite can be reprogrammed if necessary.

Most of the other problems in the first months' testing involved software details and conventions. In fact, VAS produced recognizable pictures of the earth in all 12 channels by 9OCT80. However, the lack of dump and debug facilities in the S/DB at the Wallops, Virginia ground station prevents the rapid analysis and repair of their problems. Consequently, UW and GSFC have developed front-end software to do quality assurance of the incoming raw VAS radiances.

The scientifically important problems involved establishing zero radiance for outer space, since algorithms must correct for: voltage biases on the detectors, radiance from the telescope foreoptics, and accidental views of the moon or stars during the zero point "space look." The VAS calibration chain is outlined in more detail in a subsequent section on quantitative radiometric quality.

---

[4]The largest conceivable radiance corresponds to a scene temperature of 340° K.

4.3.2 Miscellaneous Postlaunch Irregularities

A few minor data processing anomalies still remain, such as confusion over the logical bit used to indicate either north-to-south or south-to-north scanning of the mirror. (Current operations ignore it by assuming all scans are done north to south.) Perhaps only 30 percent of the telemetry documentation associated with each spin scan of radiance data is used regularly enough to insure that it is completely "debugged."

Postlaunch checkout of VAS-D occurred during the equinoctal "eclipse season," when the satellite is thermally shocked by passing through the earth's shadow each night. The only noticeable effect upon regular (daytime) sounding operations was the inability of the local radio reception to function for an hour at midday when the satellite appeared nearly aligned with the sun.

Operations with VAS-D on GOES-4 were regularly plagued with sudden stoppages in the flow of data. The majority of the cases clearly arise in the S/DB[5] and not in the VAS instrument or in the local computers. In November 1980, the mean time to failure was a few hours. This caused roughly half of the attempted dwell soundings to fail, especially those in the morning corresponding to the 1200GMT radiosonde launches. In fact, the radiosondes themselves can occasionally interfere with the reception of VAS data at the S/DB in Wallops, Virginia, since the backup frequency for local RAOB broadcasts is within the bandwidth of the GOES 28 Mbit sec^{-1} telemetry downlink. Other data processing problems are noted in the following sections.

4.4 UNITED STATES APPEARANCE ON 7NOV80

Quick-look, wide-angle visible images were available as WEFAX pictures[6] from the GOES-EAST VISSR operations. Figure 4 shows the VISSR picture of the United States taken at 2000GMT

---

[5] Subsequent analysis indicates that the cause is in the S/DB hardware where several hundred integrated circuits have silver coated leads, which have been gradually corroding and causing uninterpretable voltage levels. These chips have since been refurbished.

[6] No GSFC VISSR picture was available from GOES-4 itself at 98°W, because the Laser Beam Recorder (LBR) attached to the VASPP system for the production of full earth, full resolution VISSR pictures was inoperative. The cost of maintaining the LBR is deemed to be too great to risk its operation as a routine aid to the VAS data users at GSFC.

7NOV80 from GOES-EAST, at 75° W. Most of North America was quite clear, and the SE United States was experiencing unseasonably warm weather.

The GSFC VASP data handling capacity was designed for mesoscale field analysis, so that sounding experiments can encounter software and hardware bottlenecks[7] for areas larger than a subsynoptic region. Consequently, the SE United States was selected for the first VAS soundings at GSFC, since the area was seen at a good aspect angle, the air was clear, and there was "ground truth" available from the radiosonde stations there, as well as "satellite truth" from the afternoon pass of TIROS-N.

4.5 SE UNITED STATES RADIOSONDES ON 7NOV80

The afternoon radiosonde releases in the SE United States started about 2330GMT, roughly 3 hours after the VAS dwell radiances were observed in that area. There are 19 sites in the area of interest, from Oklahoma to North Carolina and down to the Gulf of Mexico. Table 5 lists the 19 site locations, and the secant of the zenith angle from the site to GOES-4 at 98° W. Figure 20 shows the locations of the 19 radiosonde sites projected on an image of the SE United States produced from the VAS 3.9 micron window radiances. Zenith angles with $\sec\theta > 2.0$ ($\theta > 60°$), as would be viewed in New England or the Pacific Northwest, are too large to produce accurate retrievals reliably.

Tables 6, 7 and 8 list the 19 radiosonde measurements of temperature, dewpoint and dewpoint depression (all ° K). The tables were interpolated onto the 40 levels used for transmission function and radiation transfer calculations to be described in section 7.1. These lists were derived

[7]The GSFC VASP is a minicomputer (a PDP 11/70 under RSX 11M) with sufficient CPU, memory, bandwidth and mass storage capacity for the flow of VAS data, but the 16-bit address word size limits each task to 64 kbytes. This has proved to be undersized for general purpose scientific programming, even with overlays, subtasking and memory paging. The worst VASP bottlenecks are being reprogrammed by striking a new balance among factors of CPU speed, memory availability, data management delays, overlay complexity, software flexibility, programmer skills, and user convenience.

from printouts of the entire radiosonde reports mailed from the National Climate Center (NCC) in Asheville, NC. Tropospheric radiosonde reports are more directly available from the National Weather Service (NWS) "604 line" attached to the AOIPS computer at GSFC[8].

Figure 12 shows plots of temperature and dewpoint profiles for three sites within the region of interest (Amarillo, Texas, Jackson, Mississippi and Tampa Bay, Florida). The temperature profiles resemble the subtropical mean far more than the U.S. Standard Atmosphere (not shown) with a sharp, cold tropopause and unseasonably warm air at the surface. The air is very stable, with a noticeable gradient toward the cooler air in the east. The moisture profiles are substantially drier than the subtropical default with large midtropospheric variations. No site reports moisture above 300 mb, and many eastern stations reported only a few of the lowest mandatory levels with a nominal (i.e., too dry to measure) dewpoint depression of "30° C." Considerable moisture layering can be seen in many of the dewpoint depression profiles of Table 8.

4.6 OPERATIONS ON 7NOV80

On Friday afternoon, 7NOV80 during 1901-2052GMT, the VAS data processing systems executed the first successful dwell averaged observations. The VAS instrument was programmed with a Processor Data Load (PDL) with 54 spins per line over all 12 channels (see Table 1), surveying scan lines 200 to 600[9] (roughly 50° to 20° N latitudes). The southern United States, in lines 400 to 596, was observed at roughly 2030GMT, about 3 hours before the actual release of the "0000GMT" radiosondes at 2330GMT. The spin budget in the dim stratospheric channels was greatly reduced in order to trade that loss in radiometric accuracy for increased speed and coverage.

---

[8] Unfortunately, the AOIPS processing of the "604" profiles routinely truncates the data above 100 mb, which is too low to verify many of the VAS radiances, as one can see from the vertical extent of the weighting functions in Figures 2 and 3.

[9] Only lines 200 to 596 were received; the loss of the end lines from every PDL is a common fault somewhere in the data processing system.

4.7 SUMMARY OF VAS-D OPERATIONS TO 7NOV80

VAS-D was launched on 9SEP80 with one of a redundant pair of detectors broken, reducing useful data rates by a factor of 2. A month of postlaunch checkout was used for debugging software throughout the VAS system, principally the A/D conversions on the satellite, the calibration in the S/DB at Wallops, and the calibration and quality assurance in the VASPP and VASP. The first orderly, calibrated dwell radiances were gathered over North America on the afternoon of 7NOV80, 1900-2100GMT. The weather was remarkably clear and warm over most of the SE United States, where radiosonde reports were available 3 hours later from 19 clear sites.

SECTION 5
VAS-D IMAGE QUALITY

Images of VAS radiances are used for qualitative detection of gross processing problems. Quantitative analysis will be discussed in the section on radiometric quality assurance. The dwell sounding data of 7NOV80 is examined visually for continuity, registration, landmark location, and obvious radiometric problems. In fact, infrared images with higher resolution can be made from VAS data taken in the Multi-Spectral Imaging (MSI) mode than are shown here in the Dwell Sounding Averaged (DSA) mode. More exact image testing has been deferred to pursue atmospheric soundings with the first VAS dwell sounding data.

5.1 IMAGES IN ALL 12 VAS CHANNELS

The raw VAS radiances consisted of 12 dwell averaged channels of 3822 samples taken along 198 large detector (15 km nadir resolution) scan lines. This data was undersampled by taking every 10th sample from the central 1912 samples on every 2nd line.[10] This resampling makes pictures with a geometrically comfortable aspect ratio. (The original oversampling along a scan line produces images of the earth that appear stretched E-W by a factor of 5.) The result is 12 channels of radiances with 191 pixels by 99 lines of 30 km resolution (nominal nadir view) over North America viewed from 98° W. The entire range of radiance in each channel was then interpolated onto an 8-bit grey scale (2^8=256) for maximum contrast. Finally, the grey scale images were converted to digital TV files (512 X 512 dots) on the VASP and were each annotated with identifying information. Black and white photographs of these files are shown in Figure 5 with one V. S channel image per page for 12 pages.

The images in Figure 5 have been contrast reversed so that the cold, low radiance cloud tops will appear conventionally white. Other cosmetic editing of these images causes unpredictable black or white representations for outer space, which are seen in the upper corners of the images.

---

[10] The VASP software for making images from DSA datasets had an upper limit of 20,000 total pixels (bytes) so that pictures of more than 200 X 100 SFOV's were not possible.

The "landmarks" in the VAS images shown in Figure 5 are found in the GOES-EAST VISSR picture in Figure 4. There are characteristic cloud formations over Montana and the Pacific Northwest, over the upper Midwest and central Appalachians, and across the southern tip of Florida. The United States seacoast from the Carolinas to Texas is clear, as is Baja, Mexico and southern California. These features are all apparent in the VAS window and lower tropospheric sounding channels. Only the higher clouds appear in the mid-tropospheric channels. For instance, the low cloud band running from North Dakota to the Great Lakes is visible in VAS channels 5 to 8 and 12, but is indistinguishable in VAS channels 4 and 11. The mid-tropospheric clouds over Montana and the Great Lakes can be seen in VAS channels 4 and 9 to 11, but scarcely affect the upper tropospheric radiances in VAS channel 3. Likewise, the highest level clouds in the flow across the tip of Florida appear in all of the images in Figure 5 except for the two stratospheric bands, VAS channels 1 and 2. The only "landmarks" in the stratospheric channels are the edges of the earth in the upper corners of the pictures. The mid-tropospheric water vapor bands, VAS channels 9 and 10, have very similar images in Figure 5, although the somewhat greater penetration of channel 9 manifests itself as sharper contrast for the mid-level clouds. These water vapor images also display a remarkably complicated pattern of clear air dry "slots" (dark streaks of maximum upwelling radiance in the contrast-reversed images of Figure 5), such as the convex and concave pair across Oklahoma and Arkansas and along the Gulf Coast. In channel 12, the 3.9 micron VAS window channel, there are local surface warm features (darker areas) in southern Texas and in the central clear areas of the Gulf of Mexico. The autumnally chilled shallow waters just off of the Gulf and Atlantic coasts make the sunlit land and the warmer deep waters stand out in greater contrast in VAS channel 12, with the Gulf Stream quite visible. Finally, there are noticeable limb gradients in all of the channels except channel 1, which presents an almost flat, grey appearance of low intensity at all viewing angles. The blank appearance of the earth in channel 1 has not yet been explained.

5.2 IMAGE QUALITY DISCUSSION

Images for sounding purposes were designed to have rather coarse resolution (15 to 60 km) to average out radiometric noise in a SFOV. Consequently, infrared imaging errors are not rigorously tested here, but are only noted where they obviously affect sounding.

5.2.1 Continuity

These images have been correctly de-interleaved from the original multiplexed telemetry stream of samples, channels, lines, and internal documentation. This is worthy of mention because VAS channel images taken before and after 7NOV80 sometimes show N-S discontinuities where one channel's image suddenly jumps to another channel.[11]

5.2.2 Registration

The six infrared detectors on VAS have substantial E-W and N-S offsets from each other, so that software must carefully remove these fixed differences to make landmarks in different channels coincide in a multispectral image. Also, the starting point and spin rate of the VAS sampling is irregular enough that the S/DB must resample every spin to make the edges of the earth look circular and registered. Both of these operations can be tested by looking at the difference between two similar channels.

Figure 6 shows the difference of brightness temperature between the VAS "split window" (channels 8-7, at 11 and 12 microns, respectively) over an image of the SE United States. The raw data was resampled to decrease radiometer noise by averaging 10 pixels and 2 lines into each SFOV at 30 km nominal resolution, yielding a scene of 34 lines with 73 pixels each. Both channels used the same detector at nearly the same wavelength, and there is no hint of mis-registration (which would show up as high contrast "double image" borderlines around the clouds and along the coastline). Figure 7 is a similar image of the brightness temperature difference between the two VAS

[11] This problem was later traced to the S/DB where one entire spin's worth of data can be lost, confusing the downstream de-interleaving algorithms. This problem became acute by mid-December 1980 and seriously interfered with the collection of scientific data. It was eventually traced to corroding leads on some of the integrated circuits in the S/DB.

windows (channels 12-8 at 4 and 11 microns), which use different detectors. The image shown in Figure 7 has been contrast-enhanced to make the coastline more apparent and artificially emphasizes the internal features, such as the Mississippi valley. Figure 7 shows no "double imaging" due to the offset between the longwave and shortwave detectors.

This simple multispectral testing indicates that the registration algorithms in the S/DB and the VASP are correct for the large (15 km) lower detectors. The registration with the large upper detectors must await testing with VAS-E, since the large longwave upper detector is inoperative on VAS-D. Registration with the small longwave detectors has not yet been rigorously tested at GSFC.

5.2.3 Navigation

At this time,[12] there are no automated transformations on VASP to convert infrared line and pixel locations at some time to or from latitude and longitude locations on the earth. Consequently, convenient grid lines and geo-political boundaries cannot be supplied to the VAS images. Fortunately, by working on a clear day, one can roughly identify locations in an image from major landmarks and from cloud masses seen in the navigated VISSR pictures from the operational GOES-EAST satellite.

5.2.4 Single Sample Noise.

Since the radiances in Figure 5 were "contrast-stretched," the channels with less intrinsic dynamic range (such as the stratospheric channels) show their noise plainly. Although we only

---

[12] VASP navigation software has been developed and tested on VAS data from 13 to 14NOV80, but the navigation parameters must still be manually developed for each frame, and there are still some bugs in the VASPP/VASP software conventions. Development of infrared transformation software is underway, but it has been hampered in the incomplete state of VASPP software for replaying archived raw VAS data.

Using the GSFC VASP computer to determine the orbit and attitude (O/A) for the GOES satellite has exposed a potential operational problem. The O/A determination requires much of the VASP hardware capability for 8 hours of each observing day in parallel with the 8 hours of sounding determinations. Consequently, two shifts of data processing may be required for each shift of VAS data taking: one for sounding and one for navigation.

selected every 10th sample along every other line, there is no sign of organized single sample noise, such as "herring bone" patterns. There is, however, considerable line-to-line variation in the average brightness, which is discussed in the next paragraph.

Occasional "wild radiance" points are observed in the dataset that produced Figure 5. The grey images photographed to make Figure 5 have been edited to remove these "blemishes," so that an exact count of wild radiance points is not available (one such unedited point is visible in the clouds over Montana in VAS channel 10). A rough estimate of the significant bit error rate (BER) is a few SFOVs per 191 X 91 SFOV picture, or roughly 10^{-4}. Since these errors are obvious only in the most significant of 8 bits, the inferred bit error rate must be close to 10^{-3}, which is considerably larger[13] than the expected rate of about 10^{-6}.

5.2.5 Line-by-Line Variation

Line intensity variations are a qualitative indicator of the relative calibration instability. The variation in the average brightness of the lines in Figure 5 is very noticeable in the contrast-enhanced stratospheric channels. Also, groups of lines with slightly offset average brightness are noticeable in some of the channels in Figure 5 and as a broad dark band across the center of the "split window" in Figure 6. These line-to-line variations are but the visible result of variations in the relative stability of the line-by-line calibration procedure used on VAS, as discussed quantitatively in the following section on radiometric quality.

5.3 IMAGE QUALITY SUMMARY

Images of the 7NOV80 VAS dwell sounding radiances are well registered multispectral views of the North American atmosphere and are suitable for sounding. Some problems exist with a high bit error rate and with line-to-line relative calibration stability. The upper stratospheric channel shows no significant brightness variation across the earth. Navigation of VAS line and pixel to

---

[13] The large BER in the infrared video data probably reflects the aforementioned hardware problems with the corroding leads on the integrated circuits in the S/DB.

or from latitude and longitude coordinates is not available. This dwell sounding dataset is not a high resolution test of VAS imagery, since it has been resampled to 30 km SFOV resolution.

SECTION 6
VAS-D RADIOMETRIC QUALITY

This section summarizes some of the quantitative radiometric studies done in the VASP in the process of analyzing the VAS calibration of dwell data from 7NOV80.

6.1 PRELAUNCH RADIOMETRIC SPECIFICATIONS

Prelaunch radiometric specifications for the VAS channels are listed in Table 3, using both radiance R (erg/etc) and brightness temperature T* (Kelvin) units. The wavenumbers are the mean of the measured spectral response, and the typical scenes are from radiance simulations for the tropical mean atmosphere (see section 7.1). The noise equivalent delta radiance (NEΔR) single sample noise is from prelaunch tests (Malinowski and Ruiz, 1980) and has been converted to noise equivalent delta brightness temperature (NEΔT) for the typical scene radiances. The SFOV noise requirements are design specifications (Arking, 1977) again converted to T* for the scene. The absolute ($\pm$1.5° K) and relative ($\pm$0.5° K) T* calibration values are drawn from a general statement about testing (Malinowski and Ruiz, 1980) over the range of terrestrial brightness (200° to 300° K) and are converted to R for the typical scene.

Since there is no "VAS Users Guide" with official radiometric specifications, Table 3 was constructed to provide radiance benchmarks. Minor discrepancies in scene temperatures and noise estimates exist between Tables 3 and 1, because Table 1 was based upon the original specifications (Arking, 1977) and the U.S. Standard Atmosphere. The large measured noise values for the upper-air sounding channels listed in Table 3 seem much too conservative (VAS channel 1 would be useless with a NEΔT of $\pm$11° K), so that the specified noise values in Table 1 are used for radiometric quality assurance in this section.

6.2 OUTLINE OF THE VAS CALIBRATION CHAIN

VAS radiometric calibration is complicated by the lack of external references (except for outer space) and by the fact that the VAS instrument itself glows. Calibration algorithms are

defined by UW, developed by SBRC, and coded by Westinghouse Corp. in the S/DB and the VASPP. As was described in section 4.1, calibration calculations are executed throughout the entire VAS data processing chain: in the GOES satellite, in the S/DB, and in the VASPP and VASP. When mis-calibrated radiances initially arrived for dwell soundings, quality assurance software was developed in the GSFC VASP in order to help debug the upstream errors.

6.2.1 Calibration on GOES

In the VAS instrument, each scan line is calibrated by viewing an internal hot body (nominally at 320° K) and outer space (nominally at 3° K, but effectively at zero radiance for VAS noise levels). The glowing foreoptics, which view outer space and the earth but not the internal hot standard, introduce radiance that is removed by monitoring the temperature of many parts of the VAS instrument. The raw positive voltage from the flux falling on a detector through one of the infrared filters is converted to a 10-bit "count" for every one of the 3822 samples on the scan line. As mentioned in Paragraph 4.3.1, the positive bias and the leeway allowed in this conversion leaves no more than 8 significant bits (roughly 0.4 percent truncation error) of useful signal. Slow changes in the detector bias during a scan line is termed "droop," since a steady discharge in the electronics will appear as a downward drift in the zero-level radiance.

6.2.2 Calibration in the S/DB

At the S/DB, the 2-point (3° K to 320° K) calibration curve is determined, and the 10-bit counts are converted to positive (i.e., still offset) values proportional to radiance. The proportionality factor for each scan line is passed as a single number representing the "binary point" position for the 10-bit samples. The S/DB redefines the zero-point space values from 34 samples at the east and west ends of the 3822 sample scan line, choosing the end with the smallest mean value to avoid confusion by some bright object, such as the moon or stars. The S/DB also edits out the highest and lowest values from the 34 samples at the lower end of the scan line, leaving 32 points to redefine a mean zero point.

6.2.3 Calibration in the VASPP

At the VASPP, the 10-bit values are unpacked into 16-bit integer words, the offset removed, and dwell averaging over the "spin budget" of each channel performed. The removal of the offset produces some negative radiances, which are often observed in the noise when viewing outer space. The user can also acquire *unaveraged* dwell sounding (DSU) radiances from the VASPP, so that problems with the spin-by-spin data processing can be diagnosed.

6.2.4 Calibration in the VASP

At the VASP, the integer radiance counts are converted into 32-bit floating point numbers, using the "binary point," i.e., a factor equal to the $(k-15)^{th}$ power of 2 for dwell data and the $(k-10)^{th}$ power of 2 for MSI data, which is supplied in the documentation of each scan line. The VASP user can choose to average lines and/or pixels together into larger, less noisy SFOVs. The VASP can also re-interleave the samples, channels, lines and documentation into datasets more conveniently organized for sounding or imaging.

6.3 DISCUSSION OF UNAVERAGED VAS DWELL RADIANCES

One of the clearest displays of VAS radiometric quality which has been developed in GSFC's VASP has been plots of radiance versus sample number, such as shown in Figures 8, 9 and 10. These plots show sample-by-sample values of the observed radiance for the first 700 samples in the west end of the scan line and a 32-point running mean. The running mean has been added to display average radiance more clearly in the noisy channels and explicitly demonstrate the accuracy of the zero point value of the 32-point "space look" at the end of the scan line. Figures 8, 9 and 10 all show data from scan line number 390 (roughly 40° N latitude), with the limb of the earth occurring at roughly sample number 500.

*Un*averaged VAS radiances along each spin scan line were taken on 7NOV80 from the dwell frame at 1600GMT, a few hours before the successful averaged dwell sounding at 2000GMT. These

unaveraged radiances are displayed for a few channels in Figures 8 and 9, and statistics for unaveraged radiances are used in a subsequent section that discusses the figures of merit (FOMs) in Figure 11.

The following subsections are a semi-quantitative discussion of scattered light, noise, and calibration errors, as found by the scientific users in the radiance sampling plots. Quantitative FOMs are presented in yet another subsection.

6.3.1 Scattered Light

The ideal test for scattered light would be the shape of a radiance scan line passing through a bright point source. The available test is restricted to the shape of the scan line in outer space on either side of the earth. The broad bandpass of the 11 micron window gives VAS channel 8 the best single sample signal/noise. Consequently, this window is used to study scattered light in the sounding instrument.

Figure 8 shows one spin of unaveraged radiances for VAS channel 8 (11 micron window) with a 32-point running mean drawn through it. Light scattering appears in Figure 8 as a 1.0 erg/etc increase in the brightness of the scan line from distant outer space up to the limb of the earth (samples 1 to 500). This slope is not drift in the electronics, because there is a mirror image slope away from the earth on the other end of the scan line (not shown). Hence, the scattered light at 11 microns amounts to about 1 percent of the average earth intensity with a roughly linear decrease of 1.0 erg/etc over 500 samples of outer space.

It is not clear how to relate this observation to prelaunch performance specifications. The impact on normal VAS imaging and sounding is not expected to be significant, since the loss of contrast on the face of the earth will be comparable to noise and calibration errors.

6.3.2 Noise

The radiometer noise is independent of calibration along each scan line, if the detection system is stable and fast enough.[14]

[14] In reality, VAS samples have very high correlations for a few samples, and noticeable correlations over hundreds of samples (Menzel, 1980). Nevertheless, this initial analysis will treat noise as the variance about the mean of a line of samples.

Due to the 8-bit digitization limit discussed in section 4.3.1, truncation noise can be observed in Figure 8 as a quantized step size in the noise seen in outer space. For this case (VAS channel 8), the quantization is comparable to the detector noise (±0.25 erg/etc). For the noisier channels (such as VAS channel 11 in Figure 9), the truncation is less noticeable, and it should be masked by dwell averaging for most sounding purposes.

Indeed, detector noise dominates single radiance samples in most VAS channels, either because of a narrow bandpass filter (e.g.,VAS channels 1 to 5) or because the earth is relatively faint at shorter infrared wavelengths (e.g., VAS channels 6 and 11). For example, Figure 9 shows one spin of unaveraged radiances for VAS channel 11 (4.4 micron sounding), with a 32-point running mean drawn through it. The earth's limb (samples 500 to 700) is scarcely brighter than the noise in outer space (samples 1 to 500), so that no sounding could possibly be done with a single scan line of VAS channel 11. Signal averaging and quantitative noise estimates are discussed in subsequent subsections.

6.3.3 Relative Calibration

Relative calibration refers to the independent reproducibility of a radiance measurement of the same object. For VAS, each scan line of data is independently recalibrated, except for some of the foreoptics temperature monitoring, which takes 20 spins (at 100 rpm) to be completely documented. Relative calibration is tested by examining repeated observations of spin scans of the same line and channel (i.e., unaveraged dwell data), by looking at the variance of the mean of a line of samples. Relative stability along a line ("droop") is tested by comparing the brightness of outer space at the ends of a scan line.

6.3.4 Absolute Calibration

Absolute calibration refers to the ability to correctly measure external radiances. Unfortunately, outer space is the only external reference, and the VAS radiances have already been forced

to zero at the low end of the 3822 samples. Absolute zero can be tested by examining outer space elsewhere on the line of samples, even though this is also a relative test of stability and scattered light.

The "space look" zero point at the end of the scan line in Figure 8 is noticeably negative (roughly −0.25 erg/cm²/sec). Most other channels are likewise negative (not shown), although the scan line plotted in Figure 9 is not. Since the size of the negative bias in the zero point is comparable to the digitization error, it is probably caused by truncation within the integer arithmetic used throughout most of the VAS calibration chain, since truncation acts to "round down" calculated values. More quantitative FOMs of this effect are shown in a subsequent subsection.

6.4 AVERAGING VAS RADIANCES

VAS' low signal/noise is imposed by the attempt to do high resolution, narrow band multichannel radiometry with a small telescope at geosynchronous altitude. Obviously, considerable signal averaging must be done without averaging together data with uncorrectable biases, data processing errors, or unexpected noise characteristics. The averaging steps designed into the VAS data processing system for the production of the signal/noise required in a SFOV (see Table 1) are:

1. Dwell averaging several successive spin scans of the same line with the same channel, as assigned by the "spin budget" sent to the satellite.
2. Averaging the adjacent (overlapping E-W) samples along a scan line.
3. Averaging data for the same location, whenever the redundant (upper/lower) detectors have viewed the same spot through the same filter at different positions of the scan mirror.
4. Averaging data from adjacent (N-S) lines.

Obviously, the improvement in signal/noise that comes from these averaging techniques is at the expense of coverage and/or resolution in space and/or time. Because the first VAS radiances were taken for sounding purposes rather than error analysis purposes, it is not possible to carry out a detailed quantitative analysis of the error budget associated with each averaging technique. The following sections discuss the expected subtleties of averaging VAS data where correlations and

biases prevent one from obtaining optimal noise reduction (i.e., without a mean error and with the noise reduced by the square root of the number of samples averaged together, $\sqrt{N}$).

6.4.1 Dwell Averaging

Figure 10 shows one line of dwell averaged (7 spins) radiances from VAS channel 11 (4.4 micron sounding) with a 32-point running mean drawn through it. Comparing Figure 10 to 9, which was the unaveraged radiance from just one spin scan, it can be seen that dwell averaging reduces the standard deviation in the radiances, leaving a net negative bias in outer space (samples 1 to 500). Dwell averaging of independent samples should produce a standard deviation which behaves like $NE\Delta R_\lambda/\sqrt{N}$. Unfortunately, the spin budget used for the first VAS radiances is too meager to test this behavior. This test is worth doing, because the calibration of each spin scan is not truely independent, due to the time that it takes to monitor all of the foreoptics' temperatures (20 spins). Consequently, the error budget associated with dwell averaging is not clearly established for the first VAS dwell soundings.

6.4.2 Averaging along a Line

Because the VAS infrared detectors move only a fraction of their own width before being sampled again, the VAS detection system was permitted to have substantial correlation between successive samples (Menzel, 1980). In fact, the averaging of samples along a line into a single SFOV was envisioned as the normal operating mode. However, since single sample noise is then highly correlated along a line, the SFOV noise is more than $NE\Delta R_\lambda/\sqrt{N}$. At this time, not enough analysis of the error budget for averaging samples along a line has been done with the first VAS radiances to present quantitative results. Nonetheless, averaging along a line does reduce the noise, as the 32-point running means (with nominal 45 km E-W resolution) show qualitatively in Figures 9 and 10.

6.4.3 Averaging Detectors

The VAS instrument can be commanded to view the same geographical E-W line with redundant (upper/lower) detectors as it steps the scan mirror N-S. In fact, such overlap will occur

whenever contiguous dwell soundings in all 12 channels are made with the smaller (7 km nominal resolution) longwave detectors, since the shortwave detectors only come in the large size (15 km nominal resolution). Comparison of the upper/lower detector radiances would test the relative calibration and pointing accuracy of VAS. Unfortunately, the VAS-D instrument was launched with the longwave upper detector broken, and the first VAS radiances on 7NOV80 do not use the small detectors in the dwell mode.[15] It appears that any thorough examination of the relative accuracy of the upper/lower detector error budget will have to be done with VAS-E data.[16]

6.4.4 Averaging Lines

The VASP user can average adjacent N-S lines of data into larger SFOVs. Like dwell averaging, line averaging should reduce noise by a factor of $1/\sqrt{N}$, limited by the stability of the relative calibration. Quantitative tests of the line averaging error budget have not yet been made with the first VAS radiances. Qualitative examination of the VAS images in Figure 5 indicated some line-to-line correlation in the relative calibration of the 54 spin dwell averaged data, so that this test of the actual error budget for line averaging seems worthwhile. Nevertheless, 2 line averages (30 km nominal resolution) were used to make SFOVs for the soundings discussed in later sections of this report, because there did seem to be less noise in such images.

6.5 QUALITY ASSURANCE FOMS FOR VAS-D RADIOMETRY

The mean, RMS and standard deviations of VAS radiances from successive scan lines are compared to the prelaunch radiometric specifications in Tables 1 and 3, in order to do quantitative quality assurance. Figure 11 plots figures of merit for noise, zero point accuracy, droop, and relative calibration stability. Most FOMs are presented as dimensionless ratios of observed radiances

[15] The mirror stepping mode automatically sends data from the small longwave upper and lower detectors in the 11 micron channel. Software errors in the S/DB at this time were mangling the small upper longwave detector data, so no comparison could be made in this way either.

[16] VAS data at GSFC is archived on a special High Density Tape Recorder (HDTR) attached to the VASPP. However, replay of the HDTR archive tapes has yet to be successfully demonstrated for VAS-D dwell sounding data.

to the specified limits, so that values greater than 1 are worse than requirements. The first orderly VAS radiances are found to roughly meet basic quantitative requirements for noise, zero point, droop and calibration stability from the scientific user's point of view, although the systematic biases are comparable to NEΔR. The shortwave detectors are found to have noise and stability FOMs which are significantly better than prelaunch specifications.

6.5.1 Noise FOMs

Figure 11-A plots VAS-D noise in each channel. The noise FOM is the ratio of the standard deviation of the radiance observed in one unaveraged line of data, looking at outer space away from the "zero point" (samples 50 to 250 for the large lower detectors from scan line 390), to the NEΔR listed for each channel in Table 1.

The longwave channels (1 to 5 and 7 to 10) roughly meet prelaunch specifications, and the shortwave channels (6, 11 and 12) are roughly a factor of 2 better than prelaunch specifications. The latter observation is a pleasant surprise, since it means that the "spin budget" in the faint shortwave sounding channels (6 and 11) can indeed be cut without rendering these channels useless. Improvements in detector technology should eventually make it possible to modify future VAS instruments to use higher resolution detectors with the same NEΔR.

6.5.2 Zero Point FOMs

Figure 11-B plots a "zero point" FOM observed in each VAS channel. The "zero point" FOM is the ratio of the "space look" radiance divided by the NEΔR listed for each channel in Table 1. The "space look" radiance was calculated from one unaveraged scan line in the same manner as that used for the S/DB:

1. Two segments of 34 samples (8 to 42 and 3782 to 3816) were selected from the scan line.
2. The largest and smallest radiance values were deleted from each segment, leaving 32 samples in each.
3. The segment with the lower 32 sample mean value was declared the "space look" radiance value.

As noted in connection with Figures 8 and 10, the "space look" average radiance tends to be negative, probably due to truncation errors in the upstream integer arithmetic. Indeed, 8 of the 12 channels in Figure 11-C have negative average radiances in outer space. The mean "zero point" error is roughly 0.5 NEΔR in the longwave channels (1 to 5 and 7 to 10) and is roughly zero for the shortwave channels (6, 11 and 12). The bias from this truncation error in the "zero point" will not subside with dwell averaging, leaving roughly a -1° K systematic bias in the observed longwave channels. Since this is less than the anticipated absolute calibration accuracy of the VAS channels ($\pm 1.5^\circ$ K), it is a significant but not a serious error for sounding calculations.

6.5.3 Droop FOMs

Figure 11-C plots the "droop" observed in the VAS channels. The "droop" FOM is the ratio of the difference between the east and west "space look" radiances (described in the previous section on "zero point" radiances) to the NEΔR listed for each channel in Table 1. Negative values of the "droop" FOM mean a decrease in the radiance as the scan proceeds. Indeed, 10 out of 12 channels in Figure 11-C do "droop." The longwave channels (1 to 5 and 7 to 10) are observed to "droop" by roughly 0.8 NEΔR across the scan, while the shortwave channels are stable. Once again, this bias will not decrease with radiance averaging, and the error amounts to less than the anticipated error in absolute calibration.

6.5.4 Relative Stability FOMs

Figure 11-D plots a FOM for judging the relative stability of the calibration between spin scans in each VAS channel. The "spin/spin" FOM is the variation in the mean radiance from most of the earth (samples 956 to 2868) divided by the sensitivity of the Planck function to a change in brightness temperature at the earth's radiance ($dB(\nu)/dT^*$ at R (earth)). Effectively, the "spin/spin" FOM is the variation in the earth's mean brightness temperature ($^\circ$K) from spin to spin in the unaveraged VAS dwell radiances. Since VAS channels 8, 10 and 12 received only 1 spin in the "spin budget" for 7NOV80 (see Table 1), their "spin/spin" variations were calculated from a much later VAS frame, on 18FEB81.

The VAS-D longwave channels (1 to 5 and 7 to 10) show a spin to spin relative calibration stability in the mean earth brightness temperature of roughly ±0.5° K, and the shortwave channels (6, 11 and 12) are somewhat better. This FOM is roughly equal to the prelaunch specification (±0.5° K) for relative calibration accuracy in Table 3. The concern raised by the line-to-line variations in the VAS images (Figures 5, 6 and 7) is somewhat alleviated by this quantitative analysis, although this does not really analyze the longer term relative stability of the VAS instrument over many minutes of operation. This stability analysis does assure us that dwell averaging earth radiances should not suffer from relative calibration variations that are worse than anticipated.

6.6 COMPARISON OF VAS RADIANCES TO HIRS2 ON TIROS-N

Simultaneous observations of the earth with a better sounding instrument (i.e., HIRS2 on TIROS-N) can provide a "secondary standard" for calibration. However, questions of exact registration, viewing angle, bandpasses, etc., will always prevent such comparisions from being conclusive. Since TIROS-N for 7 NOV80 is not available from the University of Wisconsin for comparison, it is being ordered on tape from NOAA.[17]

6.7 RADIANCE QUALITY SUMMARY

Radiometric quality assurance specifications are developed for VAS-D from prelaunch specifications for noise and calibration. When mis-calibrated radiances initially arrived for dwell soundings, quality assurance software was developed in the GSFC VASP to help debug the entire data processing chain: detection and A/D conversion in the satellite; gain and offset determination in the S/DB; offset removal and dwell averaging in the GSFC VASPP; and conversion to sample averaged floating point radiances in the GSFC VASP.

Plots of raw unaveraged VAS dwell radiances along a scan line are examined qualitatively, with the findings that: scattered light in outer space amounts to roughly 1 percent of the earth's

[17] The direct data communications line between GSFC and UW is functional, but the high level software for transmitting formatted datasets is still incomplete. In any case, the UW TIROS-N system was not operating on 7NOV80.

brightness at 11 microns; the 8-significant-bit limitation in the A/D conversion produces a digitization error comparable to the NEΔR noise; and truncation errors in the integer arithmetic of calibration produce negative values for the radiance of outer space with a bias comparable to the NEΔR noise.

The correlations and biases in VAS radiances will prevent ideal data averaging (i.e., with no mean error and $1/\sqrt{N}$ noise reduction) of dwell spins, adjacent samples, adjacent lines, and redundant detectors to construct a SFOV. The first orderly VAS radiances are found to roughly meet basic quantitative requirements for noise, zero point, droop and calibration stability from the scientific user's point of view, although there are systematic biases comparable to NEΔR. The shortwave detectors are found to have noise and stability FOMs which are significantly better than prelaunch specifications. HIRS2 radiometer data from TIROS-N on 7NOV80 is not yet available for use as a "secondary standard" of comparison to the corresponding VAS-D data.

SECTION 7
RADIATION TRANSFER VERIFICATION

The GSFC Sounding Studies Group plans to develop a VAS sounding algorithm based on physical radiation transfer models and using local meteorological statistics to help resolve vertical ambiguities (Chesters, 1980). The first step in establishing the validity of the radiation transfer model is to compute radiances from "ground truth" and compare them to VAS observations. This section discusses the first attempt to make this comparison with the 7NOV80 data.

7.1 RADIATION TRANSFER

The VAS radiance simulations use line-by-line transmission functions, $\tau(\nu,p)$, computed for each temperature, T(p), and mixing ratio, Q(p), profile. Radiances $R(\nu)$ in each channel, at nominal wavenumber ν, are computed up from a perfectly emitting surface by radiation transfer of the Planck function, $B(\nu,T)$:

$$\tau(p) = \tau(\nu,p;T(p),Q(p);\text{lines,continuum}),$$
$$R = B(T(s))\tau(s) + \int_s^0 B(T(p))d\tau(p). \qquad (7\text{-}1)$$

A subtropical mean profile (rather than the U.S. Standard Atmosphere) was used for the stratospheric profile above the last reported radiosonde level. Topographic irregularities are accounted for by setting the 1000 mb and surface temperatures equal to the first reported radiosonde level. Surfaces are 100 percent emissive, giving isothermal bottomside structures with no radiance contrast. This assumption results in radiances that appear correct for the actual topography, but it also results in a strong correlation between the lower troposphere and the surface, so that the lower tropospheric retrievals rely very heavily upon the window radiances. This does not account for actual skin temperatures observed by VAS but not by the radiosondes.

Absorption-adjusted radiances, $R[\gamma]$, are calculated from equation 7-1 by using the γ'th power of τ, in order to bring the radiation transfer calculation into line with observation. This

parameterization is a rough physical model for multiplicative errors in the net molecular cross section, $k(\nu,p)$, the gaseous mixing ratio, $Q(p)$, or the airmass, $\sec\theta$, since the total absorption, $\alpha(\nu,p)$, is proportional to all of these:

$$\tau[\gamma] = \tau^{\gamma}(p) = \exp\{-\gamma\alpha(\nu,p)\} = \exp\{-\gamma Q(p)k(\nu,p)\sec\theta\}. \qquad (7\text{-}2)$$

For dry sounding channels in the troposphere, where Q, k and $\sec\theta$ are all known to a few percent, values of $\gamma<0.9$ or $\gamma>1.1$ should be regarded as a disagreement that is too large to be reasonably explained as an error in transmission. For unmixed gases, such as water vapor or ozone or for atmospheric conditions far from laboratory measurement, such as the tropopause and stratosphere, values of $0.5<\gamma<2.0$ are plausible adjustment factors.

The Planck function calculates energy emitted per time per area per solid angle per spectral interval (erg sec^{-1} cm^{-2} $sterradian^{-1}$ $wavenumber^{-1}$, abbreviated "erg/etc") from a black body:

$$B(\nu,T) = a\nu^3/[\exp(b\nu/T)-1],$$

$$a = 2hc^2 = 1.190636\times10^{-5},$$

$$b = hc/k = 1.4388318, \qquad (7\text{-}3)$$

ν is measured in wavenumbers (cm^{-1}),

T is measured in absolute temperature (°K).

For the VAS channels, we use the bandpass mean wavenumber $\langle\nu\rangle[f]$ averaged over the spectral response $f(\nu)$ of each channel:

$$\nu = \langle\nu\rangle[f] = \int_0^{\infty}\nu f(\nu)d\nu\left\{\int_0^{\infty}f(\nu)d\nu\right\}^{-1}. \qquad (7\text{-}4)$$

Since the earth's radiance spectrum is far from a black body's, there is no general agreement on the definition of an effective wavenumber, ν, or a brightness temperature function, $T^*(\nu,R)$, to convert observed radiance R in a bandpass ν to a number useful for interchannel comparisons. GSFC work uses the bandpass mean wavenumbers (Table 3) in the algebraic inverse of the Planck function to calculate T* for VAS:

$$T^* = b\nu\{\ln[1+a\nu^3R^{-1}]\}^{-1}. \qquad (7\text{-}5)$$

By contrast, UW uses a Planck-like formula with its own set of wavenumbers ν' and an empirical rescaling of the resulting brightness temperature T'^*:

$$A+BT'^* = b\nu' \{ \ln[1+a\nu'^3 R^{-1}] \}^{-1} . \qquad (7\text{-}6)$$

where A is small, B is approximately 1, and both A and B are channel dependent.

7.2 RADIANCES COMPARED

The forward radiation transfer calculation must work before one can do the inverse, since the forward calculation converts a first-guess profile into first-guess radiances. Radiosonde observations in clear air are used as "ground truth" for the forward calculation of radiances, R(calc), and brightness temperatures, $T^*(\nu,R(calc))$. These calculated radiances are compared to VAS observations at the RAOB sites. The best figure of merit for the comparison is the difference in brightness temperatures, $\Delta T^*=[T^*(calc)-T^*(obs)]$, since this FOM has roughly the same magnitude for all VAS channels (see Table 3). The 3-hour mismatch between the VAS observations at 2030GMT and the radiosondes at 2330GMT on 7NOV80 is certainly large enough to confuse our comparison, but no better coincidence is available.

7.2.1 Calculated Brightness

The 19 radiosonde profiles listed in Tables 6 and 7 were used, along with the zenith angles listed in Table 5, to calculate line-by-line clear column transmission functions and radiances. Observed VAS radiances were selected with the interactive imaging machinery on the VASP from 19 points that appear to be located at the positions of the radiosonde sites. Brightness temperature values for all 12 VAS channels at all 19 sites are listed in Table 9, along with the mean and standard deviation in each channel. The observed brightness temperatures, $T^*(obs)$, in Table 9 show values and variability which are roughly consistent with the atmospheric conditions and with the VAS noise specifications. The location of the 19 selected SFOVs is shown in Figure 13, projected both on the 3.9 micron window (VAS channel 12) and on the 6.7 micron water vapor band (VAS channel 10). The contrast in the water vapor band in Figure 13 is consistent with the variability in the moisture profiles listed in Tables 7 and 8, although its structure is far more organized than could be

deduced from the widely scattered radiosonde sites. The excellent visibility of the surface in the shortwave window shown in Figure 13 suggests very clear air, and allows us to select the 19 radiosonde sites with little geographical error despite the lack of objective navigation.

7.2.2 Brightness Differences

Table 10 lists the differences in brightness temperatures, ΔT^*, for all 12 VAS channels at all 19 sites, along with mean and standard deviations of the differences. The statistics from this table are plotted in Figure 15-A. The radiation transfer calculations are in substantial disagreement with the VAS observations, considering the SFOV noise (0.0° ±0.3° K) and calibration errors (0.0° ±0.5° K) expected from Table 3. The discrepancies show little pattern with respect to radiosonde location, but they do follow a pattern with respect to channel type: windows, shortwave CO_2, longwave CO_2, and upper air moisture.

7.2.3 Window Channels

The window channel calculations (VAS channels 7, 8 and 12) are all too faint compared to observations. This discrepancy could be caused by the fact that the VAS observations were taken in midafternoon, and the radiosondes were 3 hours later in early evening. The warmer than calculated surface could account for the discrepancy in VAS channel 12 ($\Delta T^* = -6.4° \pm 2.9°$ K) if 6° C of surface cooling occurred during this time. This much cooling would be rather large for midday conditions. In fact, a quick inspection of the hourly surface reports during this period showed nearly constant temperatures in western Texas and only modest cooling toward the East Coast. In addition, the discrepancies for the window channels listed in Table 10 are worst for the western sites. While reflected sunlight in the shortwave window (VAS channel 12) might account for the excess brightness observed in the western part of the region, it cannot account for the same gradient in the longwave windows (VAS channels 7 and 8). The most likely (but not verifiable) explanation is that the window channels view a true *skin* temperature, not a radiosonde or shelter air temperature. Consequently, the window channels view a sun-drenched surface that is much warmer than the air temperature reports used for the calculated radiances with the western sites closer to the local solar noon.

7.2.4 Shortwave Channels

The shortwave sounding channels (VAS channels 6 and 11) appear to be in fair agreement with observations. The calculated radiances are systematically warmer ($\Delta T^*=+1.6^\circ \pm 0.8^\circ$ K). This difference should be explained by an underestimate of the shortwave absorption. Such a correction could be fairly large, since the warmer than calculated surface radiance leaking into these channels works against an absorption underestimate, leaving a small remainder of two substantial errors of opposite sign in Table 10 and Figure 15-A. The lower tropospheric shortwave band (VAS channel 6) has more contamination by the surface brightness, as can be seen in the images of Figure 5.

7.2.5 Longwave Channels

The calculated radiances for the longwave bands (VAS channels 1 to 5) are generally warmer than observed. The semitransparent channels (4 and 5) appear to agree well, until one considers the fact that the calculations did not properly include the warmer than calculated surface radiances that also contaminated the windows (VAS channels 7, 8 and 12) and the comparable shortwave sounding bands (VAS channels 6 and 11). The lower tropospheric longwave band (VAS channel 5) has more contamination by the surface brightness, as can be seen in the images of Figure 5.

A systematic underestimate of the 14 micron absorption has been suggested to produce better agreement. We will show that even this adjustment is not enough to account for the discrepancy in the stratospheric channels, since the tropopause is neither cold nor broad enough to reduce the model calculations to match the observations. Other unverifiable possibilities are:

1. There is a source of strong absorption concentrated near the tropopause.
2. The VAS sounding channels are miscalibrated by $-4^\circ \pm 1^\circ$ K at intermediate brightness levels.

7.2.6 Upper Air Moisture Channels

The calculated mid-tropospheric water vapor radiances are in poor agreement with observations, being inconsistently too warm ($\Delta T^*=+3^\circ \pm 3^\circ$ K). This discrepancy is probably due to the lack of sufficient radiosonde moisture data above 500 mb. The default subtropical moisture profile

(see Figure 12) is relatively dry above 500 mb. Thus, the upper troposphere is being calculated to be too transparent, although it is not clear how to correct this objectively. The scatter in ΔT^* in the water vapor bands has yet to be explained.

7.3 NUMERICAL ADJUSTMENTS

The discrepancies outlined above showed some patterns of behavior which suggest adjustments that might verify the VAS radiances to within specifications ($0° \pm 1°$ K), so that radiation transfer models can be trusted for use in retrieval algorithms. The following adjustments were considered:

1. Transmission functions and related model parameters were carefully recomputed and tested.
2. The observed radiances were closely examined for clues to justify an empirical recalibration algorithm.
3. Radiosonde data was completely reprocessed for maximum vertical coverage and the most reasonable defaults for missing data, but without compensation for the space-time mismatches or the lack of true surface temperatures.

7.3.1 Radiation Transfer Model Adjustments

The systematic disagreement between calculated and observed VAS radiances in the longwave sounding channels is serious. The discrepancies cannot be dismissed as a mismatch between the radiosonde and satellite observations in either space or time. Two attempts were made to adjust the radiation transfer model to match the observations:

1. By including ozone absorption.
2. By creating a total absorption strength "γ-factor."

7.3.1.1 Ozone Absorption

Ozone absorption was included for the weak band from 600 to 800 cm^{-1}, supposing the tropical mean ozone profile (not shown). This adjustment yielded transmission functions with a few percent more absorption between 10 and 50 mb, but the discrepancies in radiance scarcely

changed. For exactness, the calculated radiances used in the ΔT^*s of Table 10 included ozone in the calculations. Ozone cannot provide the hoped for abnormally strong, concentrated absorption at the tropopause, since it is normally produced by more diffuse processes near the thermopause 5 to 10 km higher.

7.3.1.2 Absorption Strength γ-Factor

An attempt to rescale the absorption coefficients with an overall strength γ-factor was made. The underlying assumption is that the line coefficients were systematically under- or overestimated in the laboratory measurements of the molecular band strengths (McClatchey, *et al.*, 1973). Since the total absorption affects the transmission exponentially, the adjustment is determined by trying γ'th powers of $\tau(p)$ in the radiation transfer equation 7-1, until the calculation matches the observation.

Figure 14 shows plots of resynthesized radiances versus the γ-factor for all VAS channels at one site (Tampa Bay, Florida), which has a typical pattern of radiance disagreements between calculations and observations. The different channels show that it is not always possible to find a γ-factor which adjusts the calculated radiance by enough to agree with the observation. This condition is particularly true for the channels near the tropopause (VAS channels 1 to 3). Either increasing or decreasing the total absorption moves the weighting functions in Figure 2 away from the coldest part of the atmosphere, causing the calculated radiances to increase their already high values. The window channels (7, 8 and 12) have no satisfactory γ-factor because there is little absorption to adjust over the hotter than calculated surface. Some γ-factor adjustment can always be made for the mid-tropospheric channels (4 to 6 and 9 to 11) in Figure 14, since the γ-factor moves their weighting functions up and down the steep temperature profile (compare Figures 2 and 12).

Table 11 lists γ-factors for all 12 channels at all 19 sites, wherever they are computable. The γ-factors for Tampa Bay (site 19) are drawn from Figure 14, with "*****" indicated for unadjustable channels. Figures 15-A and 15-B show plots of the mean and RMS values of ΔT^* and the

γ-factor for all 12 VAS channels, using these 19 sites. Figure 15-B shows a "?" where the γ-factor cannot be computed for some sites (VAS channels 1, 3 and 8), and it shows a "??" where the γ-factor cannot be computed for any site (VAS channels 2 and 12). No consistent, realistic absorption strength adjustments are found for the upper atmospheric sounding channels (1, 2 and 3). The adjustments in the windows (8 and 12) and the water vapor channels (9 and 10) are not meaningful, since the brightness discrepancies are more readily explained as radiosonde-to-satellite mismatches in time and vertical coverage. In addition, the warmer than calculated surface in the observations causes the γ-factors for the sounding channels (4, 5, 6 and 11) in Figure 15-B to be underestimated.

7.3.2 Radiance Adjustments

Since the assessment of VAS radiometric quality in the earlier sections did not indicate calibration errors, there is no justification for adjusting the observed VAS radiances themselves. However, this possibility should stay open for consideration, since the ΔT^*s in the sounding channels are consistently positive, and they have about the same magnitude ($\Delta T^*=4^\circ \pm 1^\circ$ K) if one allows up to 6° C of surface temperature mismatch between the calculations and the observations. The absorption strength γ-factors do not show such a simple consistent pattern (compare Figures 15-A and -B).

An empirically forced agreement by adding 4° K to the upper air sounding channels will produce reasonable looking soundings, but there is no physical justification for doing this. In fact, such an adjustment would destroy the value of using a physical model, since there is no way to trace the error propagation of such an *ad hoc* "fudge factor." The bias between VAS observations and forward radiation transfer models is too large to permit the use of physically determined retrieval algorithms on the VAS data of 7NOV80.

7.3.3 Radiosonde Limitations for Radiation Transfer

As mentioned in a previous section, the radiosonde data from the 19 sites at 2330GMT 7NOV80 was carefully reduced from the original station reports supplied as printouts from the

National Climate Center (NCC)[18] in Asheville, NC, with the hope of finding a sufficiently cold tropopause and stratosphere to explain the low observed brightness in the upper air sounding channels. The improved reduction used a more appropriate subtropic mean profile for missing data (see Figure 12) and included a corresponding ozone profile (not shown) in the transmission function calculations. Without these improvements, the upper air sounding channels and water vapor bands were in even less agreement (roughly 2° ±2° K worse) than shown in Table 10 and Figure 15-A.

Figures 2, 3 and 12 show that there is a serious mismatch in the kind of vertical information available from satellite and radiosonde data even when they coincide in space and time. While radiosondes make measurements on a finer vertical scale, they are not as complete. Comparisons depend significantly upon the method used to supply the "missing data" in the radiosonde report. In particular, the moisture instrumentation on radiosondes is almost worthless in the dry, cold air in the middle and upper troposphere where the two best VAS moisture channels peak. Likewise, the window channels see a *skin* temperature, not a lowest mandatory level or even a shelter temperature. The skin temperature is the emission from the surface millimeter of open water, vegetation or (rarely) bare soil.

Figures 16-A and -B summarize how the 12 VAS channels collect their observed radiance. Radiance accumulation functions are plotted in the style of ordinary weighting functions derived from transmission calculations – as a fraction of the total radiance seen per unit scale height. These functions are really the total integrand in the radiation transfer equation 7-1. They show where the observed radiance actually comes from in the atmosphere.

The bands with a substantial contribution from the surface are indicated in Figures 16-A and -B by having their VAS channel numbers (4 to 8 and 11 to 12) written at the appropriate fractional

[18]The RAOB data gathered from the NWS "604 line" on the AOIPS computer at GSFC were less useful than the reduced profiles shown in Tables 6, 7 and 8, since the "604" data was cut off above 100 mb and any missing data was extrapolated to the U.S. Standard Atmosphere.

radiance value on the 1000 mb level. These estimates roughly agree with the apparent visibility of surface features in the VAS images in Figure 5. The weighting functions, $d\tau/d\ln P$, of Figures 2 and 3 only show where the radiance would come from if the atmosphere were isothermal. By comparing Figures 16-A and -B to Figures 2 and 3, one can see that the cold tropopause is radiometrically depressed, and the warm lower troposphere and surface are radiometrically enhanced. This situation is particularly true of the shortwave channels (VAS channels 6, 11 and 12).

For instance, the weighting functions in Figure 2 make VAS channels 3 and 11 seem the same, but the radiance accumulation in Figure 16 indicates that VAS channels 4 and 11 are the better pair. The same is true of VAS channels 5 and 6. This pair was designed to match in clear air, but not in air with unresolved fractional cloud cover. The appearance of the VAS images in these channels, shown in Figure 5, bear out the sensitivity calculations shown in Figure 16.

7.3.4 Potential Radiation Transfer Model Adjustments

Techniques to adjust the radiation transfer model to agree with VAS observations are obviously a future research effort. Now that the limitations of radiosondes as a first-guess for surface temperature and upper air moisture have been recognized, it appears that previous VAS soundings themselves may have to be used instead. Likewise, previous or average VAS radiances may have to be part of the first-guess radiances. While efforts will be made to calculate transmission functions even more accurately (using a current list of line-by-line parameters, instead of McClatchey's 1972 data), the upper air sounding channels may likewise require previous VAS observations as a first guess. Such an approach can still incorporate physically determined weighting functions with objective statistical conditioning, while turning the GSFC VASP retrieval algorithm into a completely *relative* space-time extrapolation sounding system.

7.4 RADIATION TRANSFER VERIFICATION SUMMARY

VAS radiances were selected at 19 clear air radiosonde sites in the SE USA from the 2030GMT 7NOV80 dwell sounding. Exact line-by-line transmission functions and radiances were calculated

at these 19 sites, using the radiosonde reports taken 3 hours later at 2330GMT 7NOV80. The calculations and observations were compared for all 12 channels at all 19 sites in the form of brightness temperature differences, ΔT^*. The average differences showed several effects:

1. The window channels are calculated to be about 6° K colder than observed, probably due to the actual value of the skin surface temperature in the bright sunlight.
2. The upper air water vapor bands are calculated to be about 3° K warmer than observed, probably due to the lack of good radiosonde moisture data above 500 mb.
3. Allowing for the warmer than calculated surface temperature, all of the temperature sounding channels are calculated to be about 4° K warmer than observed. Empirical adjustments to the overall strength of the absorption in the sounding channels show no physically consistent pattern. The three channels near the tropopause cannot have radiance agreement forced by any possible simple strength adjustment. *Ad hoc* sources of abnormally strong absorption at the tropopause or *ad hoc* changes in the observed VAS radiances are not scientifically justifiable.

Analysis of the sources of radiation in the VAS channels indicates that radiosondes are poor "ground truth" for accurate radiation transfer verification. Many of the channels contain *skin temperature* radiance not available in the balloon measurements, and the upper air water vapor bands display moisture above the failure point of the radiosonde moisture sensor. Physical retrieval models may have to depend upon first guesses relative to previous VAS data in order to avoid radiosonde limitations and unaccountable biases.

SECTION 8
VAS-D SOUNDING QUALITY

Profile retrievals are done from the VAS radiances at 19 clear air RAOB sites in the SE USA by using several methods. The temperature and moisture retrievals are compared to the radiosonde data taken 3 hours after the VAS data.

8.1 RETRIEVAL MATRICES USED

VAS soundings at GSFC are based upon linearized formulations, since such algorithms allow one to trace error propagation through the retrieval process. The main retrieval methods available are synthetic regression, empirical regression, and statistically conditioned radiation transfer.

Physically modeled retrievals are not attempted on the first VAS radiances of 7NOV80. The several °K of bias between calculated and observed brightness would simply propagate as several °C of error into the retrievals. This bias must be successfully modeled scientifically before physical retrieval algorithms can be applied to VAS data.

8.1.1 Conditioned Regression Retrievals

A minimum-information linear-regression algorithm is used to retrieve temperature and mixing ratio profiles from the observed VAS radiances. This technique (Fleming and Smith, 1971) is chosen because it has enough flexibility to adjust to both VAS' programmable noise levels and the statistical conditioning available in historical mesoscale radiosonde collections. Such statistical conditioning should improve retrievals by resolving ambiguities of vertical structure in favor of the most probable structure expected from objective experience (Chesters, 1980).

Regression retrievals assume that the radiance response, $\delta R(\nu)$ in a channel at wavenumber ν, is a linear combination of atmospheric variations, $\delta X(p)$, where $X(p)$ is temperature, moisture, or other state parameter in the atmosphere as a function of pressure, p. Consequently, an estimate of the atmospheric variation, $\delta X'(p)$, can be made from a corresponding linear combination of variations in the observed radiances:

$$\delta R(\nu) = A(\nu,p) \cdot \delta X(p),$$
$$\delta X'(p) = C(p,\nu) \cdot \delta R(\nu). \qquad (8\text{-}1)$$

The "•" above symbolizes matrix multiplication with terms being summed over matching independent variable values. With many observations of X and R, a retrieval matrix, $C(p,\nu)$, can be estimated from the radiance to atmosphere cross correlations in a set of observations:

$$C(p,\nu) = \langle \delta X(p) \delta R(\nu') \rangle \cdot [\langle \delta R(\nu') \delta R(\nu) \rangle]^{-1}. \qquad (8\text{-}2)$$

The "< . .>" above symbolizes a statistical average over a sample learning set of simultaneous, co-located observations, and the "[. . .] $^{-1}$" symbolizes matrix inversion. The basis of the $\langle \delta X \delta R \rangle$ correlation is the presence of T and Q within τ and B in equation 7-1. Likewise, the $\langle \delta R \delta R \rangle$ channel-to-channel cross correlation is based both upon the underlying correlations within the state variables X and upon the overlap among the channels $d\tau/d\ln P$ (see Figures 2 and 3).

Direct application of the simple regression algorithm in equation 8-2 to a small set of available satellite and radiosonde data usually leads to retrieval matrices with large coefficients and opposing signs. This over-interprets the small fluctuations in real data. The minimum-information scheme conditions retrievals against this effect by incorporating an estimate of the radiometer noise in each channel $\langle \epsilon(\nu)^2 \rangle$.

Mathematically, the atmospheric variations and the corresponding radiance changes for a dependent set of events are linearized about the mean, and a single sample noise, $\epsilon(v)$, is included:

$$X = \langle X \rangle + \delta X,$$
$$R = \langle R \rangle + \delta R + \epsilon,$$
$$\delta X' = C \cdot [\delta R + \epsilon], \qquad (8\text{-}3)$$
$$d\langle [\delta X' - \delta X]^2 \rangle / dC = 0,$$
$$C = \langle \delta X \delta R \rangle \cdot [\langle \delta R \delta R \rangle + \langle \epsilon^2 \rangle]^{-1}.$$

Equation 8-3 uses least-squares techniques to solve for a matrix $C(p,\nu)$, which minimized the uncertainty in the retrievals $\delta X'(p)$ averaged over a training set of dependent events. The radiometer noise can be expressed directly in radiance units (ergs cm^{-2} sec^{-1} wavenumber^{-1} sterradian^{-1},

abbreviated "erg/etc"), or it can be computed from the single channel variance $<\delta R(\nu)^2>$ divided by a corresponding "signal"/noise ratio $\Gamma(\nu)$:

$$<\epsilon^2> = <\delta R^2>/\Gamma^2 \qquad (8\text{-}4)$$

Note that the "signal" is the variance in the radiance, not the total brightness of a channel. The VAS retrievals in this section are all done with a single "conditioning factor," Γ=10/1, which is realistic for most channels (see Table 2). A preliminary study of regression retrievals of temperature and mixing ratio profiles from simulated VAS radiances is done to establish the sensitivity of such soundings to various conditioning factors (Lee and Yap, 1980).

8.1.2 Simulated Retrievals using Prelaunch Studies

As part of GSFC's preparation for the launch of VAS-D, statistically conditioned regression retrieval matrices are computed from theoretically synthesized VAS radiances (Chesters, *et al.*, 1981). Line-by-line transmission functions and radiation transfer models are used to calculate radiances (see section 7.1), which are then correlated with the assumed temperature and mixing ratio profiles in a minimum-information regression-retrieval scheme. Two sets of prelaunch training profiles are available:

1. The NOAA32, a "global" set of 32 radiosonde reports from widely varying conditions over North America. Retrievals conditioned by the NOAA32 should have the correct gross sensitivity, but lack both a good first guess and the appropriate determination of ambiguities in vertical structure.
2. The NSSL210, a more "local" set of 210 profiles analyzed from NSSL radiosonde network observations of thunderstorm conditions in Oklahoma during the spring of 1976. The NSSL210 retrieval matrix is conditioned to the unstable atmosphere, characteristic of thunderstorms in the Great Plains. The result is a better first guess for the abnormally warm autumnal weather in the SE USA in the afternoon of 7NOV80, although that day's weather has stable vertical structure.

Both the NOAA32 and the NSSL210 retrieval matrices are conditioned with a crude "signal"/noise factor of 10/1, which is roughly consistent with VAS specifications (see Table 2). Both matrices have synthetic first-guess radiances which contain unexpected biases with respect to the observed VAS radiances, as previously discussed in connection with Table 10 and Figure 15.

8.1.3 Empirical Retrievals using 7NOV80 Observations

The biases between synthetic radiances and VAS observations are avoided by creating a regression-retrieval matrix entirely from empirical data taken on 7NOV80. Radiances for the VAS channels are taken from the 19 SFOVs shown in Figure 13. Corresponding profiles are taken from the 19 RAOB profiles listed in Tables 6 and 7. An estimated "signal"/noise ratio of Γ=10/1 is used to condition the minimum information scheme to be consistent with the prelaunch regression matrices. This empirical radiance-to-radiosonde approach is designed to guarantee empirically correct first guesses for both the brightnesses and the profiles. Indeed, even the 3-hour mismatch between the time of VAS observations and the radiosonde measurements is guaranteed to be unnoticeable, as long as we do retrievals upon the earlier VAS radiances and compare the results to the later radiosondes.

This empirical regression on the 7NOV80 VAS data is feasible only because it is completely clear over a large area filled with many nearly concurrent radiosonde observations, all of which are viewed by VAS with nearly the same zenith angle. Under normal or stormy weather conditions, the number of acceptable radiosonde reports available for correlation with VAS radiances will be too few and too scattered to be applicable to the local mesoscale conditions. Consequently, the planned GSFC VAS sounding algorithm is still based upon a physical model for radiation transfer.

8.2 INDEPENDENT VAS RADIANCES FOR RETRIEVAL TESTING

The radiances from the 19 SFOVs shown in Figure 13 cannot be used as an *independent* test of retrievability, since they are already used to determine the regression-retrieval matrices. Independent radiances are introduced by using SFOVs adjacent to the 19 SFOVs shown in Figure

13. The nominal 30 km resolution of the SFOVs is not a serious spatial mismatch to the radiosonde locations, and truly independent radiometric noise will be tested in the retrievals. These 19 independent sets of adjacent, observed VAS radiances are used to produce three sets of 19 temperature and mixing ratio retrievals by using the NOAA32, the NSSL210 and the SEUSA19 regression matrices. Unfortunately, there is no "ground truth" available other than the 19 profiles already used from Tables 6 and 7.

8.3 SAMPLE RETRIEVALS AT RADIOSONDE SITES

VAS retrievals are done with the empirically conditioned SEUSA19 regression matrix. Figures 17-A, -B and -C show radiosonde and retrieved temperature and dewpoint profiles at three sites: Amarillo, Texas, Tampa Bay, Florida and Jackson, Mississippi. The temperature retrievals are in good agreement with the smooth RAOB profiles. The retrieval at Amarillo below 920 mb is meaningless, due to the altitude of central Texas. The dewpoint retrievals are in fair agreement below 500 mb for Jackson and Tampa Bay, but in very poor agreement over the entire Amarillo profile.

In general, moisture data for the 300 to 500 mb layer is of uncertain quality for the radiosondes, where the retrievals are dominated by unverifiable radiances in the water vapor bands (VAS channels 9 and 10). Dewpoint disagreements in the 300 to 500 mb layer can easily result from a small error in chosing the location of the nearest SFOV, since Figure 13-B shows dramatic contrast over short distances in the moisture structures at this altitude. Moisture data above 300 mb is uninterpretable, due to the radiosonde limitations discussed in previous sections.

Satellite retrievals can be expected to produce better integrated layer averages than level values, since they are based upon radiances which arise from large vertical slabs of atmosphere, as indicated by the weighting function plotted in Figures 2 and 3. Table 12 lists the observed and retrieved values of precipitable water integrated above lower levels at the same three sites whose temperature and moisture profiles are plotted in Figure 17. Indeed, the precipitable water retrieved over Jackson and Tampa Bay agree within 20 percent of the radiosonde values. However,

the precipitable water over Amarillo has the same serious disagreement with radiosonde values as the dewpoint profile did in Figure 17-A. The cause of the failure in the moisture retrievals at Amarillo has not yet been determined.

It is not wise to give too much attention to the details of one profile from one retrieval method at one site, since each case has its own individual characteristics. Sample retrievals using the synthetic prelaunch matrices are not shown because they are very bad; such retrievals will only be discussed statistically in the following section.

8.4 RESIDUAL ERRORS IN THE PROFILE RETRIEVALS

The conventional figure of merit for profile retrievals is the RMS residual profile between the satellite soundings and radiosonde "ground truth." This FOM is the information not retrieved from independent SFOVs because of first-guess errors, unseen clouds, unmodeled surface effects, mismatches between the satellite and "ground truth" data, vertical smoothing, and noise. The information to be retrieved is the preretrieval variance in the field about the selected first-guess profile.

Generally speaking, the RMS profile residuals in satellite soundings follow a pattern of error content (Phillips, *et al.*, 1979). Uncertainties are dominated by mean residuals over several unresolved vertical layers. The temperature residuals are normally larger at the tropopause because there is little radiance upwelling. Both the moisture and temperature residuals are normally larger near the surface because of the naturally larger variance in these optically thin layers, which lie just above a surface with irregular topography and emissivity. The moisture residuals are also poorly determined in the lower troposphere, because of many problems with surface irregularities and low radiance sensitivity, as indicated in Figures 3 and 16-B. Figures 18 and 19 show the RMS residuals between all three temperature and mixing ratio retrieval attempts (NOAA32, NSSL210 and SEUSA19) and the "ground truth" in Tables 6 and 7, averaged over all 19 sites in the SE USA. The preretrieval variance about the mean of the 19 sites is also shown.

8.4.1 RMS Temperature Residuals

The RMS temperature residuals in Figure 18 follow very different patterns for the NOAA32, the NSSL210, and the SEUSA19 regression-retrieval matrices:

1. The synthetic NOAA32 temperature retrievals have a mean RMS error of about ±7° C, which is much worse than the preretrieval ±2° C variance. This information degradation is probably due to the large bias between the synthetic and observed VAS radiances, which were discussed in previous sections. The large error bulge in the 400 to 800 mb layer is probably due to the statistical bias in the NOAA32 profiles as they affect the mid-tropospheric water vapor bands.

   The "global" set teaches the NOAA32 regression matrix that VAS channels 9 and 10 correlate strongly with both temperature and moisture in the mid-troposphere, so that large ΔT^*s for these channels are interpreted as corresponding large errors in T(600±200 mb) where these channels peak (see Figure 3 or 16-B). Indeed, the RMS errors away from the bulge are only ±3° K. This suggests that temperature retrievals conditioned by the NOAA32 might have acceptable errors when they are appropriately applied to a global VAS dwell sounding without the water vapor bands.

2. The NSSL210 temperature retrievals have a mean RMS error of ±9° C, which is even worse than the NOAA32 retrievals. The errors are distributed almost uniformly over the profile, except for better agreement (±4° C) at 920 mb. The cause of this large error is not known. This result is surprising because the first-guess temperature profile from the NSSL210 set (not shown) is similar to the actual temperature profiles shown in Figure 12. One possibility is that the temperature variations learned from the unstable thunderstorm fields of the NSSL210 are completely orthogonal to the temperature variations present in the stable autumnal field of 7NOV80. The problem must be analyzed before the NSSL datasets are used to condition retrievals during the planned Midwestern thunderstorm VAS observations.

3. The synthetic empirical SEUSA19 temperature retrievals have a mean RMS error of ±1° C, which is a real information improvement over the preretrieval variance of ±2° C. By contrast, the synthetic retrievals just described actually degraded the variance from ±2° K to ±7° K and ±9° K. Most of the improvement is below 300 mb, since the radiometric noise in the upper air temperature sounding channels is too large to be useful for this spin-starved dwell sounding (see Tables 1 and 9).

   The apparently excellent agreement benefits from the cancellation of actual errors in the 3-hour mismatch between the VAS observations and the 19 RAOBs, due to the lack of *independent* "ground truth" radiosonde observations which are taken *at the same place and time* as the VAS observations. The sparseness of the synoptic radiosonde network makes it impossible to independently verify VAS soundings based upon empirical regression with the synoptic radiosondes themselves, even if there is no 3-hour mismatch. Nevertheless, the RMS improvement in these empirical temperature soundings demonstrate that the random errors in the VAS radiances are low enough to make clear air retrieval errors within specifications (±2° C) whenever there are no systematic biases in either the first-guess radiances or the first-guess profiles.

8.4.2 RMS Mixing Ratio Residuals

The RMS mixing ratio residuals in Figure 19 also have error patterns that depend upon the retrieval matrix:

1. The synthetic NOAA32 mixing ratio retrievals seriously degrade the moisture information in the lower troposphere. Similar errors are found even in the prelaunch simulated VAS retrievals when the "global" matrix is applied to a particular "local" condition (Chesters, *et al.*, 1981). The underlying problem is once again due to the strong correlation between temperature and moisture in the "global" set. For the NOAA32 retrievals, the magnitude of the error is greatest near the surface because of the large arctic to tropical contrast present in this layer for the "global" training set, so that the lower air temperature sounding channels are instead being interpreted as indicating moisture. This incorrect training

causes gross misinterpretation of the individual VAS channel radiances when applied to a situation without such a correlation.

2. The synthetic NSSL mixing ratio retrievals slightly degrade the moisture information in the lower troposphere and seriously degrade the upper troposphere. The cause of this degradation is not clear, but the large bias and scatter between calculated and observed VAS radiances in the water vapor bands is suspected (note the errors in VAS channels 9 and 10 listed in Table 10 and Figure 15-A).
3. The empirical SEUSA19 mixing ratio retrievals modestly improve moisture information over the entire profile, compared to the original moisture variance. The 1000 mb moisture retrievals are meaningless, since most of the 19 sites are located above this extrapolated level. Like the RMS temperature residuals, these mixing ratio residuals mask the errors due to the 3-hour mismatch between the VAS observations and the synoptic radiosondes. The modest improvement in the moisture residuals only suggests that unbiased VAS retrievals could improve our knowledge of clear air moisture content.

8.4.3 Profile Retrieval Error Assessment

The RMS residual profiles in Figures 18 and 19 show that retrievals on real VAS observations with synthetically developed coefficients actually degrade profile information, due to large first-guess biases and inappropriate statistics. The RMS profiles also show that unbiased retrievals do improve temperature and moisture information, implying sufficient stability in the VAS radiometry to meet sounding requirements. Sounding accuracy cannot be verified without an independent set of "ground truth" profiles taken at the same place and time as VAS observations. However, the implied internal consistency of the VAS radiances leads us to believe that the clear air between the 19 SE USA radiosonde sites can be sounded with the SEUSA19 regression matrix to produce relatively correct empirically retrieved temperature and moisture fields with 30 km resolution.

8.5 RETRIEVAL SUMMARY

Temperature and moisture retrievals are performed on the first VAS radiances in the clear air at 19 radiosonde sites in the SE USA on 7NOV80. Systematic biases between calculated and

observed VAS radiances preclude the use of physically modeled retrievals. Retrievals are tested with independent VAS radiances selected from SFOVs adjacent to the 19 SFOVs at the radiosonde sites. Retrievals with synthetic regression matrices seriously degraded the temperature and moisture information due to biases in first-guess radiances and profiles and inappropriate statistical conditioning in "global" and "local thunderstorm" datasets. Retrievals with local empirical radiance-to-radiosonde regression matrices improved temperature and moisture information. The empirical retrievals produced RMS residual profiles that exceeded requirements for VAS sounding accuracy. However, the residuals are certainly smaller than the true error, since no independent "ground truth" data is available at the same time and place as the VAS observations. The low RMS residuals from the local empirical retrieval matrix demonstrate good enough radiometric stability within a VAS radiance field to ensure good relative sounding accuracy for stable mesoscale conditions.

SECTION 9
MESOSCALE ANALYSIS OF EMPIRICAL VAS-D RETRIEVALS

VAS D retrievals derived from the local empirical radiance to radiosonde regression matrix are analyzed to determine the relative impact of VAS upon mesoscale temperature and moisture fields. An exact comparison between RAOB and VAS analyses is not possible because of the 3-hour difference between the observations. However, the comparison does provide evidence of the ability of VAS retrievals to fill in the gaps that exist in the conventional RAOB database.

9.1 MESOSCALE ANALYSIS

Figures 21-A and -B show the conventional NWS surface pressure analysis and 500 mb height field analysis over the USA late in the afternoon of 7NOV80. The weather is characterized by a rather weak 500 mb trough-ridge-trough system across the United States with a complex low pressure system in the Pacific Northwest and a weak surface low over the Great Lakes region. The clouds associated with these features are clearly visible in the VAS images in Figure 5, except for the stratospheric sounding channels, 1 and 2. The anticyclonic surface circulation extending westward from the Atlantic Ocean and the dry westerly flow in the mid- to upper-troposphere (Figure 21) provided the clear skies over the southeastern United States, as seen by VISSR operations from GOES-EAST (Figure 4) and by the VAS experiment from GOES-4 (Figure 5).

Using the locally conditioned regression matrix, VAS soundings are generated at 75 locations across the southeastern United States on a uniform grid (see Figure 20). The grid contains 5 rows by 15 columns of SFOVs with a spacing of approximately 2° latitude by 1.5° longitude, corresponding to roughly 30 km SFOV resolution with 150 km spacing.[19] Six of the 75 VAS soundings are eliminated because of significant cloud contamination, leaving 69 mostly clear soundings to be used in a contour analysis. RAOB data from the 19 stations in the SE United States are interpolated to the same grid, using a Barnes analysis scheme developed on the GSFC Atmospheric and

[19]One would like to retrieve at every clear SFOV in Figure 20, which would be 30 km resolution and spacing, but a bottleneck in the VASP regression retrieval software limited processing to fewer than 100 retrievals.

Oceanic Image Processing System (AOIPS) General Meteorological Package (GEMPAK). The gridded RAOB dataset is then contoured for comparison to the VAS retrieval fields.

9.2 MESOSCALE ANALYSIS COMPARISONS

Figures 22, 23, 24 and 25 compare the contoured analyses of the VAS retrievals to the RAOB soundings for the surface temperature, the 850 mb temperature and mixing ratio, and the 500 mb temperature, respectively. Note that the RAOB analysis in the Gulf of Mexico represents an extrapolation of data from the coastal region into a large data-void area, which restricts any comparison of the VAS and RAOB analyses over the Gulf.

The RAOB surface and 850 mb temperature analyses (Figures 22-A and 23-A) reveal a significant east-west gradient across the domain. The 850 mb temperature gradient is concentrated over the east Texas and Louisiana region. The warmest air in Texas is immediately ahead of the trough moving into that region from the northwest (Figure 21-B). The VAS retrieval analyses (Figures 22-B and 23-B) for the surface and 850 mb levels compare favorably with the RAOB analyses. At the earth's surface, the 10° C temperature gradient from the warm air over Texas to the cool air over the Atlantic seacoast has been retrieved from the VAS radiances. The concentrated temperature gradient at the 850 mb level in eastern Texas is also well represented in the VAS retrievals.

The temperature difference charts (Figures 22-C and 23-C) reveal several interesting features. First, the differences at the surface and at 850 mb are within 3° C and 2° C, respectively, indicating that gross, spurious data values are not introduced by the VAS sounding algorithm. Second, the VAS retrievals have actually strengthened the east-west gradients of the 850 mb and surface temperature fields. While the details in the gradients are not verifiable from the existing "ground truth" radiosondes, they do have a radiometric basis. For example, the cooler VAS temperatures along the Texas coast and the warmer VAS temperatures in Mexico (illustrated by the difference fields in Figures 22-C and 23-C) result from the window channel brightness difference between the

land mass and the water surface (see VAS channels 7, 8 and 12 in Figure 5). Thus, the net effect upon the VAS retrieval analysis is a stronger low level temperature gradient from the western Gulf of Mexico into Texas.

The warmer VAS surface temperatures in the Gulf of Mexico to the west of Key West, Florida are also a direct response to the brightness patterns in the VAS window channels. Apparently, the VAS retrievals fill in the details missed by the conventional RAOB analysis in the large gap over the Gulf of Mexico. Because the purely empirical regression retrievals are trained over the land, where the skin temperature, air temperature, and radiances have a different relationship than over the water, it is not possible to make quantitative confidence estimates for the sounding accuracy in the Gulf of Mexico.

The 500 mb VAS and RAOB temperature analyses (Figure 25) are included to illustrate the ability of VAS to replicate the RAOB analysis of the rather bland field in the middle to upper troposphere. The smoothness of the retrieval analysis is a good quality assurance test for the existence of any spurious points in the individual VAS soundings.

A comparison between the VAS and RAOB 850 mb mixing ratio analyses (Figure 24) illustrates significant differences in the moisture fields. The best mixing ratio retrievals are produced over an area that encompasses central Texas, Louisiana, Arkansas, Mississippi and the western part of the Gulf of Mexico where the differences between VAS and RAOB soundings are generally within 1 gm kg^{-1}.

However, the VAS retrievals along the East Coast and in northwest Texas are noticeable wetter than the RAOB analysis. The wetter satellite analysis is based somewhat upon the VAS radiances in the "split window," since the brightness differential between VAS channels 7 and 8 is stronger in these areas (Figure 6). The discrepancy in northwestern Texas may not be significant, since both analyses are based on very little data; the RAOB analysis is based upon one report, and the VAS analysis is based upon soundings from central Texas because the northern soundings are rejected

for probable cloud contamination. The VAS retrievals yield a significant moisture tongue in the eastern part of the Gulf of Mexico, the magnitude of which cannot be verified with the existing RAOB network. The images from channels 7 and 8 in Figure 5 and their brightness difference in Figure 6 indicate a region of greater water vapor content in this area and suggest that this particular moisture signature is real if it is not due to unresolved low clouds.

9.3 MESOSCALE ANALYSIS SUMMARY

The VAS temperature and moisture retrievals derived from the local empirical radiance-to-radiosonde regression matrix are analyzed and compared to the RAOB operational network. An exact comparison is not possible, because of the 3-hour time difference between soundings. However, the results indicate that VAS retrievals do capture significant lower tropospheric temperature gradients. VAS has also added significantly to the analysis of temperature and moisture fields over the Gulf of Mexico, which is a large data-void area within the operational RAOB network. From this first-analysis comparison at GSFC, VAS apparently helps to cure the "gaposis" problem, which limits the conventional RAOB network both in space and time. However, much more testing of VAS retrievals under normal and disturbed weather conditions must be done to determine the net impact of VAS soundings upon subsynoptic and mesoscale analysis.

SECTION 10
VAS-D ASSESSMENT SUMMARY

This section summarizes what has been learned from the first VAS-D radiances at GSFC and assesses their significance for future work with the VAS instrument.

10.1 COLLECTION OF THE PREVIOUS SECTION SUMMARIES

The summaries from each of the previous sections are reiterated here for the reader's convenience.

10.1.1 Summary of Objectives and Outline

The first orderly VAS dwell sounding radiances are examined by the scientific users for:

1. Image quality.
2. Radiometric precision.
3. Radiation transfer verification.
4. Regression retrieval accuracy.
5. Mesoscale analysis features.

The report is organized in the following order:

1. Objectives and outline.
2. Description of VAS.
3. Prelaunch assessments at GSFC.
4. VAS-D operations to 7NOV80.
5. VAS-D image quality.
6. VAS-D radiometric quality.
7. Radiation transfer verification.
8. VAS-D sounding quality.
9. Mesoscale analyses from empirical retrievals.
10. VAS-D assessment summary.

10.1.2 Summary Description of VAS

The VAS instrument is an improved version of the VISSR device used operationally on the GOES satellites. It was designed to provide multispectral infrared sounding data and exploits the geosynchronous station to give frequent coverage of mesoscale weather developments. VAS has 12 calibrated thermal infrared channels between 4 and 15 microns, which were chosen to distinguish the effects of tropospheric temperature, moisture and cloud cover upon the upwelling radiances. The VAS channels cover the troposphere with roughly 5 km vertical and 15 km horizontal resolution, and they suffer the usual passive infrared limitations on determining the state of the lowest atmospheric layers without ancillary surface data.

10.1.3 Summary of Prelaunch Assessments at GSFC

The measured spectral responsivity of the VAS-D channels meets prelaunch specifications. The calculated sensitivity of the brightness temperature (°K) to the VAS channels' variations in temperature and moisture (°C) indicate a typical "variance/noise" ratio of 10° C/1° K over North America throughout the year. A sounding study of thunderstorm environments, using VAS radiances synthesized from NSSL radiosondes, yielded profile and gradient retrievals with acceptable error levels, provided that the algorithm was statistically conditioned to resolve ambiguities in favor of the most probable local conditions. However, there was a serious underestimate of the moisture content of the lower troposphere, which suggests that ancillary data is needed in order to retrieve this parameter accurately.

10.1.4 Summary of VAS-D Operations to 7NOV80

VAS-D was launched on 9SEP80 with one of a redundant pair of detectors broken, reducing useful data rates by a factor of 2. A month of postlaunch checkout was used for debugging software throughout the VAS system, principally the A/D conversions on the satellite, the calibration in the S/DB at Wallops, and the calibration and quality assurance in the VASPP and VASP. The first orderly, calibrated dwell radiances were gathered over North America on the afternoon of

7NOV80, 1900-2100GMT. The weather was remarkably clear and warm over most of the Southeast United States, where radiosonde reports were available 3 hours later from 19 clear sites.

10.1.5 Image Quality Summary

Images of the 7NOV80 VAS dwell sounding radiances are well registered multispectral views of the North American atmosphere, and are suitable for sounding. Some problems exist with a high bit error rate and with line to line relative calibration stability. The upper stratospheric channel shows no significant brightness variation across the earth. Navigation of VAS line and pixel to or from latitude and longitude coordinates is not available. This dwell sounding dataset is not a high resolution test of VAS imagery, since it has been resampled to 30 km SFOV resolution.

10.1.6 Radiance Quality Summary

Radiometric quality assurance specifications are developed for VAS-D from prelaunch specifications for noise and calibration. When mis-calibrated radiances initially arrived for dwell soundings, quality assurance software was developed in the GSFC VASP to help debug the entire data processing chain: detection and A/D conversion in the satellite; gain and offset determination in the S/DB; offset removal and dwell averaging in the GSFC VASPP; and conversion to sample averaged floating point radiances in the GSFC VASP.

Plots of raw unaveraged VAS dwell radiances along a scan line are examined qualitatively, with the findings that: scattered light in outer space amounts to roughly 1 percent of the earth's brightness at 11 microns; the 8 significant bit limitation in the A/D conversion produces digitization error comparable to the NEΔR noise; and truncation errors in the integer arithmetic of calibration produce negative values for the radiance of outer space with a bias comparable to the NEΔR noise.

The correlations and biases in VAS radiances will prevent ideal data averaging (i.e., with no mean error and $1/\sqrt{N}$ noise reduction) of dwell spins, adjacent samples, adjacent lines, and redundant detectors to construct a SFOV. The first orderly VAS radiances are found to roughly meet

basic quantitative requirements for noise, zero point, droop and calibration stability from the scientific user's point of view, although there are systematic biases comparable to NEΔR. The shortwave detectors are found to have noise and stability FOMs which are significantly better than prelaunch specifications. HIRS2 radiometer data from TIROS-N on 7NOV80 is not yet available for use as a "secondary standard" of comparison to the corresponding VAS-D data.

10.1.7 Radiation Transfer Verification Summary

VAS radiances were selected at 19 clear air radiosonde sites in the Southeast USA from the 2030GMT 7NOV80 dwell sounding. Exact line by line transmission functions and radiances were calculated at these 19 sites, using the radiosonde reports taken 3 hours later at 2330GMT 7NOV80. The calculations and observations were compared for all 12 channels at all 19 sites in the form of brightness temperature differences, ΔT^*. The average differences showed several effects:

1. The window channels are calculated to be about 6° K colder than observed, probably due to the actual value of the skin surface temperature in the bright sunlight.
2. The upper air water vapor bands are calculated to be about 3° K warmer than observed, probably due to the lack of good radiosonde moisture data above 500 mb.
3. Allowing for the warmer than calculated surface temperature, all of the temperature sounding channels are calculated to be about 4° K warmer than observed. Empirical adjustments to the overall strength of the absorption in the sounding channels shows no physically consistent pattern. The three channels near the tropopause cannot have radiance agreement forced by any possible simple strength adjustment. *Ad hoc* sources of abnormally strong absorption at the tropopause or *ad hoc* changes in the observed VAS radiances are not scientifically justifiable.

Analysis of the sources of radiation in the VAS channels indicates that radiosondes are poor "ground truth" for accurate radiation transfer verification. Many of the channels contain *skin temperature* radiance not available in the balloon measurements, and the upper air water vapor bands display moisture above the failure point of the radiosonde moisture sensor. Physical

retrieval models may have to depend upon first guesses relative to previous VAS data in order to avoid radiosonde limitations and unaccountable biases.

10.1.8 Retrieval Summary

Temperature and moisture retrievals were performed on the first VAS radiances in the clear air at 19 radiosonde sites in the SE USA on 7NOV80. Systematic biases between calculated and observed VAS radiances preclude the use of physically modeled retrievals. Retrievals were tested with independent VAS radiances selected from SFOVs adjacent to the 19 SFOVs at the radiosonde sites. Retrievals with synthetic regression matrices seriously degraded the temperature and moisture information due to biases in first-guess radiances and profiles and inappropriate statistical conditioning in "global" and "local thunderstorm" datasets. Retrievals with local empirical radiance to radiosonde regression matrices improved temperature and moisture information. The empirical retrievals produced RMS residual profiles that exceeded requirements for VAS sounding accuracy. However, the residuals are certainly smaller than the true error, since no independent "ground truth" data is available at the same time and place as the VAS observations. The low RMS residuals from the local empirical retrieval matrix demonstrate good enough radiometric stability within a VAS radiance field to ensure good relative sounding accuracy for stable mesoscale conditions.

10.1.9 Mesoscale Analysis Summary

The VAS temperature and moisture retrievals derived from the local empirical radiance to radiosonde regression matrix were analyzed and compared to the RAOB operational network. An exact comparison is not possible, because of the 3-hour time difference between soundings. However, the results indicate that VAS retrievals do capture significant lower tropospheric temperature gradients. VAS has also added significantly to the analysis of temperature and moisture fields over the Gulf of Mexico, which is a large data-void area within the operational RAOB network. From this first-analysis comparison at GSFC, VAS apparently helps to cure the "gaposis" problem,

which limits the conventional RAOB network both in space and time. However, much more testing of VAS retrievals under normal and disturbed weather conditions must be done to determine the net impact of VAS soundings upon subsynoptic and mesoscale analysis.

10.2 ASSESSMENT OF THE FIRST VAS-D DATA

VAS has 12 calibrated thermal infrared channels between 4 and 15 microns, which were designed to distinguish the effects of tropospheric temperature, moisture and cloud cover upon the upwelling radiances. The geosynchronous station will be exploited to give frequent coverage at high resolution of mesoscale weather developments. Prelaunch sounding studies at GSFC indicated that "variance/noise" figures on the order of 10° C/1° K could be expected for VAS' sensitivity to atmospheric changes, leading to acceptable error levels in VAS retrievals from radiances simulated for prethunderstorm conditions. After 1 month of debugging the VAS data processing chain, the first orderly, calibrated dwell averaged radiances were gathered by the VAS-D instrument on GOES-4 looking at North America on the afternoon of 7NOV80, 1900-2100GMT. The weather was remarkably clear and warm over the entire Southeast United States where radiosonde reports were available from 19 clear sites approximately 3 hours later.

Images of the 7NOV80 VAS dwell sounding radiances are well registered, multispectral views of the North American atmosphere and represent calibrated data suitable for sounding. VAS radiometric quality meets prelaunch specifications for noise and calibration, although there are biases comparable to the radiance noise levels.

Radiances calculated from line-by-line transmission functions for the conditions at each of the 19 radiosonde sites disagreed with observations by several °K in brightness temperature in almost all VAS channels. Some of the radiance discrepancies can be attributed to the high skin temperature of the earth's surface, to the 3-hour mismatch in observation times, or to the poor moisture data above 500 mb. However, the upper tropospheric temperature sounding channels are unaccountably calculated to be roughly 4° ±1° K brighter than observed. This radiance bias would

propagate as a correspondingly large bias through retrieval algorithms that use such a physical model.

Consequently, local empirical radiosonde/radiance regression retrievals were developed, which automatically absorb unaccountable biases into the statistical averages. The empirical retrievals had temperature and moisture residuals well within prelaunch requirements, although the sounding situation did not allow a truly independent verification of VAS retrievability. The remaining VAS radiance field was sounded using a regular grid of 150 km spacing, and the resulting temperature and moisture analyses compared favorably with radiosonde analyses.

The VAS retrievals appear capable of adding valuable information under clear conditions by filling data gaps that exist in the operational RAOB network. VAS seems particularly effective as a multi-channel radiometer for computing and displaying subsynoptic gradients on a scale that is commensurate with the mesoscale-to-subsynoptic atmospheric processes that lead to severe storms. However, much more work will be involved in testing VAS within a severe storm environment under less than optimal sounding conditions to determine if this remote sounding potential can be realized.

Several technical and operational limitations of VAS usage have been mastered well enough to demonstrate clear air mesoscale sounding and show that there are areas for improvement in the entire VAS data processing system. Eventually, a small special network of frequent radiosondes in central Texas may be launched to provide a truly independent verification network at the same time and place as the VAS soundings for a few days of severe storm conditions.

Acknowledgements: This work was funded through the VAS Demonstration Project of NASA's Operational Satellite Improvement Program (OSIP). It was managed at NASA/GSFC by Mr. Richard Pinamonti and was technically coordinated by Dr. Harry Montgomery and Mr. Daniel Endres. The scientific groundwork for the VAS Demonstration at NASA/GSFC was initiated by Dr. Albert Arking and Mr. William Shenk. Development of the interactive VAS Processor at NASA/GSFC was begun by Mr. Patrick Gary and Mr. John Dalton and was completed by Mr. David Howell and Ms. Rita Jamros. It currently is operated under the direction of Mr. Joseph Johns. Ms. Mary desJardins was reponsible for the exchange of data between the VASP and AOIPS computers at NASA/GSFC, which resulted in many of the images and contour maps shown in this report. We thank Dr. Tay-How Lee and Dr. Marc Allen of Computer Sciences Corporation for their work in carefully preparing many of the datasets for our use.

Appendix A
REFERENCES

1. Arking, A., "Retrieval of Meteorological Variables," *GSFC VAS Demonstration Review*, edited by H. Montgomery, VAS Working Group Meeting, January 27, 1977.

2. Barnes, S. L., J. H. Henderson and R. J. Ketchum, *Rawinsode Observation and Processing Techniques at the National Severe Storms Laboratory*, NOAA TM ERL-53 (available as NTIS-72N12551), 1971.

3. Burch, D. E., D. A. Gryvnak, and J. D. Pembrook, *Investigation of the Absorption of Infrared Radiation by Atmospheric Gases*, AFCRL-70-0373 (available as NTIS-70N42640), 1970.

4. Burch, D. E., D. A. Gryvnak, and J. D. Pembrook, *Investigation of the Absorption of Infrared Radiation by Atmospheric Gases: Water, Nitrogen, Nitrous Oxide*, AFCRL-71-0124 (available as NTIS-71X78131), 1971.

5. Chesters, D., "Statistically Conditioned Least-Squares Retrievals Planned for the VAS Demonstration Experiment," *VAS Demonstration Workshop*, ed., D. L. Endres and L. W. Uccellini, NASA Conference Publication 2157, 55-79 (available as NTIS-81N19709), 1980.

6. Chesters, D., L. W. Uccellini, and A. Mostek, *VISSR Atmospheric Sounder (VAS) Simulation Experiment for a Severe Storm Environment* (work in progress).

7. Fleming, H. E., and W. L. Smith, "Inversion Techniques for Remote Sensing of Atmospheric Temperature Profiles," *Fifth Symposium on Temperature*, (Washington, D.C.) (available as NTIS-73A41976), 1971.

8. Hayden, C. M., "Low Level Moisture from VAS," *VAS Demonstration Workshop*, ed., D. L. Endres and L. W. Uccellini, NASA Conference Publication 2157, 57-65 (available as NTIS-81N19709), 1980.

9. Hillger, D. W., and T. H. Vonder Haar, "Deriving Mesoscale Temperature and Moisture Fields from Satellite Radiance Measurements Over the United States," *J. Appl. Meteor., 16*, 715-726, 1977.

10. Hillger, D. W., and T. H. Vonder Haar, "An Analysis of Satellite Infrared Soundings at the Mesoscale Using Statistical Structure and Correlation Functions," *J. Atmos. Sci., 36*, 287-305, 1979.

11. Lee, T. H., and F. Yap, *Prelaunch Study of VAS Linear Regression Retrievals*, CSC TM-80-6302, under NASA Contract NAS 5-24350, 1980.

12. Malinowski, F. R., and R. D. Ruiz, *VAS-D/GOES Data Book (2 vols)*. Santa Barbara Research Center for NASA/GSFC, under Contract No. 5-20769, 1980.

13. McClatchey, R. A., W. S. Benedict, S. A. Clough, D. E. Burch, R. F. Calfee, K. Fox, L. S. Rothman, and J. S. Garing, *AFCRL Atmospheric Absorption Line Parameter Compilation*, AFCRL-TR-73-0096 (available as NTIS-73N30382), 1973.

14. Menzel, P., *Prelaunch Study Report of VAS-D Performance*, under NASA contract NAS5-21965 (available from the University of Wisconsin, Space Science and Engineering Center, 1225 West Dayton Street, Madison, Wisconsin), 1980.

15. Montgomery, H., *Execution Phase Project Plan for Operational Satellite Improvement Program Plan – VISSR Atmospheric Sounder (VAS) Demonstration*, NASA/GSFC Management Copy, 1980.

16. Mostek, A., L. W. Uccellini, and W. Gross, *A Description of the NSSL Cases Used for a Simulated VAS Retrieval Study*, NASA TM 80223 (available as NTIS-81N012678), 1980.

17. Phillips, N., L. M. McMillin, A. Gruber, and D. W. Wark, "An Evaluation of Early Operational Temperature Soundings From TIROS-N," *Bull. Amer. Meteor Soc., 16*, 1158-1197, 1979.

18. Prabhakara, C., G. Dalu, and V. G. Kunde, "Estimation of Sea Surface Temperature from Remote Sensing in the 11 to 13 Micron Window Region," *J. Geophys. Res., 79*, 5039-5044, 1974.

19. Roberts, R. E., J. E. A. Selby, and L. M. Biberman, " Infrared Continuum Absorption by Atmospheric Water Vapor in the 8-12 Micron Window," *Applied Optics, 15*, 2085-2090, 1976.

20. Schlatter, T. W., "An Assessment of Operational TIROS-N Temperature Retrievals over the United States," *Mon Wea. Rev., 109*, 110-119, 1981.

21. Smith, W. L., and H. M. Woolf, "The Use of Eigenvectors of Statistical Covariance Matrices for Interpreting Satellite Sounding Radiometer Observations," *J. Atmos. Sci., 33*, 1127-1140, 1976.

22. Smith, W. L., C. M. Hayden, H. M. Woolf, H. B. Howell, and E. W. Nagel, "Interactive Processing of TIROS-N Sounding Data," *Conference on Weather Forecasting, Analysis and Aviation Meteorology*, (Silver Spring, MD) AMS, Boston, 390-395 (available as NTIS-79A31851), 1978.

23. Soumi, V. E., T. Vonder Haar, R. Kraus, A. Stamm, "Possibilities for Sounding the Atmosphere from a Geosynchronous Spacecraft," *Space Research XI*, 609-617, 1971.

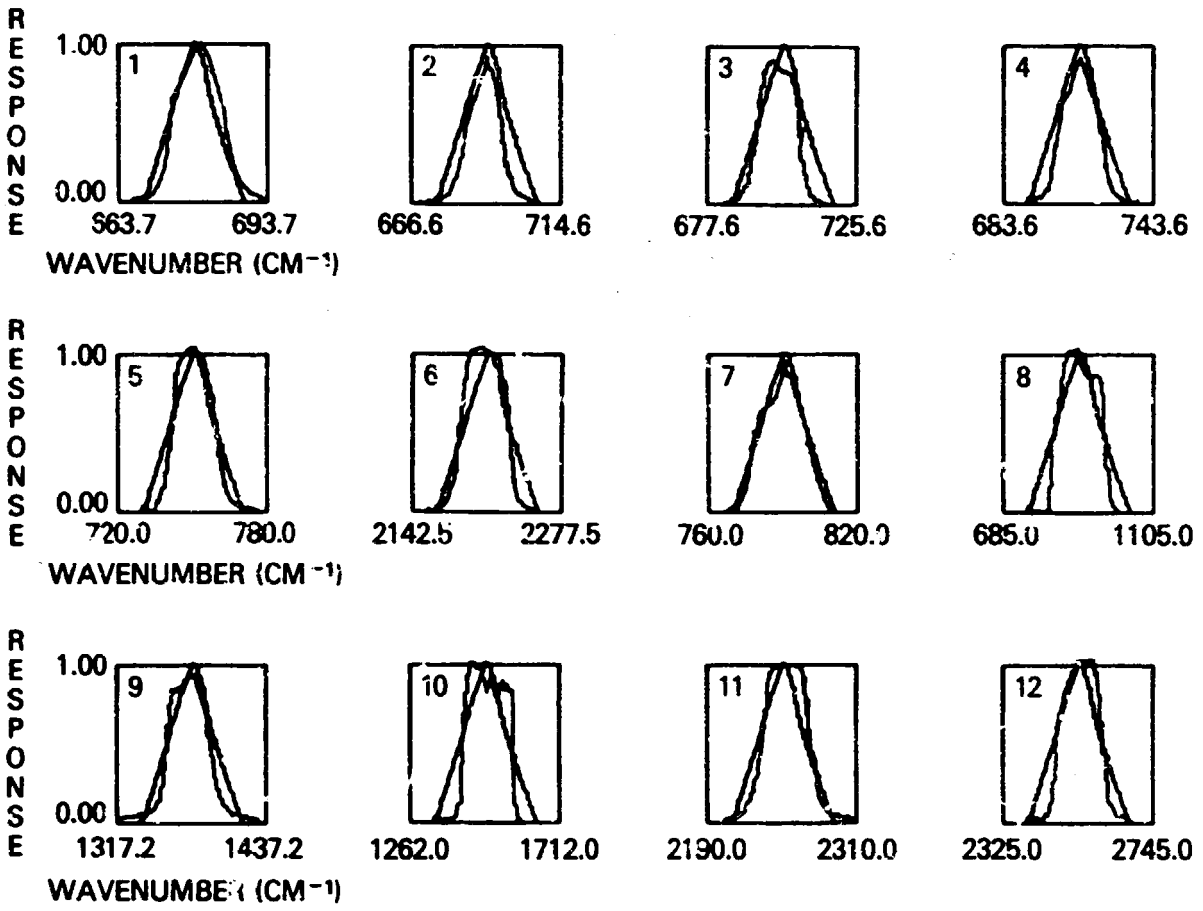

Figure 1. Measured and specified VAS-D spectral responses

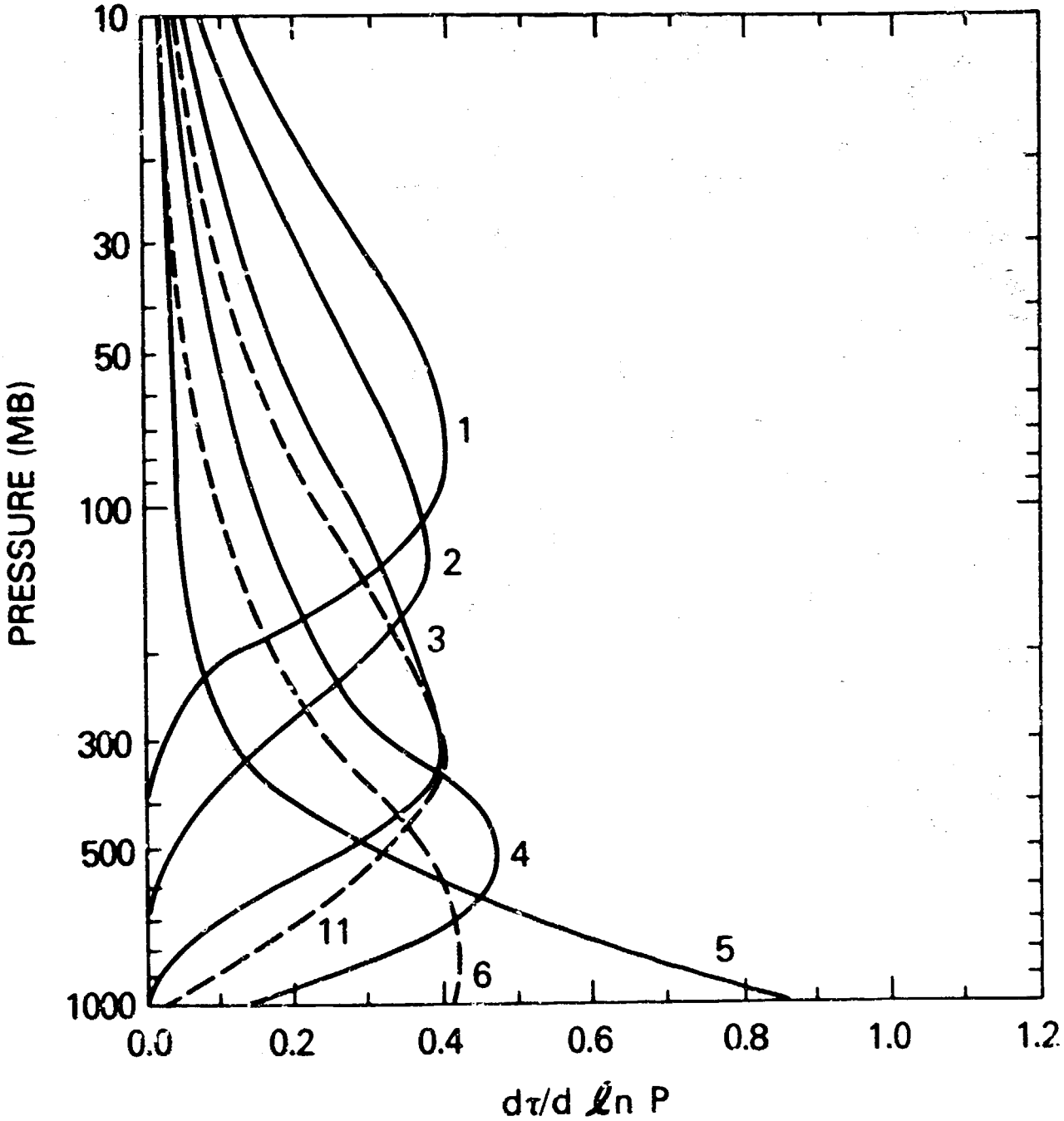

Figure 2. Weighting functions of VAS temperature sounding channels

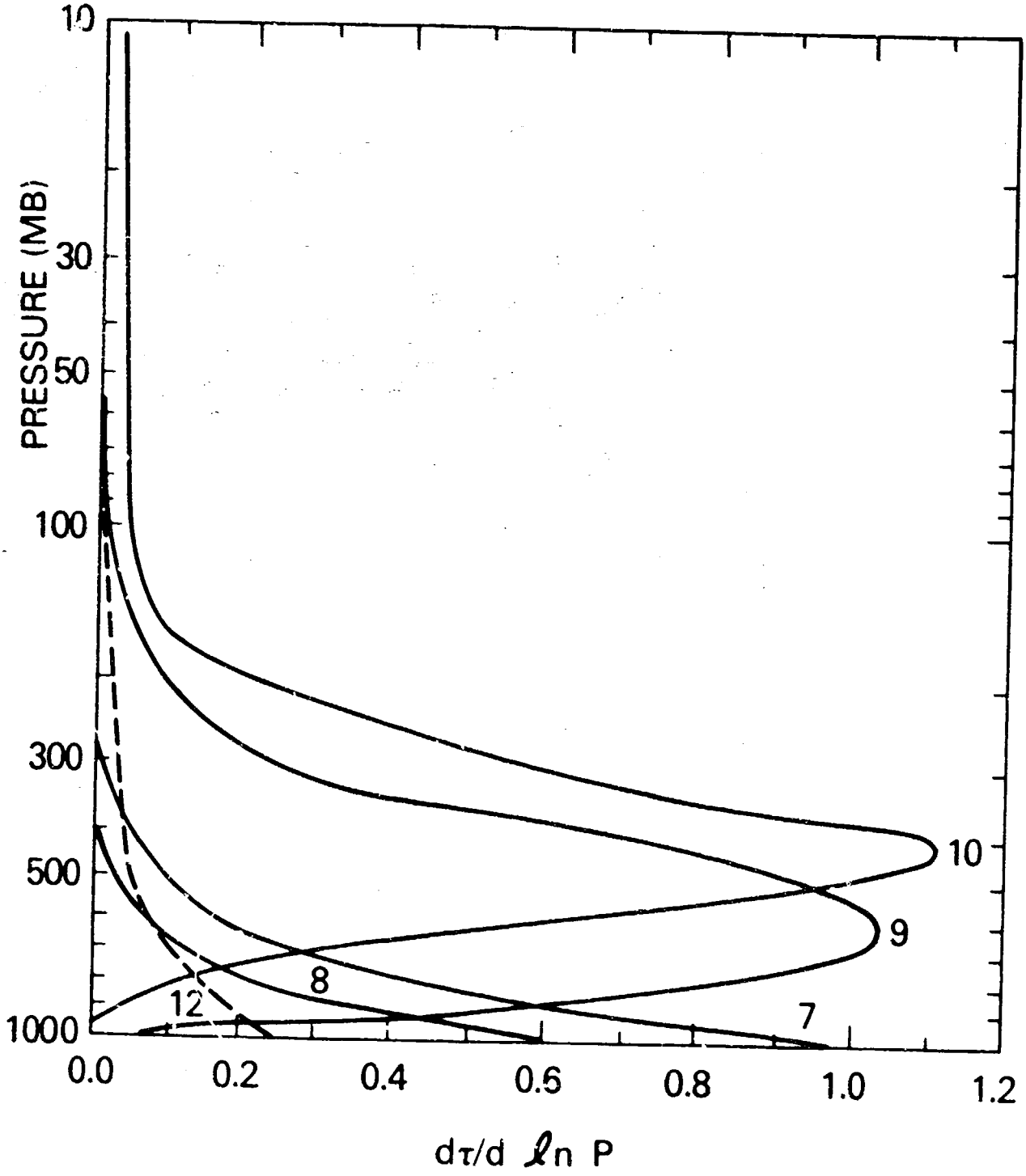

Figure 3. Weighting functions for VAS moisture and window channels

Figure 4. GOES-EAST VISSR picture of USA on 7NOV80

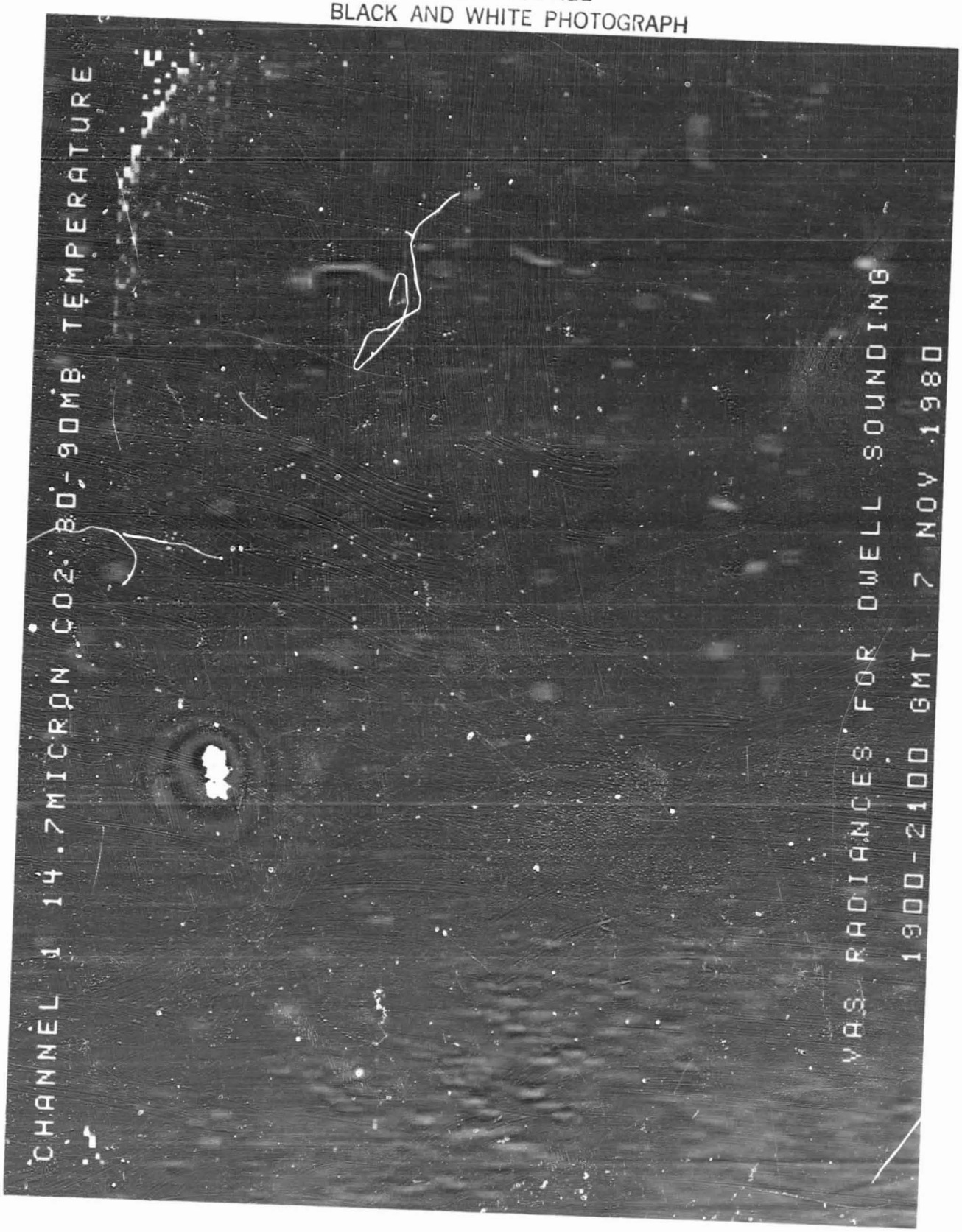

Figure 5a. VAS 12-page image sequence for SE USA on 7NOV80

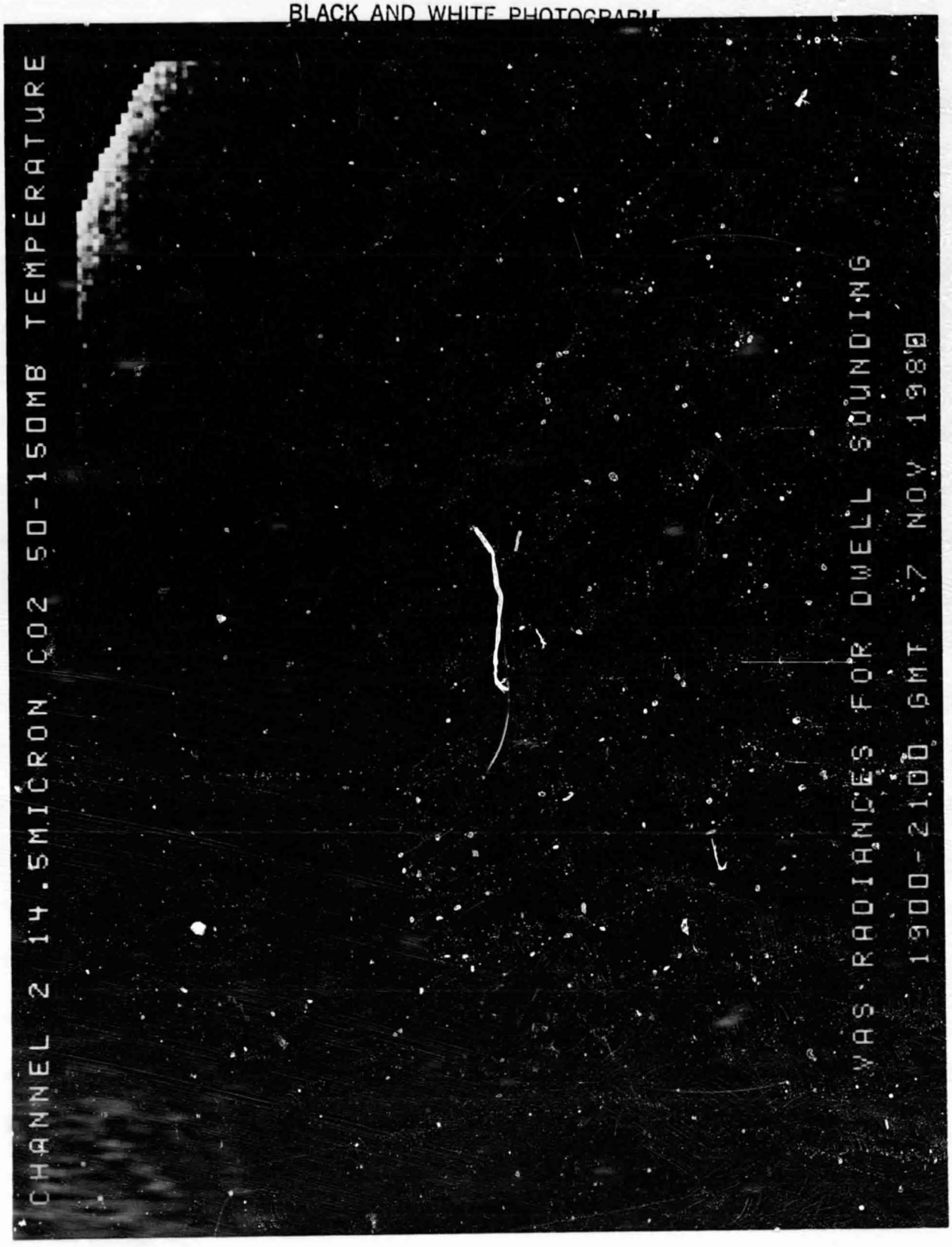

Figure 5b. VAS 12-page image sequence for SE USA on 7NOV80 (Continued)

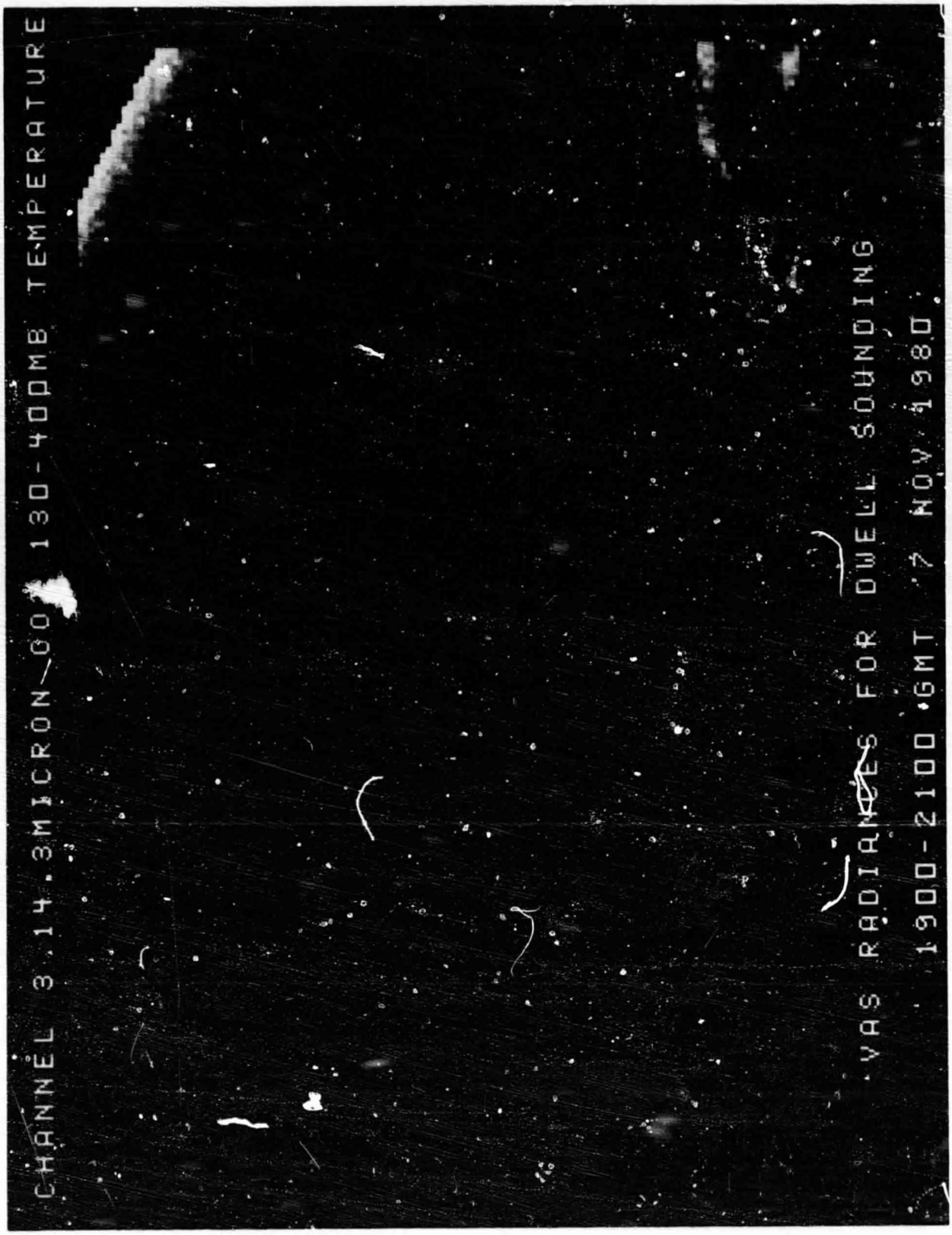

Figure 5c. VAS 12-page image sequence for SE USA on 7NOV80 (Continued)

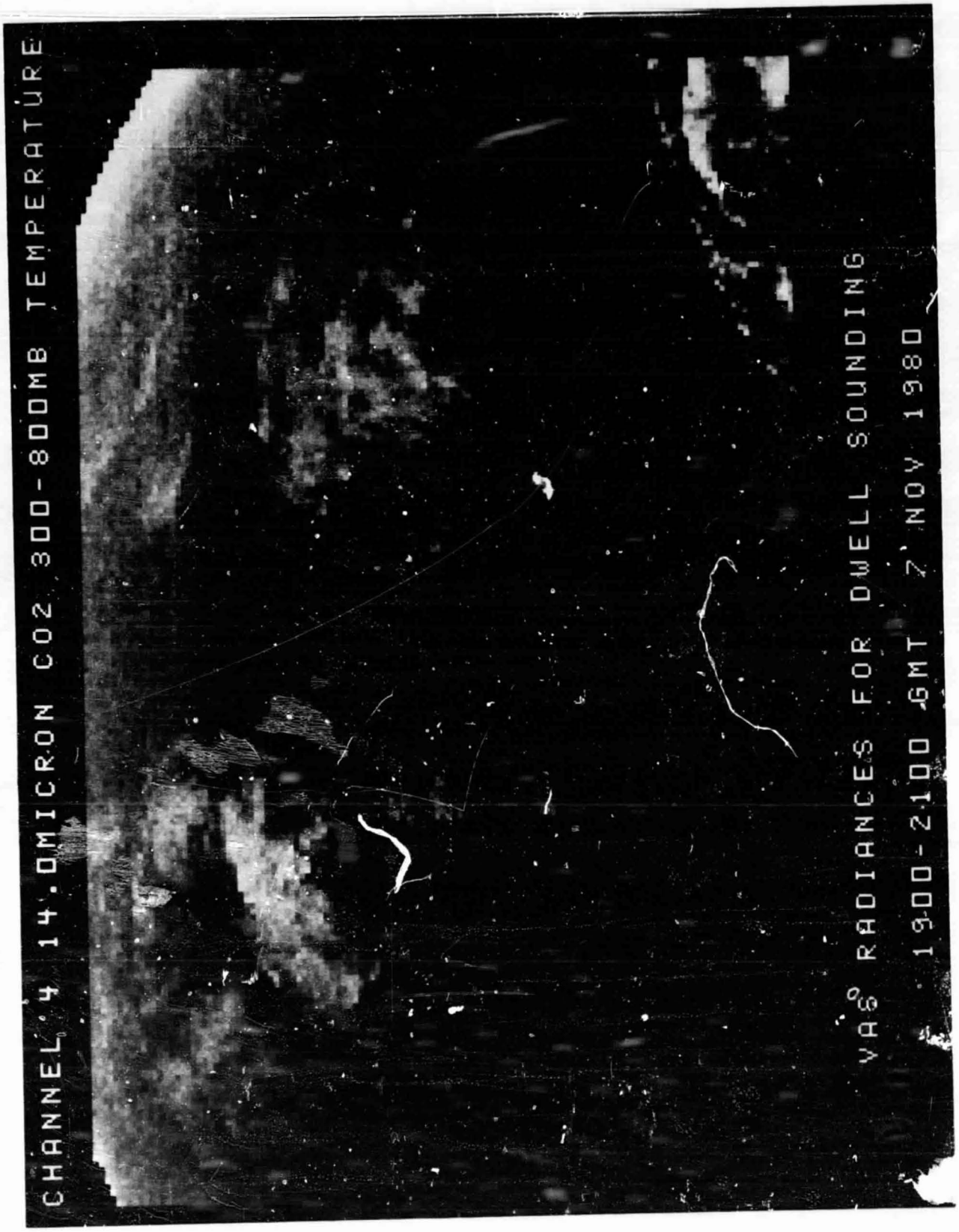

Figure 5d. VAS 12-page image sequence for SE USA on 7NOV80 (Continued)

ORIGINAL PAGE
BLACK AND WHITE PHOTOGRAPH

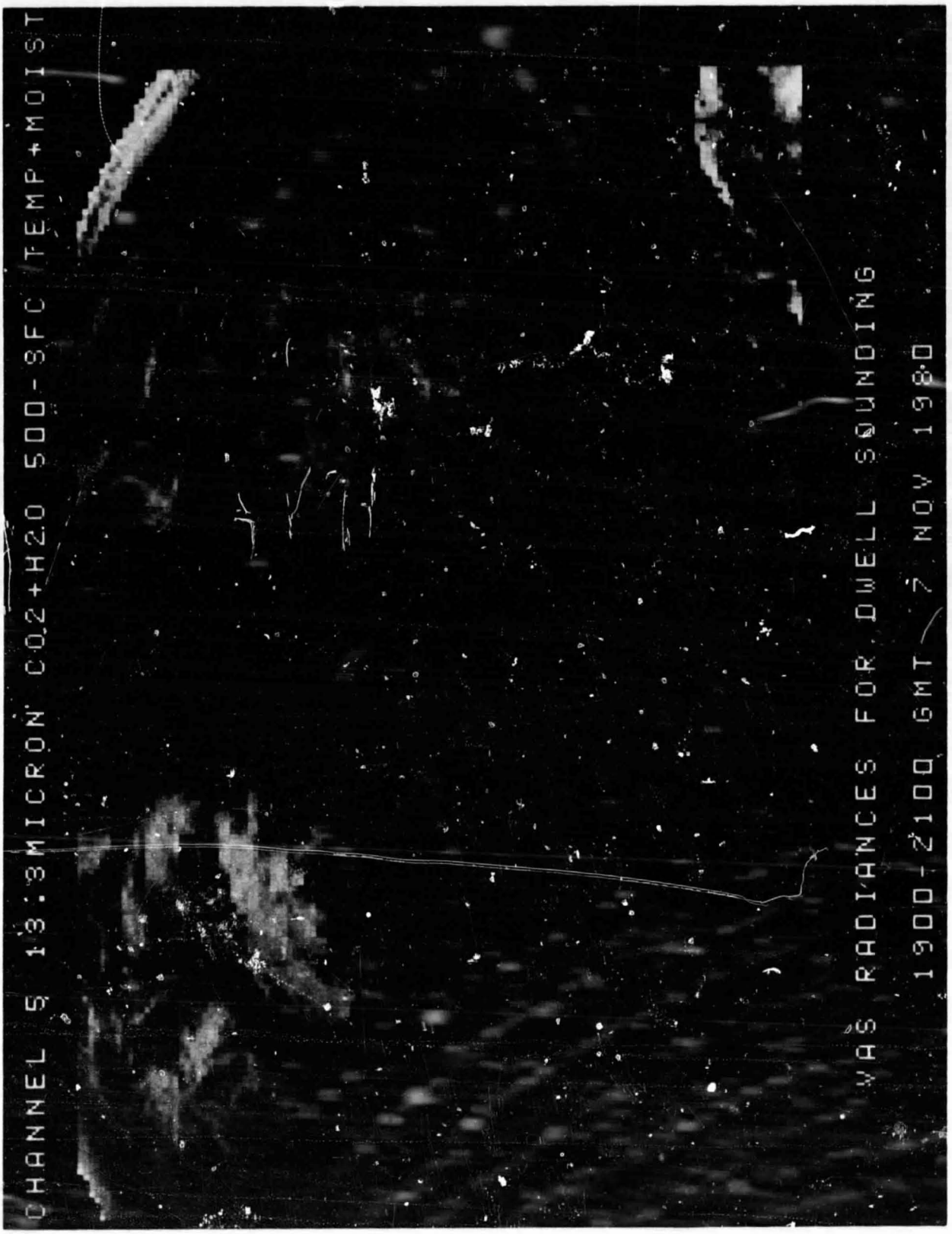

Figure 5e. VAS 12-page image sequence for SE USA on 7NOV80 (Continued)

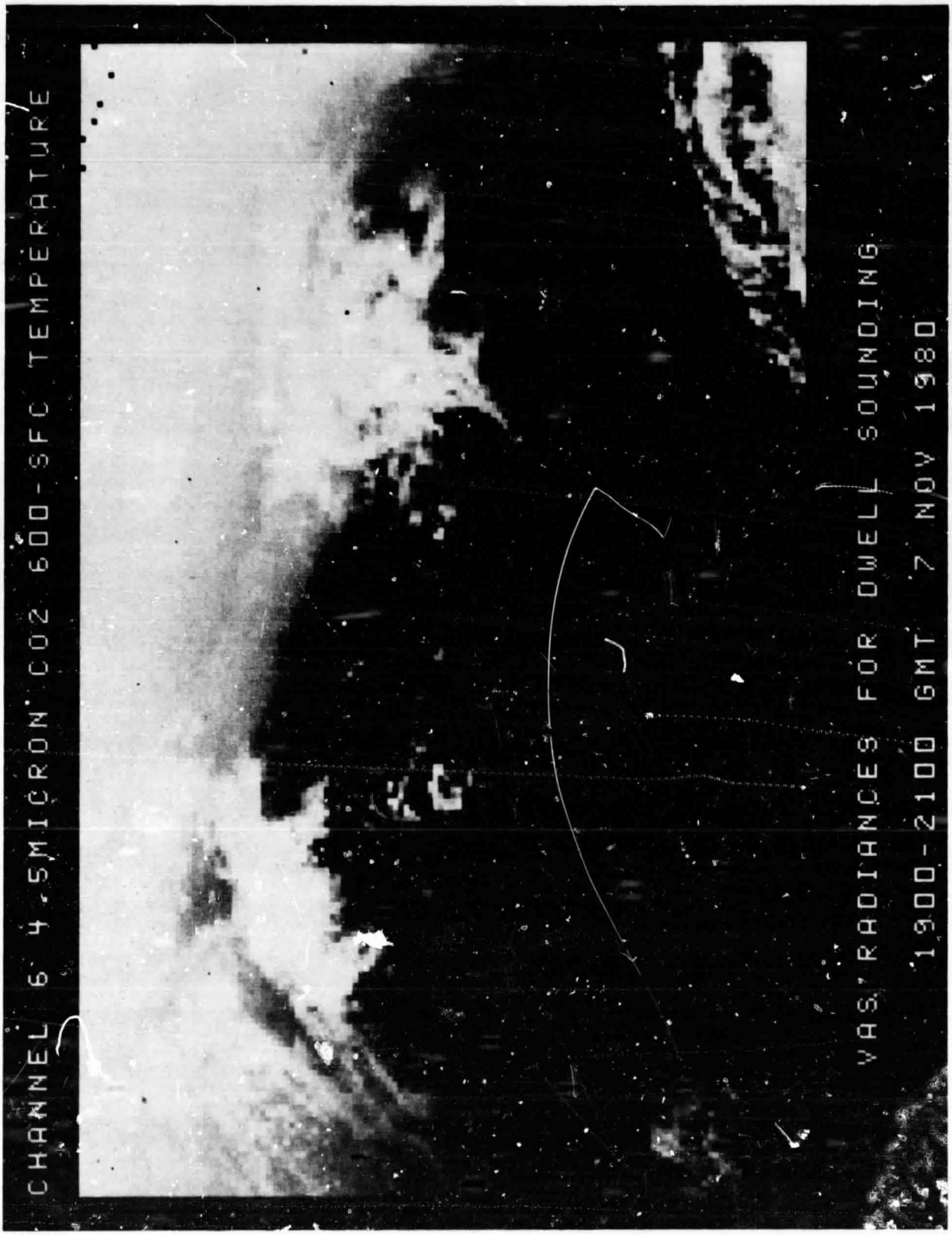

Figure 5f. VAS 12-page image sequence for SE USA on 7NOV80 (Continued)

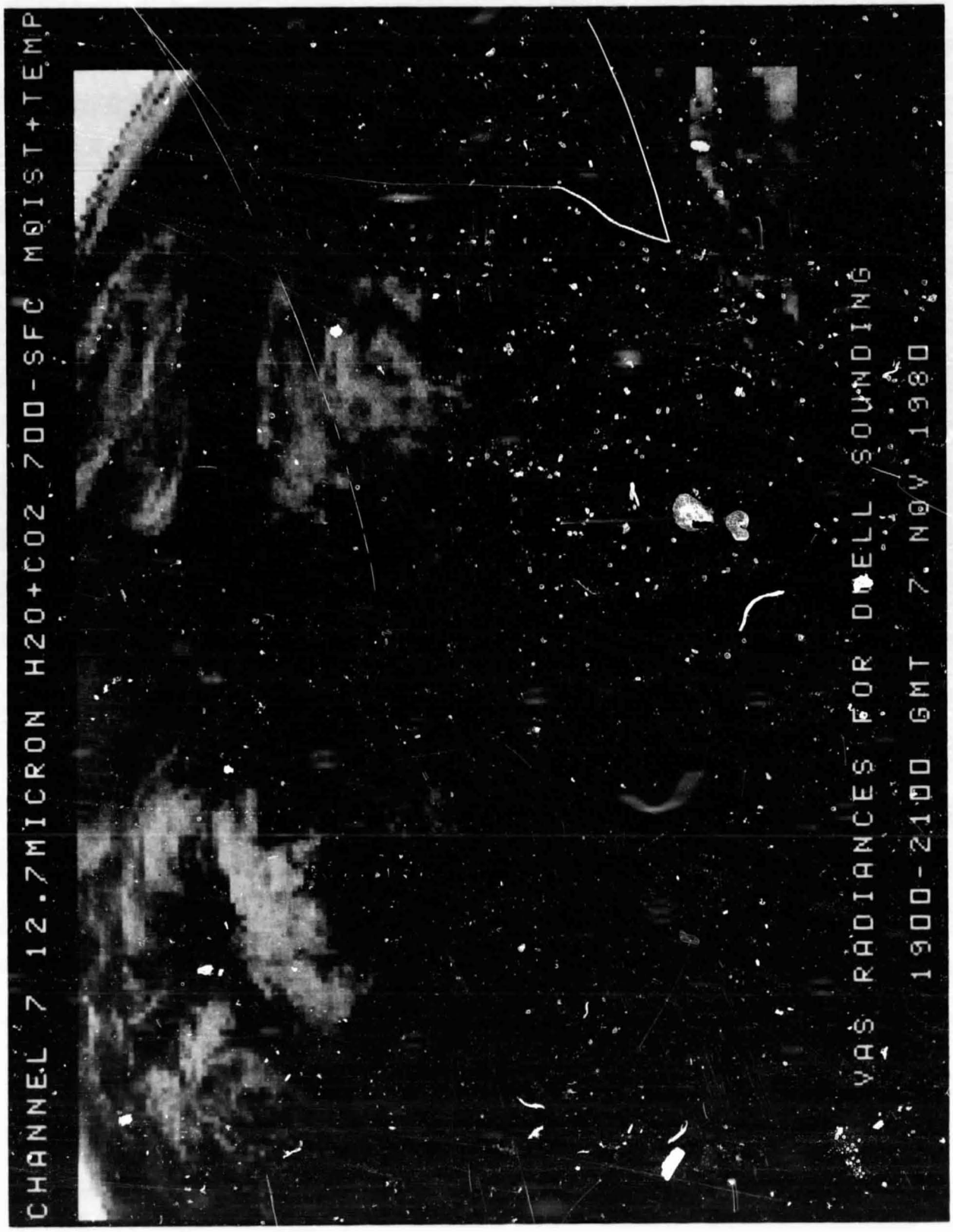

Figure 5g. VAS 12-page image sequence for SE USA on 7NOV80 (Continued)

Figure 5h. VAS 12-page image sequence for SE USA on 7NOV80 (Continued)

Figure 5i. VAS 12-page image sequence for SE USA on 7NOV80 (Continued)

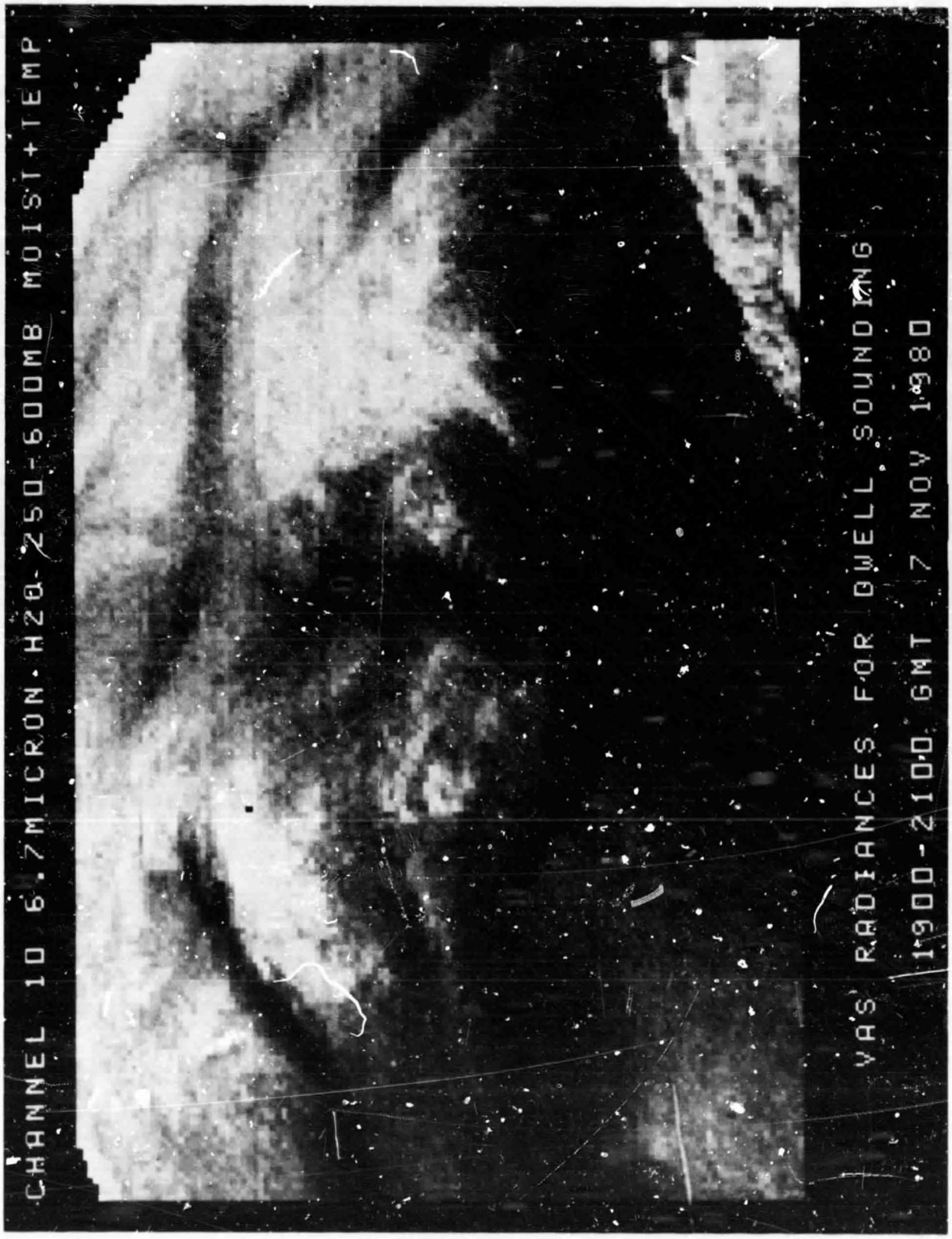

Figure 5j. VAS 12-page image sequence for SE USA on 7NOV80 (Continued)

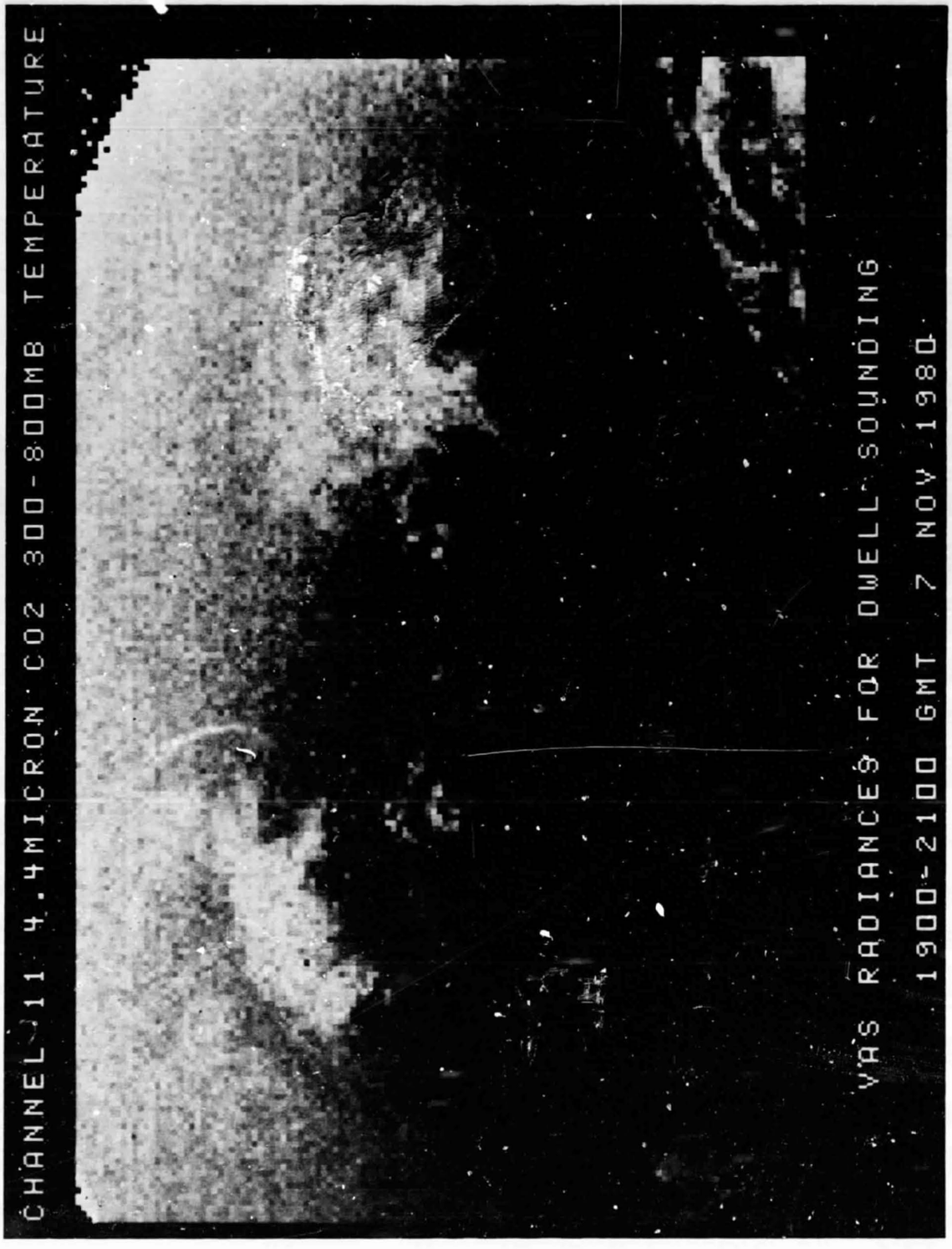

Figure 5k. VAS 12-page image sequence for SE USA on 7NOV80 (Continued)

C-2

Figure 51. VAS 12-page image sequence for SE USA on 7NOV80 (Continued)

ORIGINAL PAGE
BLACK AND WHITE PHOTOGRAPH

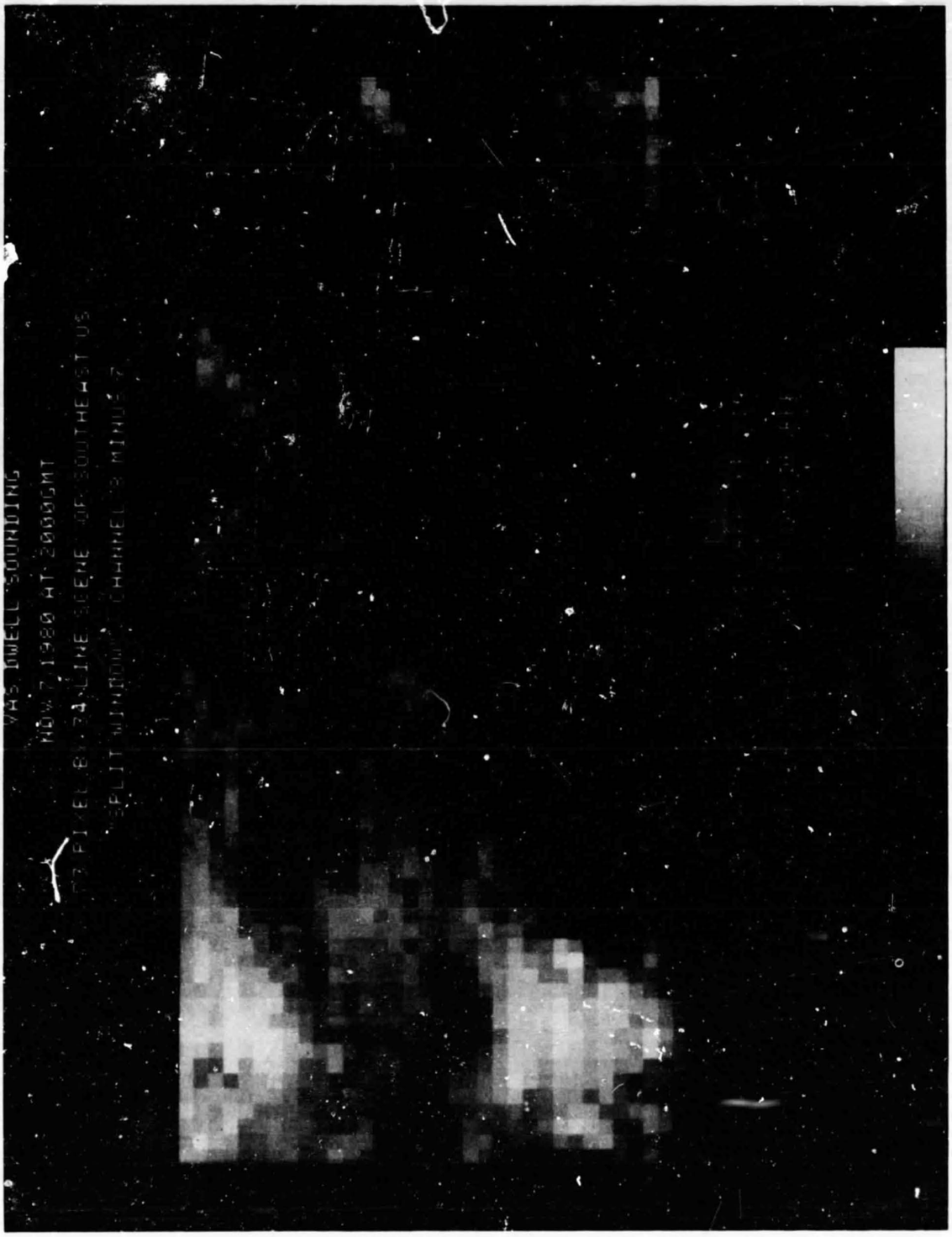

Figure 6. Image of "split window" contrast over SE USA

ORIGINAL PAGE
BLACK AND WHITE PHOTOGRAPH

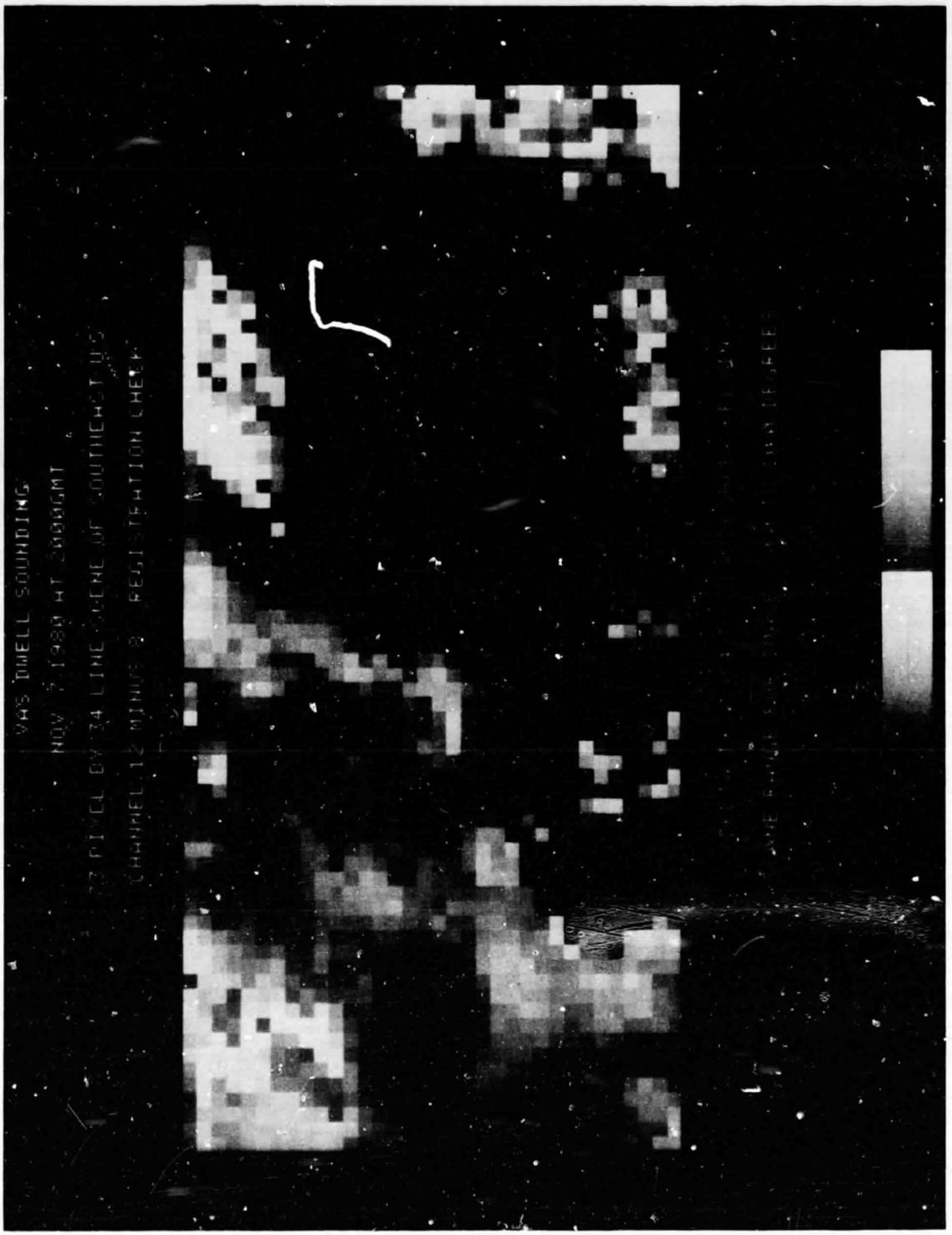

Figure 7. Image of "two window" difference over SE USA

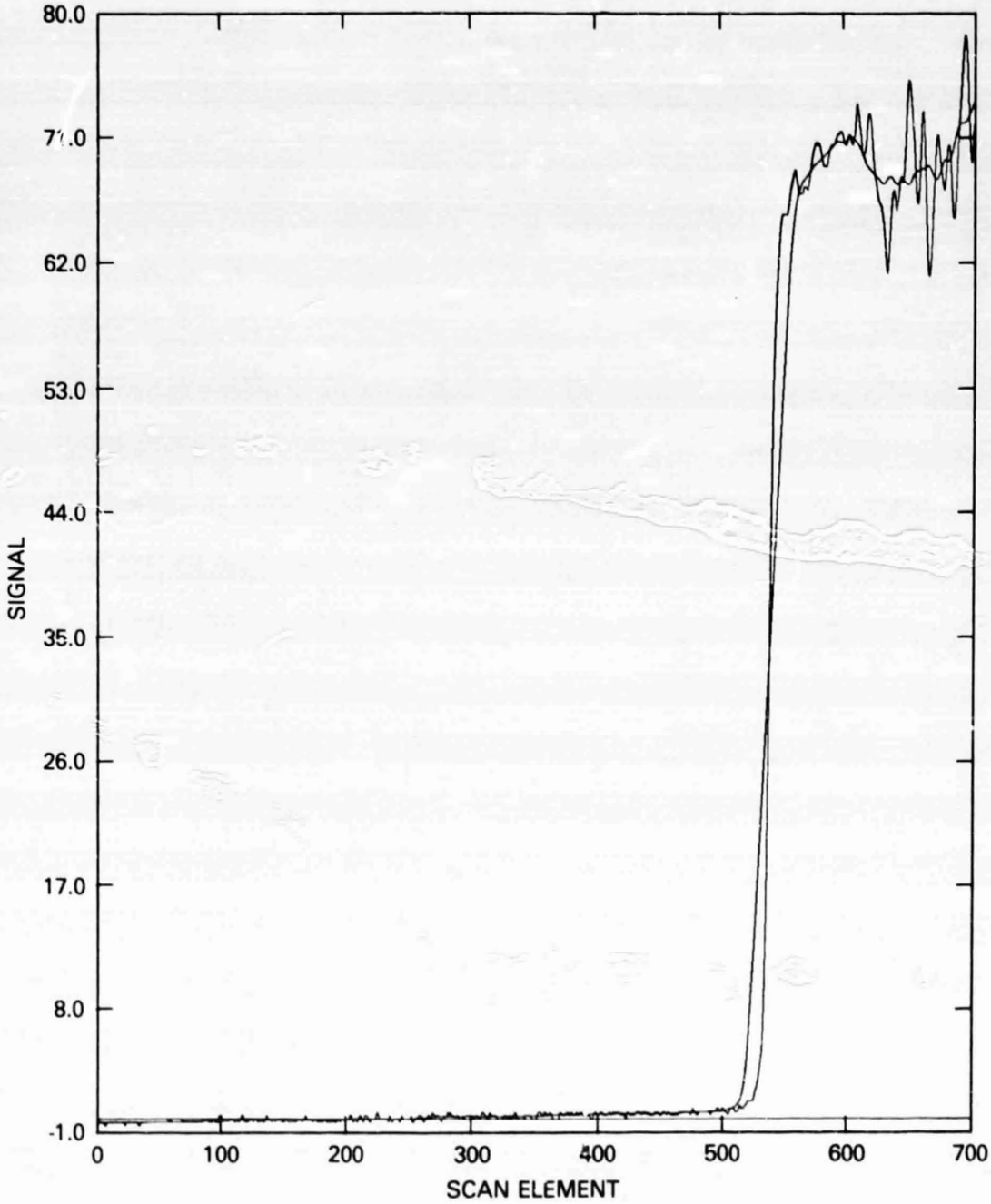

Figure 8. Western VAS pixels for one spin of channel 8

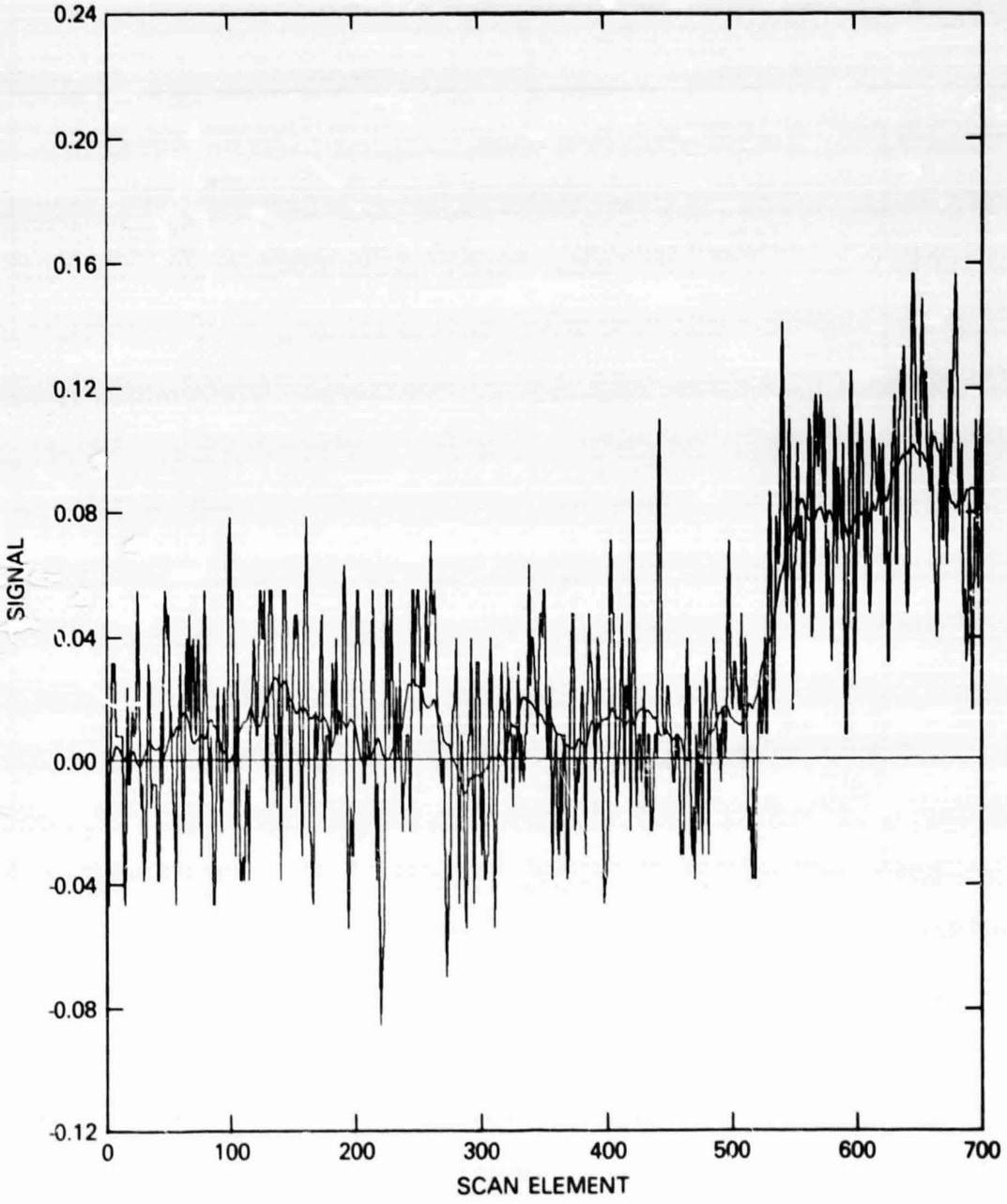

Figure 9. Western VAS pixels for one spin of channel 11

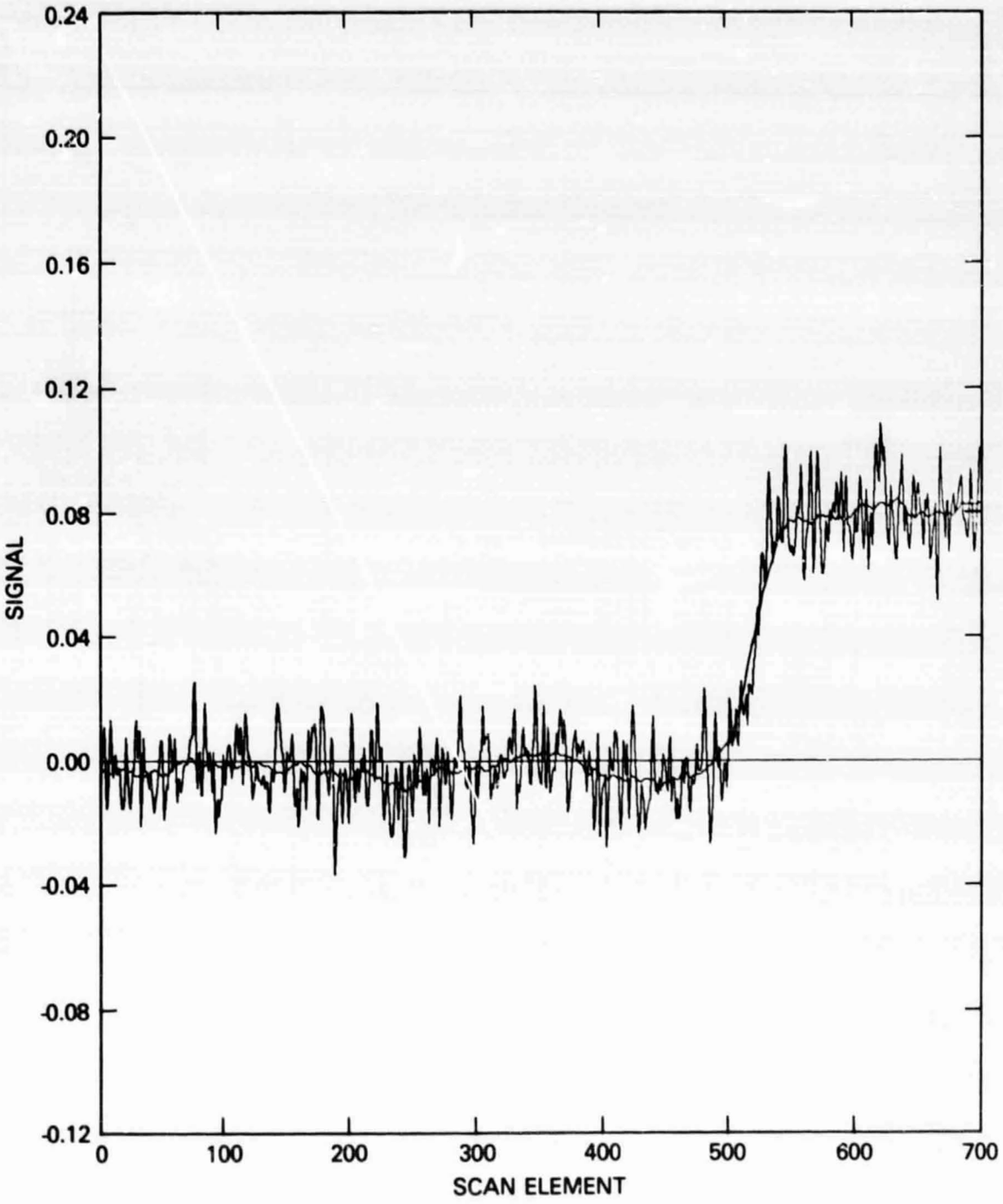

Figure 10. Western VAS pixels for one dwell line of channel 11

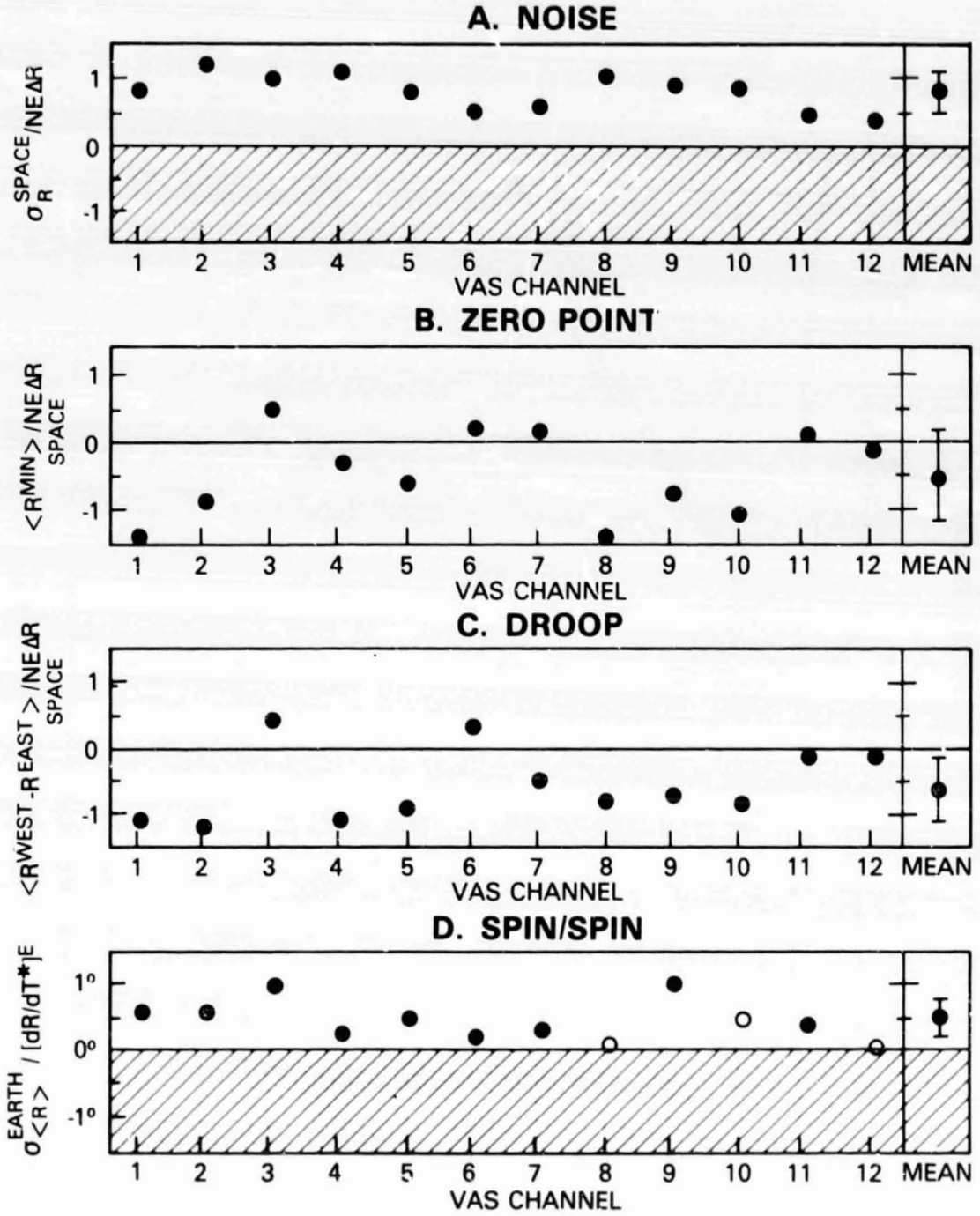

Figure 11. Quality assurance FOMs for VAS (A) noise, (B) zero point calibration, (C) droop, and (D) spin/spin stability

PRESSURE (MB)

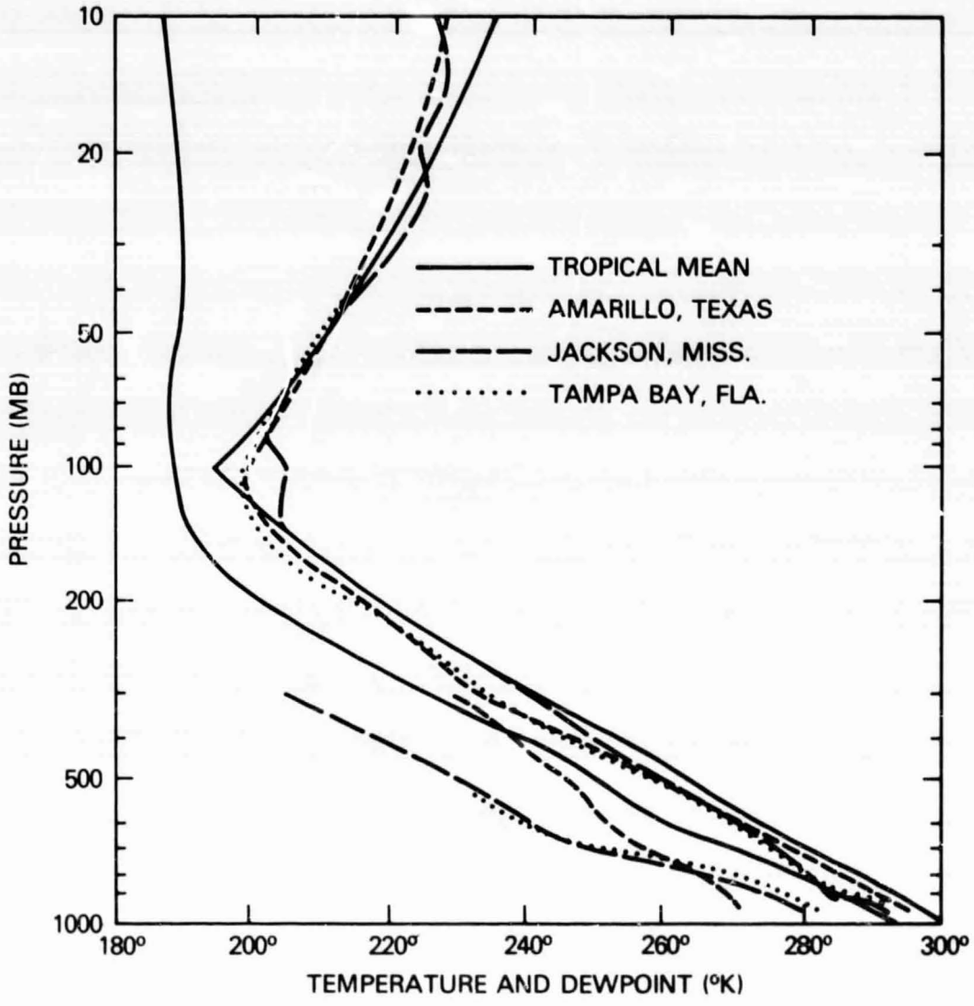

Figure 12. Temperature and dewpoint profiles at 3 key sites

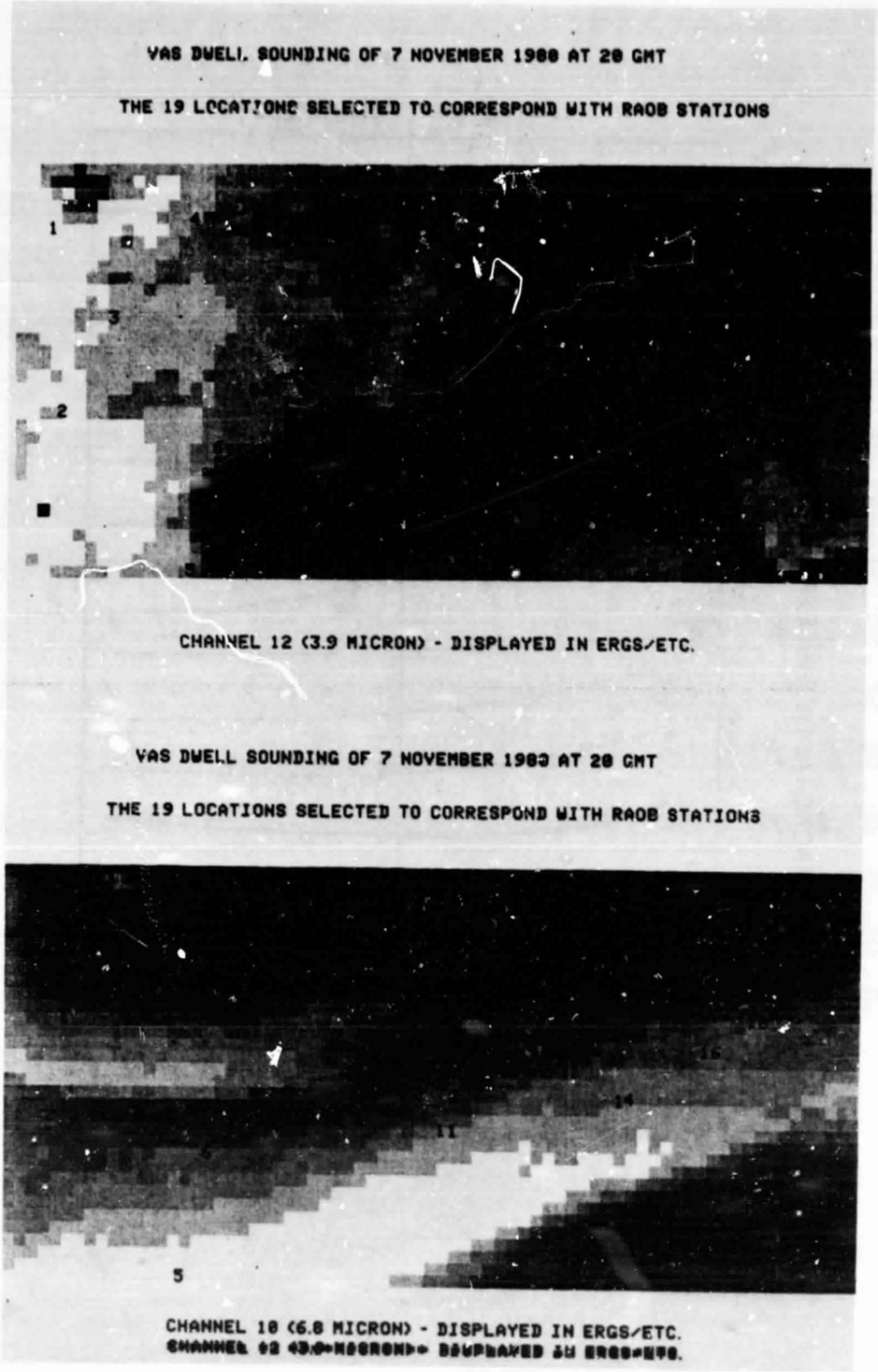

Figure 13. VAS images in channels 12 and 10 with 19 sites shown

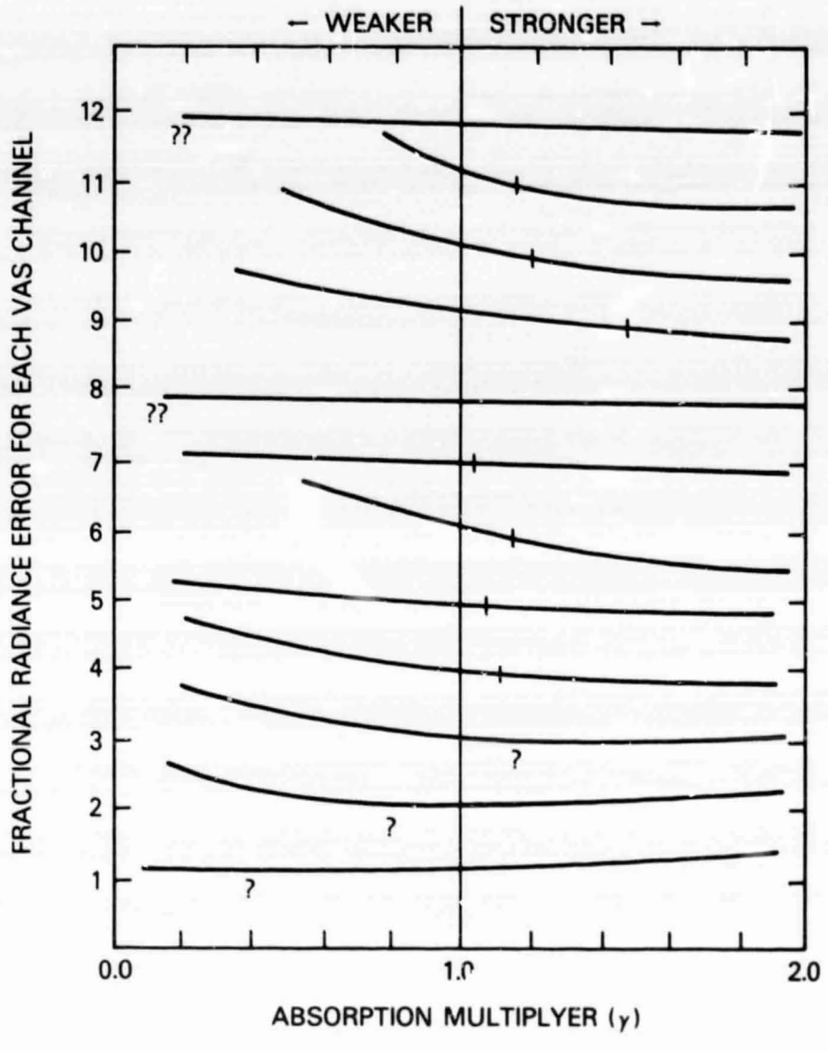

Figure 14. Calculated radiance versus the absorption strength γ-factor for each VAS channel at Tampa Bay on 7NOV80

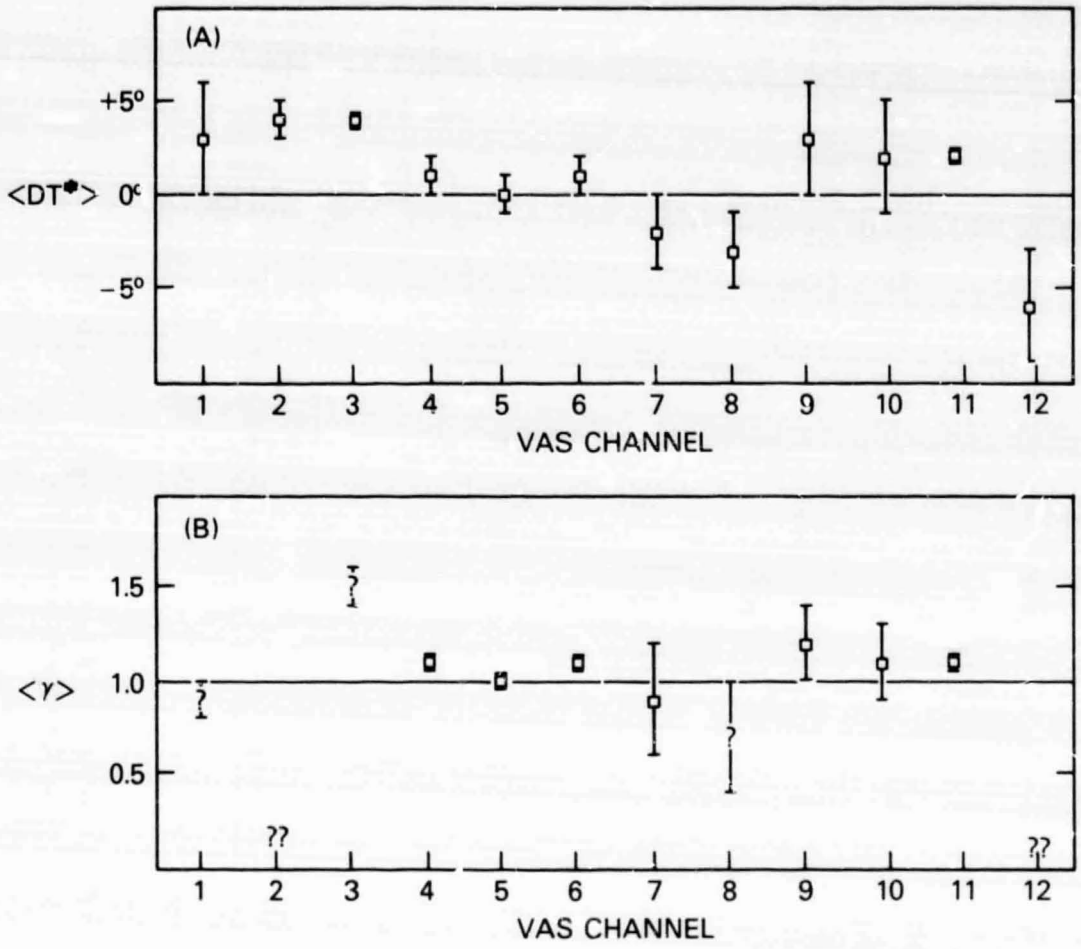

Figure 15. Mean and RMS of (A) T*(calc) – T*(obs) and (B) absorption γ-factors for the VAS channels at 19 RAOB sites

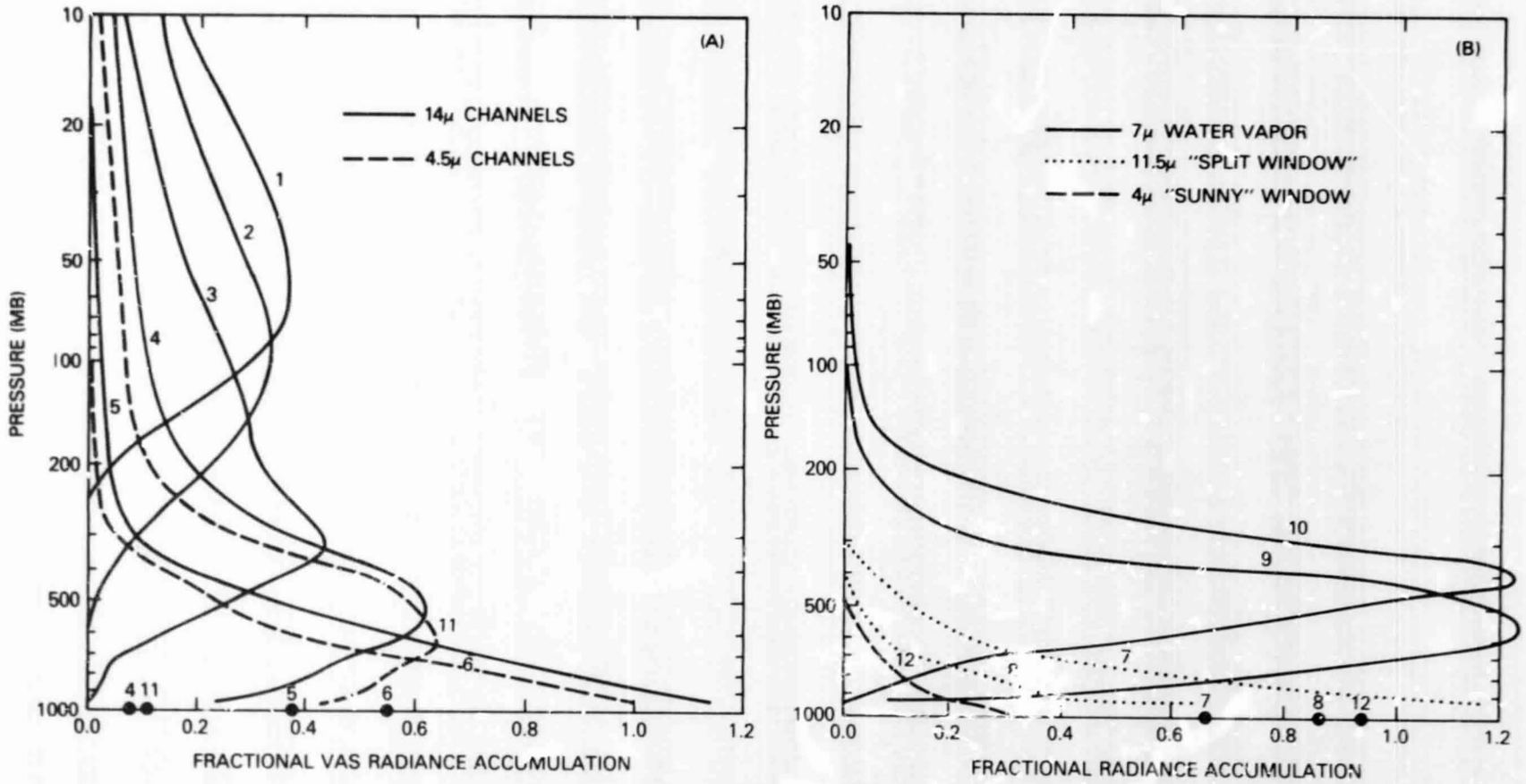

Figure 16. Fractional radiance accumulation functions for VAS (A) temperature sounding channels, and (B) moisture sounding and window channels

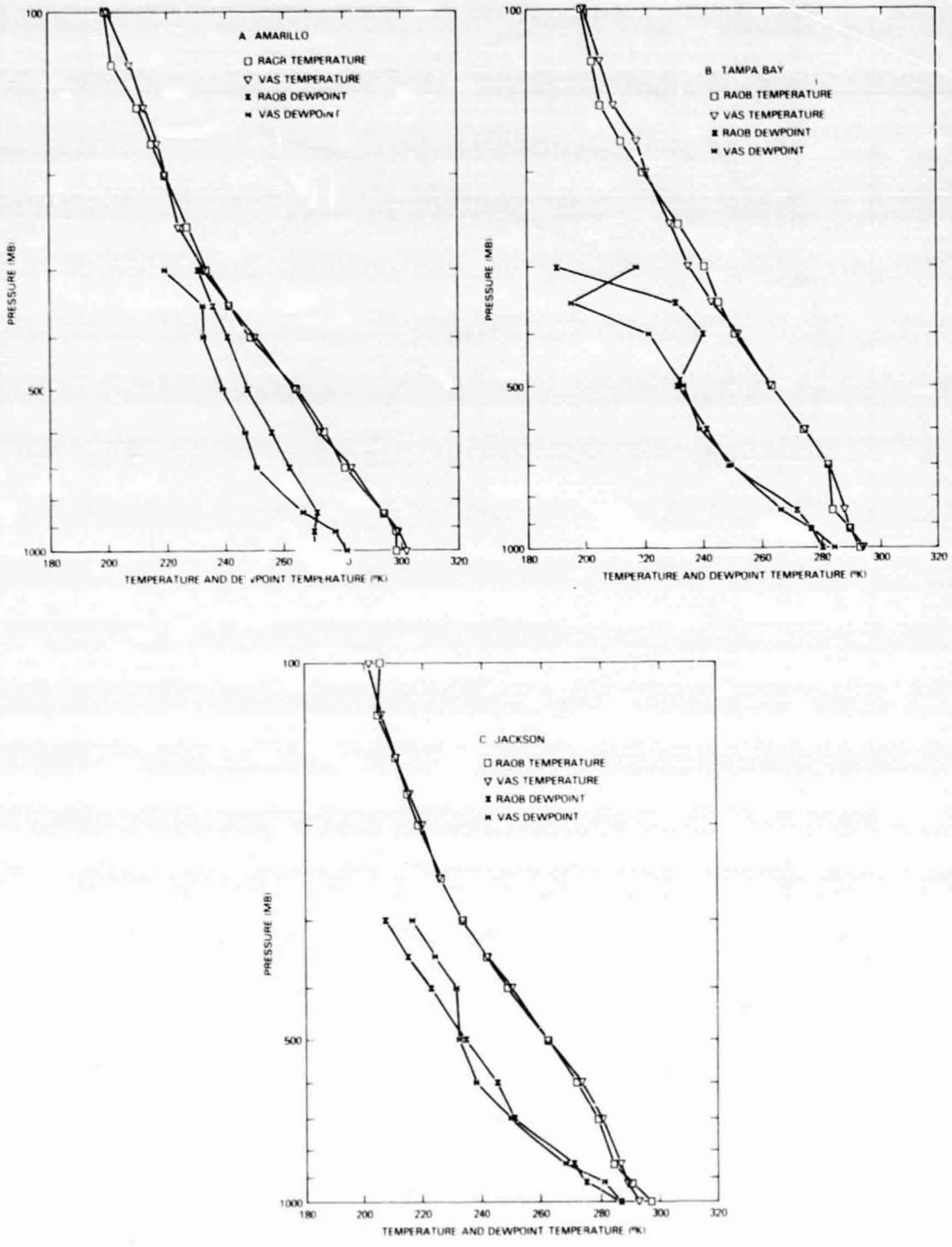

Figure 17. Temperature and dewpoint retrievals at 3 sites: (A) Amarillo, Texas, (B) Tampa Bay, Fla., and (C) Jackson, Miss.

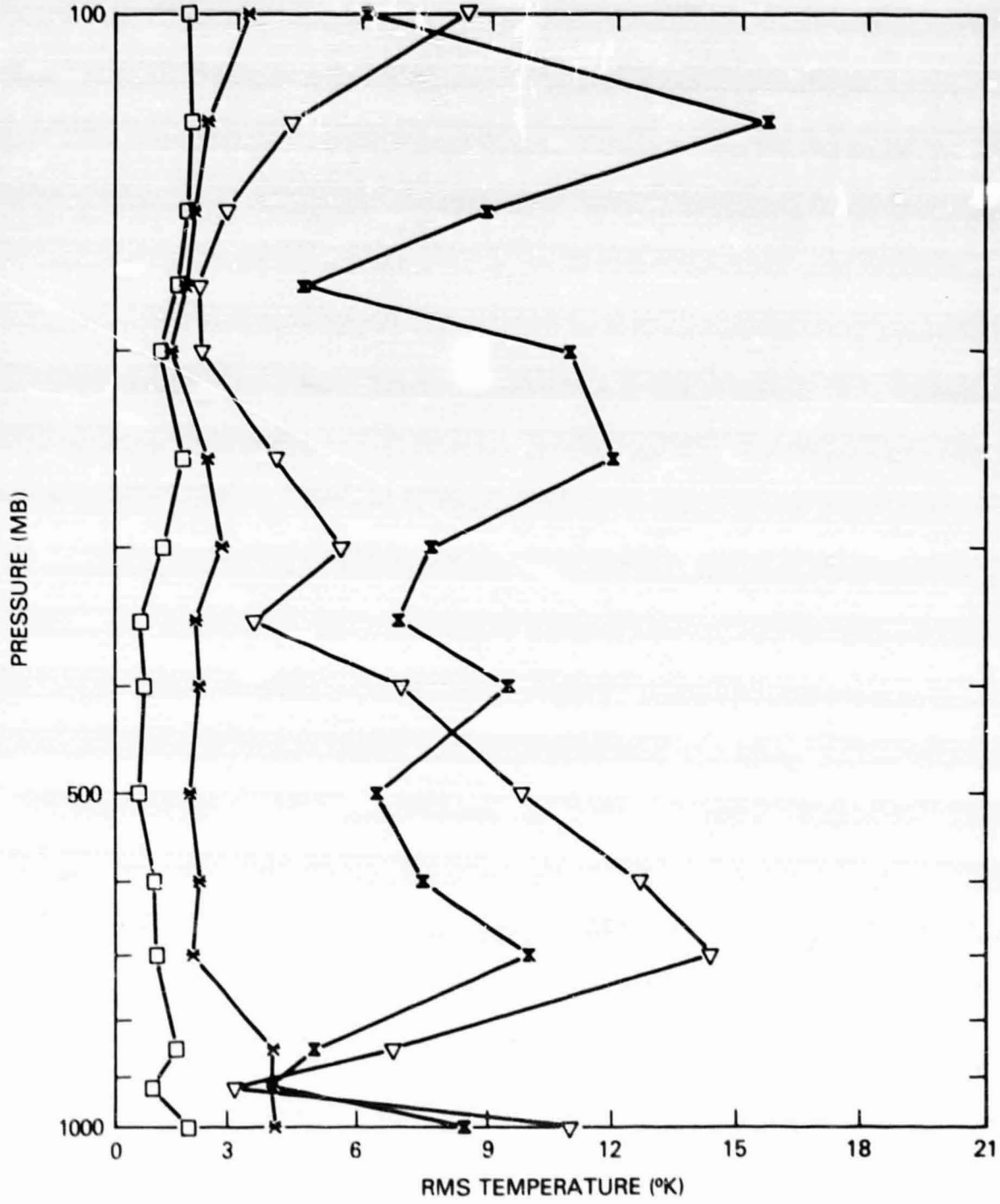

Figure 18. RMS temperature residuals, using (▽) NOAA32, (⧖) NSSL210, (□) SEUSA19 regression, compared to the (*) preretrieval variance

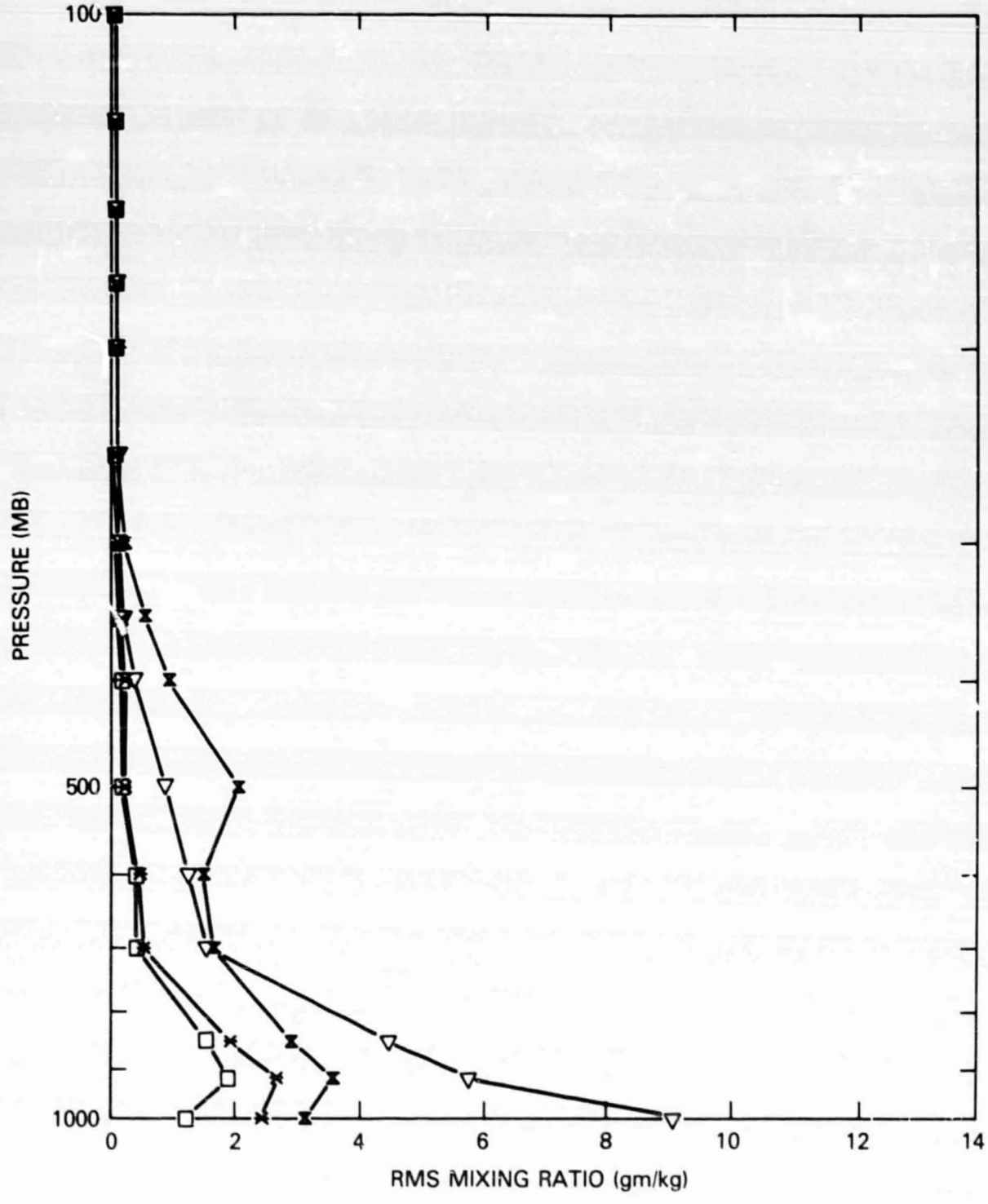

Figure 19. RMS mixing ratio residuals, using (▽) NOAA32, (⧖) NSSL210, (□) SEUSA19 regression, compared to the (*) preretrieval variance

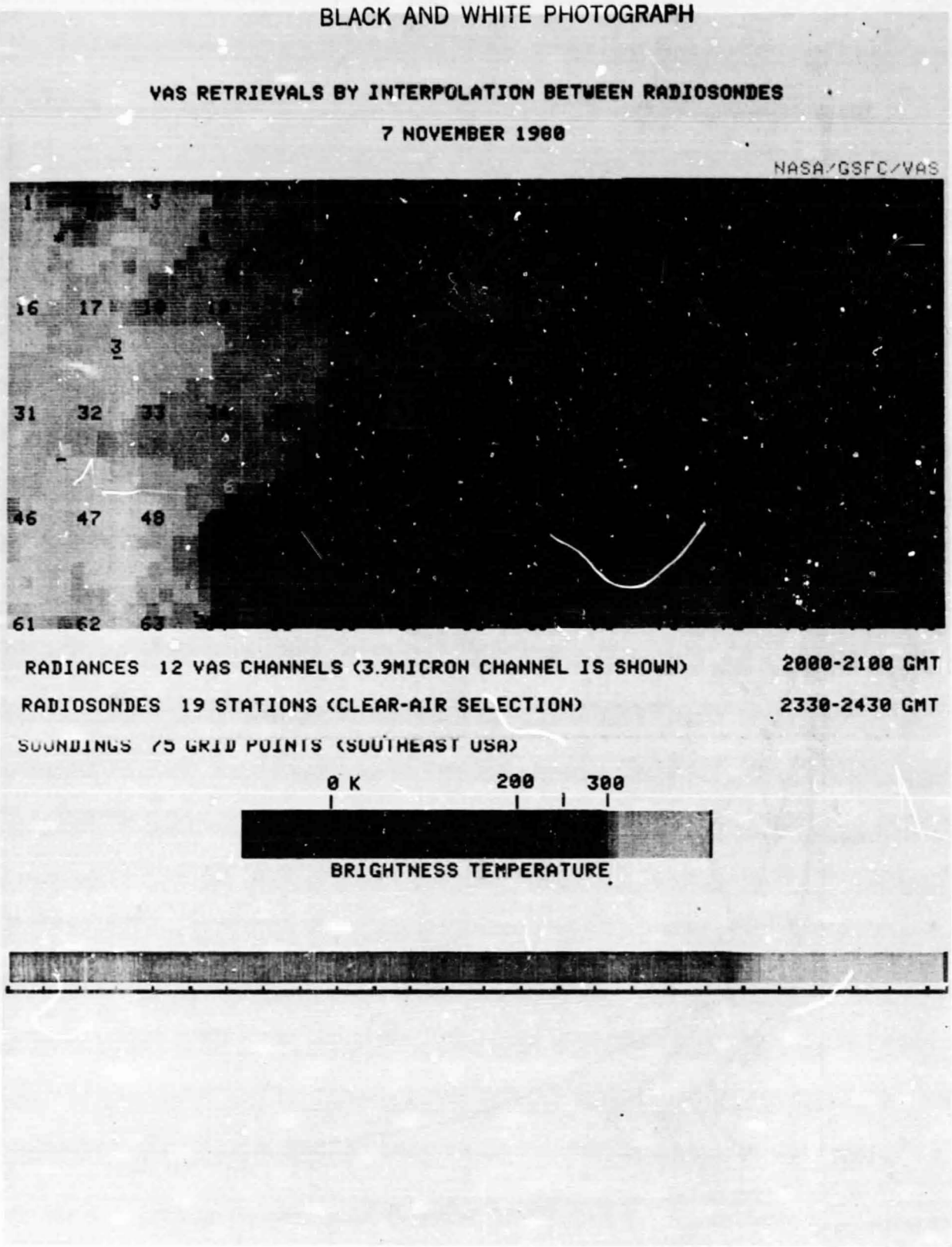

Figure 20. VAS image of SE USA, with 19 radiosonde and 75 retrieval sites

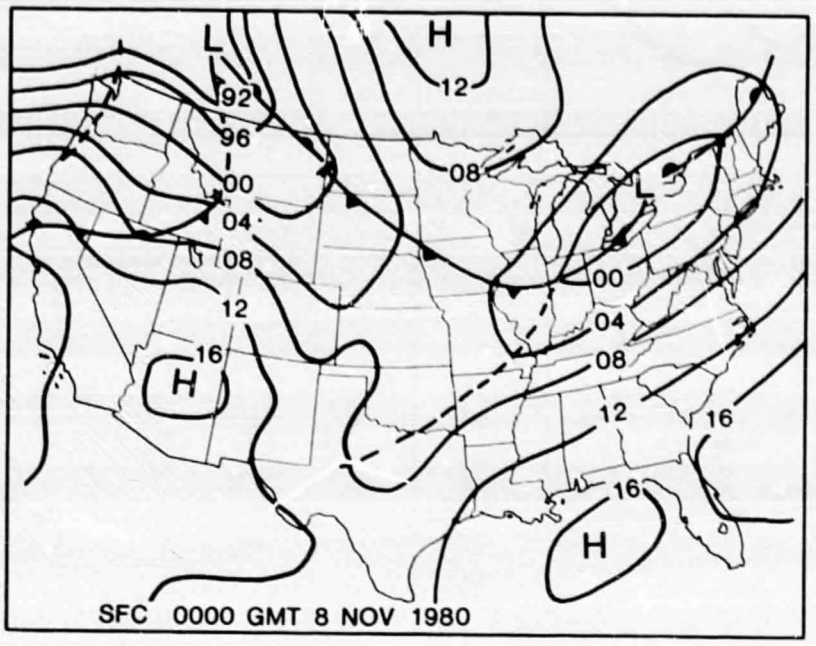

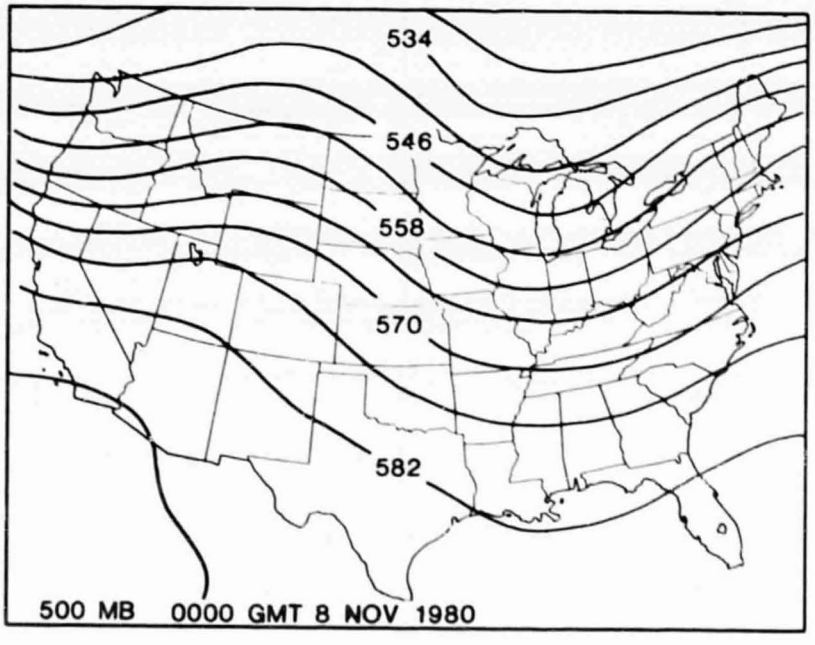

Figure 21. Conventional RAOB analyses of the (A) surface pressure and (B) 500 mb height field over the USA on the afternoon of 7NOV80

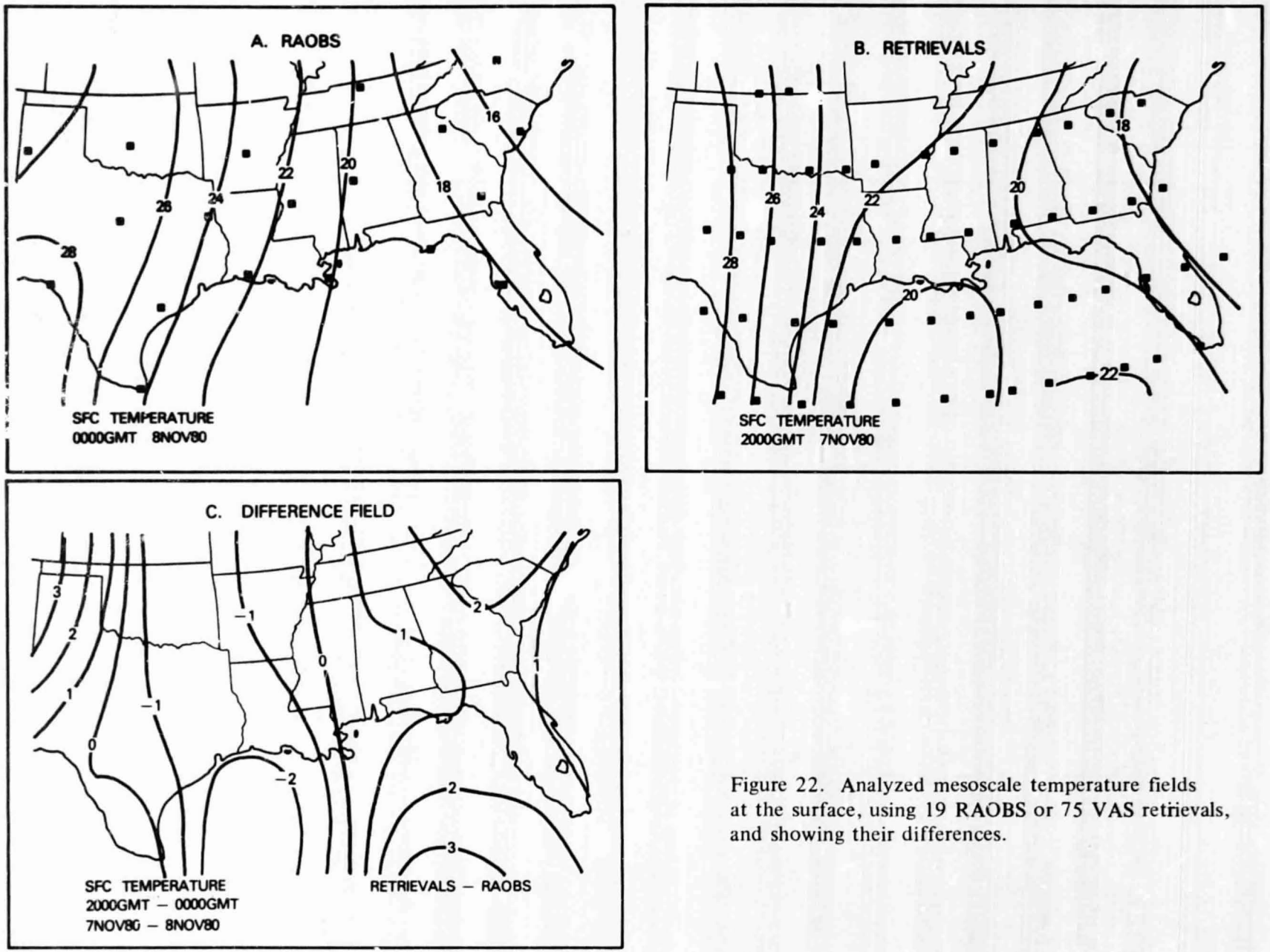

Figure 22. Analyzed mesoscale temperature fields at the surface, using 19 RAOBS or 75 VAS retrievals, and showing their differences.

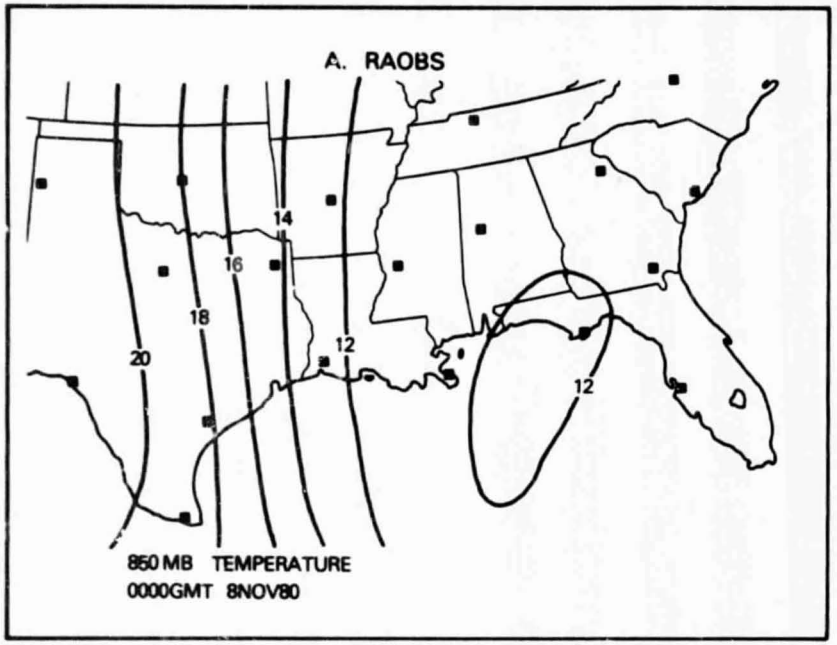

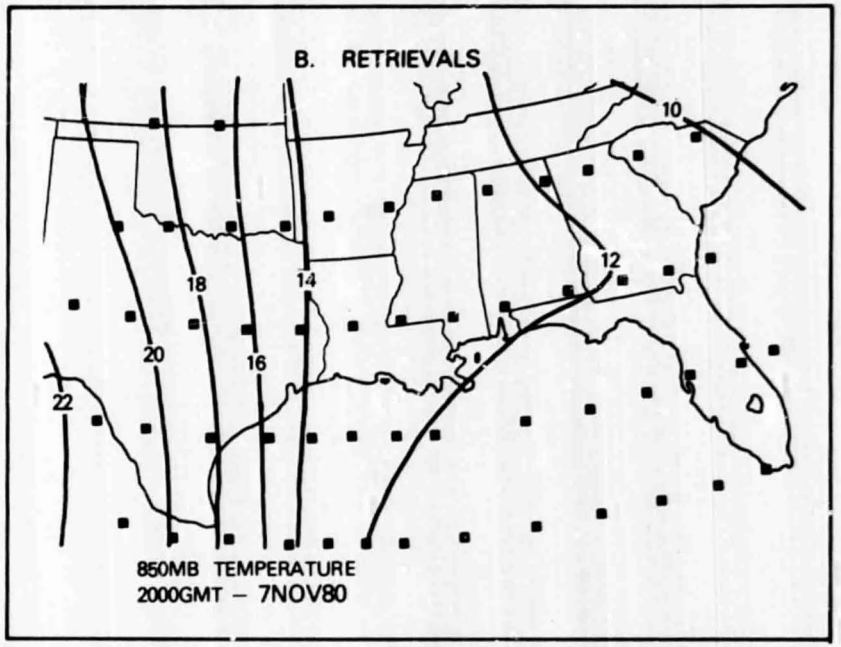

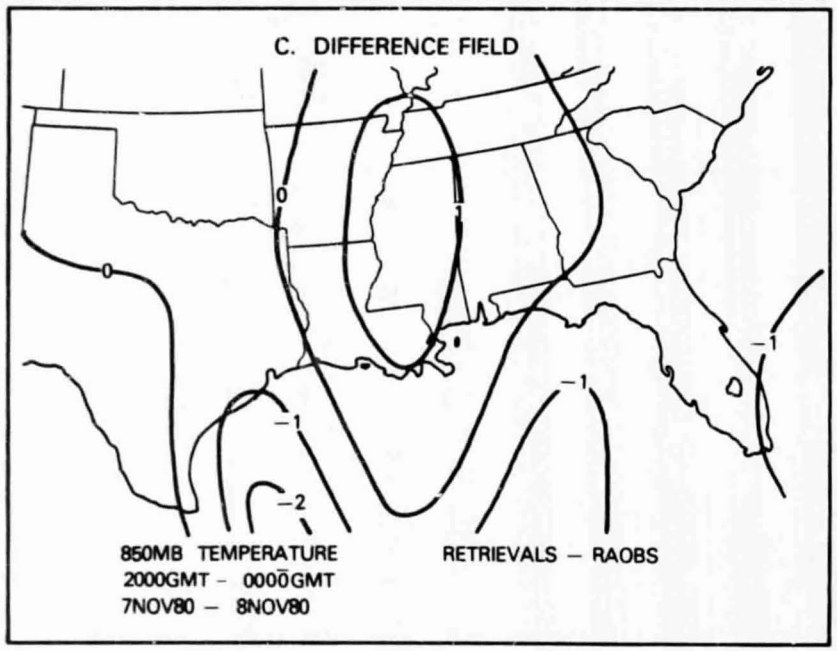

Figure 23. Analyzed mesoscale temperature fields at 850 mb

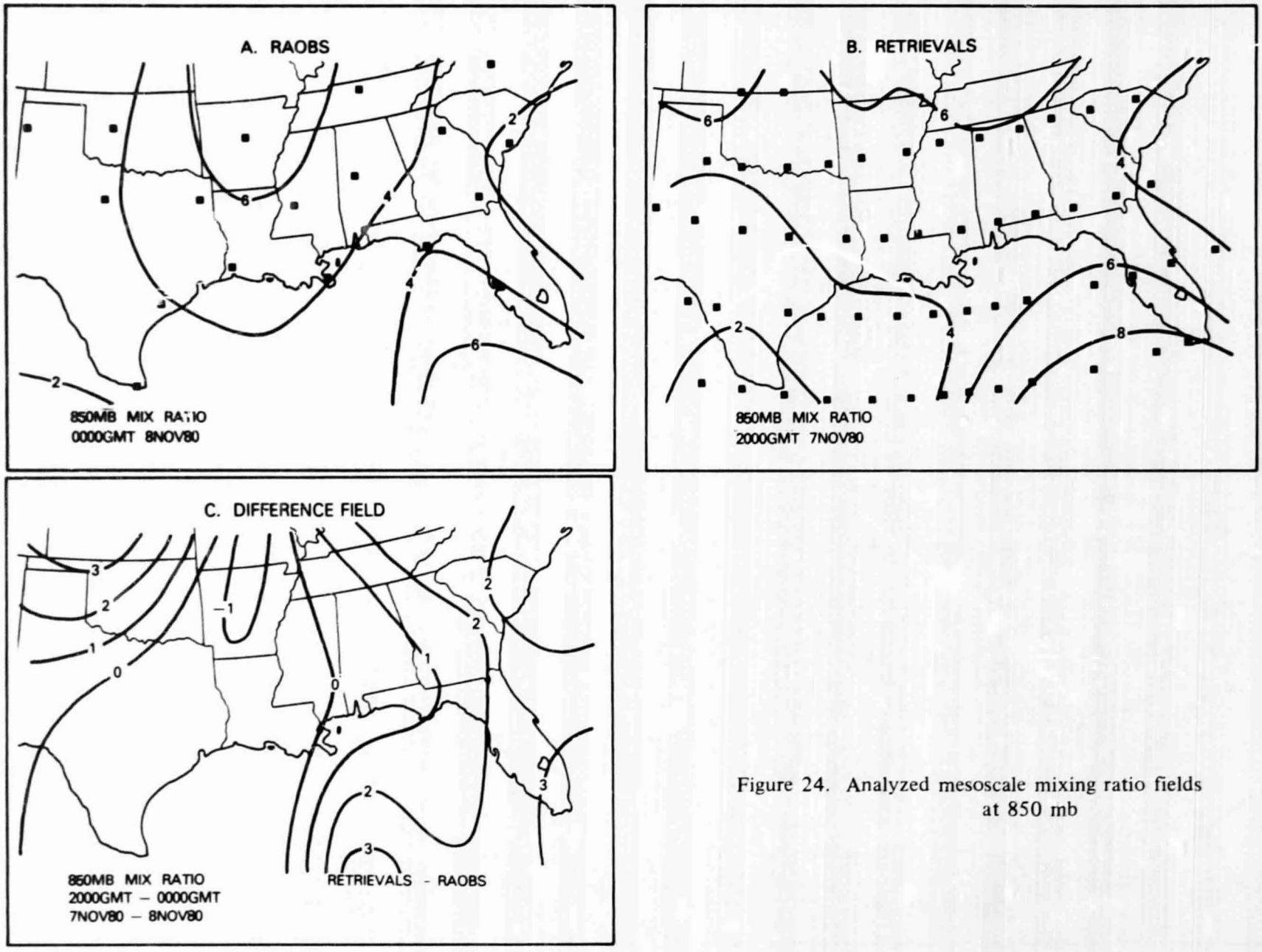

Figure 24. Analyzed mesoscale mixing ratio fields at 850 mb

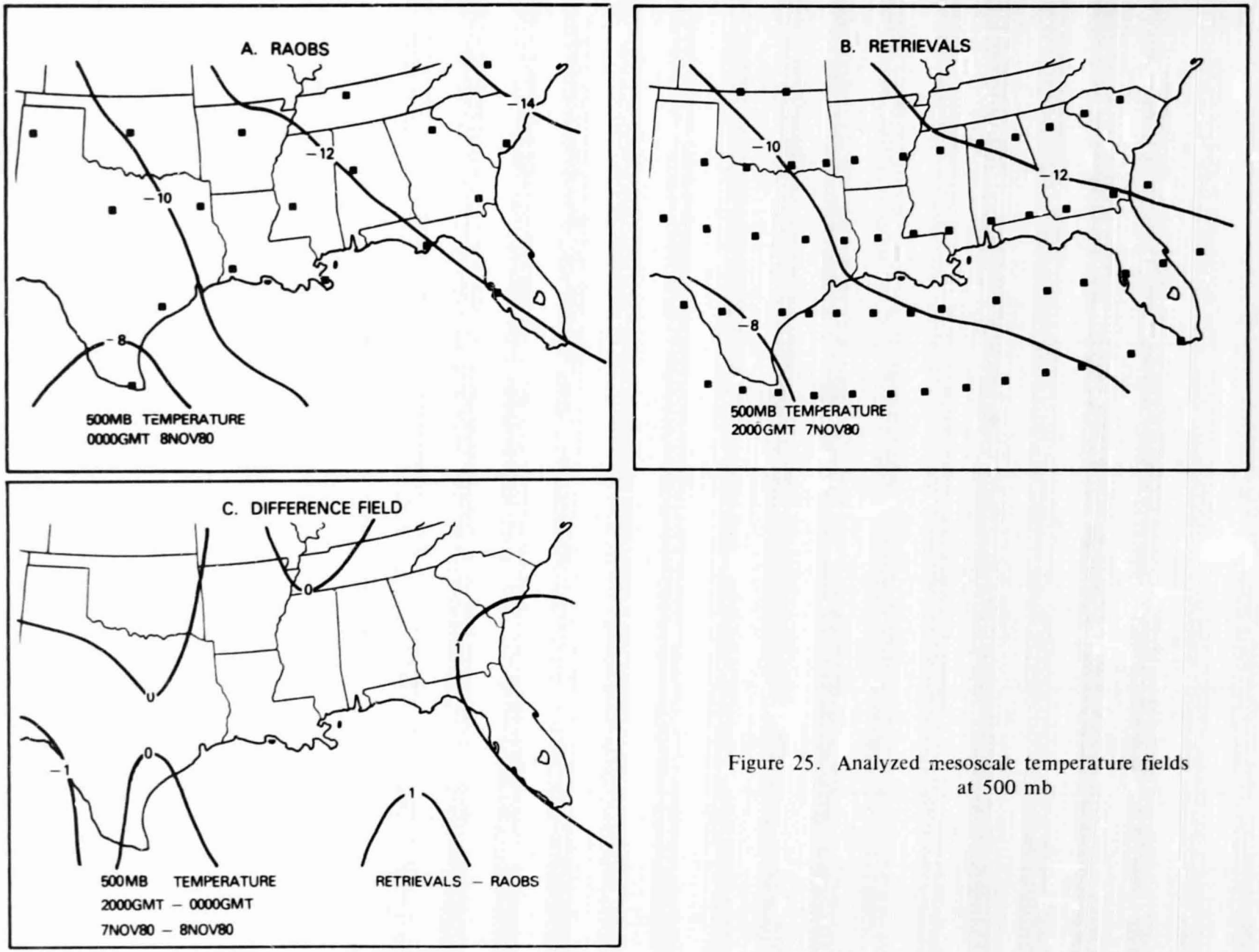

Figure 25. Analyzed mesoscale temperature fields at 500 mb

Table 1
Specifications for the 12 VAS sounding channels

VAS Ch #	Filt Cent μ	Filt Cent cm^{-1}	Filt Band cm^{-1}	Purpose for Sounding	Main Abs Gas	Other Signif Effects	Sample Noise ±°K	SFOV Req ±°K	Spin Budget Est.	Spin Budget Used
1	14.7	678	10	temp	CO_2	O_3	5.3	.3	38	2
2	14.5	691	16	temp	CO_2	O_3	2.2	.3	10	4
3	14.3	699	16	temp	CO_2	O_3	1.8	.3	7	7
4*	14.0	713	20	temp	CO_2	O_3	1.2	.2	4	7
5*	13.3	750	20	temp	CO_2	H_2O	1.0	.2	4	4
6	4.5	2209	45	temp+cloud	N_2O	sun	1.6	.1	35	7
7*	12.7	787	20	moisture	H_2O	CO_2	1.0	.2	4	3
8*	11.2	892	140	surface	–	H_2O+CO_2	0.1	.2	1	1
9*	7.3	1370	40	moisture	H_2O	–	3.4	.4	25	9
10*	6.8	1467	150	moisture	H_2O	–	1.6	.5	2	1
11	4.4	2254	40	temp+cloud	CO_2	sun	6.7	.3	46	7
12	3.9	2540	140	surface	–	sun+H_2O	0.8	.1	4	1

*Available at 7 km (nadir view) resolution.

Table 2
Estimated transmission properties of 12 VAS channels

VAS Ch #	Peak Weight (mb)	10%-90% Radiance Layer (mb)	Net sensitivity (°K/°C) Temp	Dewpt	Surf	Earth Mean (°K)	Earth σ (±°K)	"Signal" /Noise (°K/°K)
1	70	4-120	1.00	−.00	.00	219	10	2
2	125	4-225	.99	−.00	.00	219	9	4
3	200	15-475	.91	−.02	.00	223	7	4
4	500	40-900	.73	−.09	.02	238	9	7
5	920	420-surf	.47	−.30	.29	260	15	15
6	850	520-surf	.43	−.03	.44	257	17	11
7	1000	720-surf	.33	−.37	.63	270	19	19
8	surf	920-surf	.17	−.20	.84	272	21	210
9	600	110-820	.82	−.70	.02	254	10	3
10	400	240-620	.94	−.70	.00	246	7	4
11	300	7-1000	.80	−.01	.04	237	11	2
12	surf	surf-surf	.08	−.03	.92	273	22	27

Table 3
Key radiance specifications for VAS channels

VAS Ch #	Filter Waveno ν	Typical Scene R	T*	Noise Sounding NEΔR SFOV Req R	T*	R	T*	Absolute Calib. R	T*	Relative Calib. R	T*
1	679.786	40.85	216	10.40	11.2	.250	0.3	1.310	1.5	0.434	0.5
2	690.243	41.59	218	3.50	3.9	.250	0.3	1.330	1.5	0.441	0.5
3	700.170	47.94	226	3.00	3.1	.250	0.3	1.447	1.5	0.480	0.5
4	714.452	66.41	245	2.20	1.9	.250	0.2	1.744	1.5	0.579	0.5
5	750.348	99.78	274	2.10	1.4	.250	0.2	2.208	1.5	0.733	0.5
6	2208.068	1.18	274	0.06	1.2	.004	0.1	0.077	1.5	0.025	0.5
7	789.239	117.41	289	1.90	1.2	.250	0.2	2.456	1.5	0.816	0.5
8	897.400	109.52	295	0.30	0.2	.250	0.2	2.484	1.5	0.825	0.5
9	1374.872	14.06	257	1.80	4.1	.150	0.4	0.643	1.5	0.212	0.5
10	1486.125	5.69	242	0.48	2.2	.100	0.5	0.318	1.5	0.105	0.5
11	2252.566	0.23	224	0.07	5.1	.004	0.3	0.020	1.5	0.006	0.5
12	2541.064	0.84	296	0.02	0.6	.004	0.1	0.054	1.5	0.018	0.5

Table 4

VAS Plank radiances for 150°-350°K in 1°K steps

CHANNEL NUM	1	2	3	4	5	6	7	8	9	10	11	12
WAVENO 1/CM	679.786	693.243	708.170	714.452	750.348	2208.068	789.239	897.400	1374.872	1486.125	2252.566	2541.064
TEMP (K)												
151.	5.769	5.457	5.182	4.894	3.952	0.000	3.174	1.664	0.063	0.028	0.000	0.000
152.	6.011	5.699	5.414	5.024	4.142	0.000	3.335	1.760	0.069	0.033	0.000	0.000
153.	6.270	5.948	5.654	5.252	4.339	0.000	3.502	1.861	0.075	0.038	0.000	0.000
154.	6.535	6.205	5.902	5.486	4.543	0.000	3.675	1.966	0.082	0.035	0.000	0.000
155.	6.813	6.469	6.157	5.728	4.753	0.000	3.854	2.075	0.089	0.048	0.000	0.000
156.	7.092	6.740	6.419	5.977	4.970	0.000	4.039	2.189	0.096	0.044	0.000	0.000
157.	7.387	7.020	6.689	6.233	5.195	0.000	4.231	2.307	0.104	0.048	0.000	0.000
158.	7.693	7.307	6.967	6.498	5.426	0.000	4.433	2.431	0.113	0.052	0.000	0.000
159.	7.984	7.602	7.252	6.769	5.664	0.000	4.635	2.559	0.122	0.056	0.000	0.000
160.	8.298	7.906	7.546	7.049	5.910	0.000	4.846	2.692	0.132	0.061	0.000	0.000
161.	8.620	8.217	7.847	7.336	6.164	0.000	5.065	2.831	0.143	0.067	0.000	0.000
162.	8.950	8.537	8.157	7.632	6.424	0.000	5.290	2.974	0.154	0.072	0.000	0.000
163.	9.289	8.864	8.475	7.935	6.693	0.000	5.523	3.123	0.166	0.078	0.000	0.000
164.	9.636	9.201	8.801	8.247	6.969	0.000	5.763	3.278	0.179	0.085	0.000	0.000
165.	9.991	9.546	9.135	8.567	7.253	0.001	6.010	3.438	0.192	0.092	0.000	0.000
166.	10.355	9.899	9.478	8.895	7.545	0.001	6.265	3.604	0.207	0.099	0.000	0.000
167.	10.729	10.261	9.830	9.232	7.845	0.001	6.527	3.776	0.222	0.107	0.001	0.000
168.	11.110	10.632	10.190	9.577	8.154	0.001	6.797	3.954	0.238	0.116	0.001	0.000
169.	11.501	11.011	10.559	9.931	8.470	0.001	7.075	4.138	0.255	0.125	0.001	0.000
170.	11.900	11.400	10.937	10.294	8.795	0.001	7.361	4.329	0.273	0.135	0.001	0.000
171.	12.309	11.797	11.324	10.665	9.128	0.001	7.654	4.525	0.293	0.145	0.001	0.000
172.	12.726	12.203	11.720	11.046	9.470	0.001	7.956	4.728	0.313	0.156	0.001	0.000
173.	13.153	12.619	12.124	11.435	9.821	0.001	8.266	4.938	0.335	0.168	0.001	0.000
174.	13.589	13.044	12.538	11.833	10.180	0.002	8.584	5.155	0.357	0.180	0.001	0.000
175.	14.034	13.478	12.961	12.241	10.549	0.002	8.911	5.378	0.381	0.193	0.001	0.000
176.	14.489	13.921	13.394	12.657	10.926	0.002	9.246	5.609	0.407	0.207	0.001	0.000
177.	14.953	14.373	13.835	13.083	11.312	0.002	9.590	5.846	0.433	0.221	0.002	0.000
178.	15.426	14.835	14.287	13.519	11.707	0.002	9.942	6.091	0.461	0.237	0.002	0.000
179.	15.909	15.307	14.747	13.963	12.112	0.003	10.304	6.343	0.491	0.254	0.002	0.000
180.	16.402	15.788	15.217	14.418	12.525	0.003	10.674	6.603	0.522	0.271	0.002	0.000
181.	16.904	16.279	15.697	14.881	12.948	0.003	11.053	6.870	0.555	0.289	0.002	0.000
182.	17.416	16.779	16.186	15.355	13.381	0.003	11.442	7.145	0.589	0.309	0.003	0.000
183.	17.937	17.289	16.686	15.838	13.823	0.004	11.839	7.427	0.625	0.329	0.003	0.000
184.	18.469	17.809	17.194	16.331	14.275	0.004	12.246	7.718	0.663	0.351	0.003	0.000
185.	19.010	18.339	17.713	16.833	14.736	0.004	12.663	8.016	0.703	0.373	0.003	0.001
186.	19.561	18.878	18.242	17.346	15.207	0.005	13.088	8.323	0.744	0.397	0.004	0.001
187.	20.122	19.428	18.780	17.868	15.688	0.005	13.524	8.638	0.788	0.423	0.004	0.001
188.	20.692	19.987	19.329	18.401	16.179	0.006	13.969	8.962	0.833	0.449	0.004	0.001
189.	21.273	20.557	19.887	18.943	16.680	0.006	14.424	9.294	0.881	0.477	0.005	0.001
190.	21.854	21.137	20.456	19.496	17.190	0.007	14.888	9.635	0.931	0.506	0.005	0.001
191.	22.455	21.726	21.035	20.058	17.711	0.008	15.363	9.984	0.983	0.537	0.006	0.001
192.	23.076	22.326	21.624	20.631	18.242	0.008	15.847	10.342	1.037	0.569	0.006	0.001
193.	23.697	22.936	22.223	21.214	18.784	0.009	16.342	10.709	1.094	0.603	0.007	0.001
194.	24.328	23.556	22.832	21.808	19.335	0.010	16.846	11.086	1.154	0.638	0.008	0.001
195.	24.970	24.187	23.452	22.412	19.897	0.011	17.361	11.471	1.216	0.676	0.008	0.001
196.	25.621	24.828	24.082	23.026	20.470	0.012	17.886	11.865	1.280	0.714	0.009	0.002
197.	26.283	25.479	24.723	23.651	21.053	0.013	18.422	12.270	1.348	0.755	0.010	0.002
198.	26.956	26.140	25.374	24.286	21.646	0.014	18.968	12.683	1.418	0.798	0.011	0.002
199.	27.638	26.812	26.035	24.931	22.250	0.015	19.524	13.107	1.491	0.844	0.011	0.002
200.	28.331	27.494	26.707	25.587	22.865	0.016	20.091	13.539	1.567	0.889	0.012	0.002

Table 4
VAS Plank radiances for 150°-350° K in 1° K steps (Continued)

CHANNEL NUM	1	2	3	4	5	6	7	8	9	10	11	12
WAVENO 1/CM	679.785	690.243	700.170	714.452	750.348	2208.068	789.239	397.400	1374.872	1486.185	2252.566	2541.064
TEMP (K)												
201.	29.034	28.187	27.389	26.254	23.490	0.018	20.669	13.982	1.646	0.937	0.014	0.002
202.	29.745	28.890	28.082	26.932	24.126	0.019	21.257	14.435	1.728	0.988	0.015	0.003
203.	30.472	29.608	28.785	27.620	24.773	0.020	21.856	14.897	1.813	1.041	0.016	0.003
204.	31.206	30.327	29.499	28.318	25.430	0.022	22.466	15.370	1.902	1.096	0.017	0.003
205.	31.951	31.062	30.224	29.028	26.099	0.024	23.087	15.853	1.994	1.153	0.019	0.004
206.	32.705	31.807	30.959	29.748	26.778	0.026	23.719	16.346	2.090	1.213	0.020	0.004
207.	33.472	32.563	31.705	30.479	27.469	0.028	24.362	16.849	2.189	1.276	0.022	0.004
208.	34.249	33.329	32.461	31.221	28.170	0.030	25.015	17.363	2.292	1.341	0.023	0.005
209.	35.034	34.106	33.228	31.973	28.882	0.032	25.681	17.888	2.399	1.410	0.025	0.005
210.	35.831	34.894	34.006	32.737	29.606	0.034	26.357	18.423	2.509	1.482	0.027	0.005
211.	36.639	35.692	34.795	33.511	30.340	0.037	27.044	18.969	2.624	1.556	0.029	0.006
212.	37.457	36.501	35.594	34.296	31.086	0.040	27.743	19.526	2.742	1.634	0.031	0.006
213.	38.285	37.320	36.405	35.092	31.843	0.043	28.453	20.093	2.865	1.717	0.034	0.007
214.	39.125	38.150	37.226	35.899	32.611	0.046	29.174	20.672	2.992	1.804	0.036	0.007
215.	39.974	38.991	38.057	36.717	33.391	0.049	29.907	21.262	3.124	1.894	0.039	0.008
216.	40.834	39.842	38.900	37.546	34.181	0.052	30.651	21.863	3.260	1.988	0.041	0.009
217.	41.705	40.704	39.753	38.386	34.983	0.056	31.407	22.475	3.400	2.086	0.044	0.009
218.	42.586	41.577	40.617	39.237	35.797	0.060	32.174	23.099	3.545	2.188	0.048	0.010
219.	43.478	42.461	41.492	40.099	36.621	0.064	32.953	23.734	3.695	2.297	0.051	0.011
220.	44.380	43.355	42.378	40.972	37.458	0.069	33.743	24.380	3.850	2.369	0.054	0.012
221.	45.293	44.260	43.275	41.856	38.305	0.073	34.545	25.038	4.010	2.454	0.058	0.013
222.	46.216	45.175	44.182	42.751	39.164	0.078	35.359	25.708	4.175	2.564	0.062	0.014
223.	47.150	46.101	45.101	43.657	40.034	0.084	36.185	26.389	4.346	2.677	0.066	0.015
224.	48.094	47.038	46.030	44.574	40.916	0.089	37.022	27.083	4.521	2.794	0.071	0.016
225.	49.049	47.986	46.970	45.502	41.809	0.095	37.871	27.788	4.702	2.915	0.075	0.017
226.	50.015	48.944	47.921	46.441	42.714	0.101	38.732	28.505	4.889	3.040	0.080	0.018
227.	50.990	49.913	48.882	47.391	43.630	0.107	39.605	29.234	5.081	3.170	0.086	0.020
228.	51.977	50.892	49.855	48.352	44.558	0.114	40.489	29.975	5.279	3.304	0.091	0.021
229.	52.973	51.883	50.838	49.325	45.498	0.121	41.386	30.728	5.483	3.442	0.097	0.023
230.	53.981	52.884	51.833	50.308	46.449	0.128	42.294	31.493	5.693	3.584	0.103	0.024
231.	54.999	53.895	52.838	51.303	47.411	0.136	43.215	32.271	5.909	3.731	0.110	0.026
232.	56.027	54.917	53.853	52.308	48.385	0.145	44.147	33.061	6.131	3.883	0.117	0.028
233.	57.065	55.950	54.880	53.325	49.371	0.153	45.092	33.863	6.359	4.040	0.124	0.030
234.	58.114	56.994	55.918	54.352	50.368	0.163	46.048	34.678	6.595	4.202	0.131	0.032
235.	59.174	58.048	56.966	55.391	51.377	0.172	47.017	35.505	6.836	4.368	0.139	0.034
236.	60.243	59.112	58.025	56.441	52.397	0.183	47.997	36.345	7.084	4.540	0.148	0.037
237.	61.324	60.188	59.095	57.502	53.429	0.193	48.990	37.198	7.340	4.717	0.157	0.039
238.	62.416	61.274	60.175	58.573	54.473	0.204	49.995	38.063	7.602	4.899	0.166	0.042
239.	63.515	62.370	61.267	59.656	55.528	0.216	51.012	38.941	7.871	5.087	0.176	0.044
240.	64.625	63.477	62.369	60.750	56.595	0.228	52.041	39.831	8.147	5.280	0.186	0.047
241.	65.748	64.594	63.482	61.855	57.674	0.241	53.082	40.735	8.430	5.479	0.196	0.050
242.	66.880	65.722	64.605	62.971	58.764	0.255	54.135	41.651	8.721	5.684	0.208	0.054
243.	68.022	66.861	65.739	64.098	59.866	0.269	55.201	42.580	9.020	5.894	0.219	0.057
244.	69.174	68.010	66.884	65.236	60.979	0.284	56.279	43.522	9.326	6.111	0.232	0.061
245.	70.337	69.169	68.040	66.384	62.104	0.299	57.368	44.478	9.640	6.333	0.245	0.065
246.	71.509	70.339	69.206	67.544	63.241	0.315	58.470	45.446	9.962	6.562	0.258	0.069
247.	72.692	71.519	70.383	68.715	64.389	0.332	59.585	46.427	10.291	6.797	0.272	0.073
248.	73.885	72.710	71.571	69.896	65.549	0.350	60.711	47.422	10.629	7.039	0.287	0.077
249.	75.089	73.911	72.769	71.089	66.720	0.369	61.850	48.429	10.975	7.287	0.303	0.082
250.	76.302	75.123	73.979	72.292	67.903	0.388	63.001	49.450	11.330	7.541	0.319	0.087

Table 4
VAS Plank radiances for 150°-350°K in 1°K steps (Continued)

CHANNEL NUM	1	2	3	4	5	6	7	8	9	10	11	12
WAVENO 1/CM	679.785	690.243	700.170	714.452	750.348	2208.068	789.239	897.400	1374.872	1486.125	2252.566	2541.064
TEMP (K)												
251.	77.525	76.345	75.[illegible]7	73.506	69.098	0.408	64.164	50.484	11.693	7.833	0.336	0.092
252.	78.739	77.577	76.427	74.732	70.304	0.429	65.339	51.532	12.064	8.071	0.353	0.098
253.	80.003	78.819	77.667	75.968	71.522	0.451	66.527	52.592	12.445	8.347	0.372	0.103
254.	81.256	80.072	78.918	77.214	72.751	0.474	67.727	53.667	12.834	8.629	0.391	0.110
255.	82.520	81.335	80.179	78.472	73.992	0.498	68.939	54.754	13.232	8.917	0.411	0.116
256.	83.794	82.608	81.451	79.740	75.244	0.523	70.163	55.855	13.639	9.216	0.432	0.123
257.	85.077	83.891	82.733	81.019	76.508	0.548	71.399	56.969	14.056	9.520	0.454	0.130
258.	86.371	85.185	84.026	82.309	77.783	0.575	72.648	58.097	14.482	9.836	0.477	0.137
259.	87.674	86.488	85.329	83.610	79.070	0.603	73.909	59.238	14.917	10.162	0.500	0.145
260.	88.987	87.802	86.643	84.921	80.369	0.632	75.182	60.393	15.362	10.498	0.525	0.153
261.	90.311	89.126	87.966	86.243	81.678	0.663	76.467	61.562	15.817	10.815	0.551	0.161
262.	91.643	90.460	89.300	87.576	83.000	0.694	77.766	62.744	16.281	11.159	0.577	0.170
263.	92.986	91.804	90.645	88.919	84.332	0.727	79.076	63.939	16.756	11.511	0.605	0.179
264.	94.339	93.158	91.999	90.273	85.676	0.761	80.396	65.149	17.240	11.871	0.634	0.189
265.	95.701	94.522	93.364	91.637	87.032	0.796	81.730	66.372	17.735	12.239	0.664	0.199
266.	97.073	95.896	94.739	93.012	88.399	0.833	83.076	67.608	18.240	12.617	0.695	0.210
267.	98.454	97.280	96.125	94.398	89.777	0.871	84.434	68.859	18.756	13.002	0.728	0.221
268.	99.845	98.674	97.520	95.794	91.166	0.911	85.805	70.123	19.282	13.397	0.761	0.232
269.	101.246	100.078	98.926	97.200	92.567	0.952	87.187	71.400	19.818	13.800	0.797	0.244
270.	102.657	101.491	100.341	98.617	93.979	0.994	88.582	72.692	20.366	14.213	0.833	0.257
271.	104.076	102.915	101.767	100.045	95.403	1.039	89.989	73.997	20.924	14.634	0.871	0.270
272.	105.506	104.348	103.203	101.483	96.838	1.084	91.408	75.316	21.494	15.065	0.910	0.284
273.	106.945	105.791	104.649	102.931	98.283	1.132	92.839	76.649	22.075	15.506	0.950	0.298
274.	108.393	107.244	106.104	104.389	99.741	1.181	94.282	77.996	22.667	15.955	0.992	0.313
275.	109.851	108.706	107.570	105.856	101.209	1.232	95.737	79.356	23.270	16.415	1.036	0.329
276.	111.318	110.178	109.046	107.337	102.688	1.284	97.206	80.731	23.885	16.884	1.081	0.345
277.	112.795	111.660	110.531	108.827	104.179	1.339	98.683	82.119	24.512	17.363	1.128	0.362
278.	114.281	113.151	112.027	110.327	105.681	1.395	100.174	83.521	25.153	17.852	1.177	0.379
279.	115.776	114.652	113.532	111.836	107.194	1.453	101.677	84.937	25.800	18.354	1.227	0.398
280.	117.280	116.162	115.047	113.356	108.718	1.514	103.192	86.366	26.463	18.861	1.279	0.417
281.	118.794	117.682	116.572	114.887	110.253	1.576	104.719	87.810	27.137	19.381	1.332	0.437
282.	120.317	119.212	118.106	116.427	111.799	1.641	106.258	89.267	27.824	19.911	1.388	0.457
283.	121.849	120.750	119.651	117.977	113.356	1.707	107.809	90.739	28.522	20.452	1.446	0.479
284.	123.390	122.299	121.205	119.538	114.924	1.776	109.372	92.224	29.234	21.004	1.505	0.501
285.	124.940	123.856	122.768	121.108	116.503	1.847	110.946	93.723	29.958	21.567	1.567	0.524
286.	126.499	125.423	124.341	122.689	118.093	1.921	112.533	95.236	30.695	22.143	1.630	0.548
287.	128.068	126.999	125.924	124.279	119.693	1.996	114.131	96.763	31.444	22.728	1.696	0.573
288.	129.645	128.585	127.517	125.880	121.305	2.075	115.741	98.304	32.206	23.321	1.764	0.599
289.	131.231	130.180	129.118	127.490	122.927	2.155	117.363	99.859	32.982	23.928	1.834	0.626
290.	132.825	131.784	130.730	129.110	124.561	2.239	118.997	101.428	33.771	24.547	1.906	0.654
291.	134.430	133.397	132.351	130.740	126.205	2.325	120.642	103.010	34.572	25.177	1.981	0.683
292.	136.043	135.019	133.981	132.380	127.859	2.413	122.299	104.607	35.388	25.819	2.058	0.713
293.	137.665	136.651	135.620	134.029	129.525	2.504	123.968	106.217	36.216	26.473	2.137	0.744
294.	139.296	138.291	137.269	135.689	131.201	2.599	125.648	107.841	37.059	27.139	2.219	0.776
295.	140.935	139.941	138.928	137.358	132.888	2.695	127.340	109.479	37.915	27.817	2.303	0.810
296.	142.583	141.600	140.595	139.036	134.585	2.795	129.044	111.131	38.785	28.507	2.391	0.844
297.	144.240	143.267	142.272	140.725	136.293	2.898	130.759	112.797	39.668	29.209	2.480	0.880
298.	145.905	144.944	143.958	142.423	138.012	3.004	132.485	114.477	40.566	29.924	2.573	0.917
299.	147.579	146.629	145.653	144.130	139.741	3.113	134.224	116.170	41.478	30.651	2.668	0.956
300.	149.262	148.324	147.358	145.847	141.481	3.225	135.974	117.878	42.404	31.391	2.766	0.995

Table 4
VAS Plank radiances for 150°-350°K in 1°K steps (Continued)

CHANNEL NUM	1	2	3	4	5	6	7	8	9	10	11	12
WAVENO 1/CM	679.785	693.243	700.170	714.452	750.348	2206.068	789.239	897.400	1374.872	1486.125	2202.566	2541.864
TEMP (K)												
301.	150.953	150.027	149.071	147.574	143.231	3.341	137.735	119.599	43.345	32.144	2.867	1.837
302.	152.653	151.739	150.794	149.310	144.992	3.460	139.587	121.334	44.399	32.913	2.971	1.879
303.	154.361	153.459	152.526	151.055	146.763	3.582	141.252	123.083	45.269	33.689	3.079	1.923
304.	156.077	155.189	154.266	152.810	148.544	3.708	143.087	124.846	46.253	34.481	3.189	1.969
305.	157.802	156.927	156.016	154.574	150.336	3.837	144.894	126.622	47.252	35.286	3.302	1.218
306.	159.536	158.674	157.774	156.348	152.138	3.970	146.712	128.412	48.266	36.134	3.419	1.264
307.	161.277	160.429	159.542	158.131	153.950	4.106	148.542	130.217	49.295	36.938	3.539	1.314
308.	163.028	162.193	161.318	159.923	155.773	4.247	150.382	132.034	50.339	37.782	3.662	1.366
309.	164.785	163.968	163.103	161.725	157.606	4.391	152.235	133.866	51.398	38.641	3.789	1.420
310.	166.552	165.747	164.897	163.535	159.449	4.539	154.098	135.711	52.472	39.514	3.920	1.475
311.	168.327	167.537	166.700	165.355	161.302	4.691	155.972	137.570	53.562	40.401	4.054	1.532
312.	170.119	169.335	168.512	167.184	163.165	4.847	157.858	139.443	54.667	41.303	4.191	1.591
313.	171.901	171.142	170.332	169.022	165.038	5.008	159.755	141.330	55.788	42.218	4.333	1.651
314.	173.709	172.957	172.161	170.869	166.922	5.172	161.662	143.230	56.924	43.148	4.478	1.714
315.	175.527	174.789	173.998	172.725	168.815	5.341	163.581	145.143	58.076	44.092	4.627	1.778
316.	177.323	176.611	175.844	174.590	170.719	5.514	165.511	147.071	59.244	45.050	4.780	1.845
317.	179.145	178.451	177.699	176.464	172.632	5.692	167.452	149.012	60.428	46.023	4.938	1.914
318.	180.977	180.300	179.562	178.347	174.555	5.874	169.404	150.967	61.628	47.011	5.099	1.984
319.	182.816	182.155	181.434	180.239	176.489	6.061	171.367	152.935	62.844	48.014	5.265	2.057
320.	184.663	184.029	183.314	182.140	178.432	6.253	173.341	154.917	64.076	49.031	5.434	2.132
321.	186.518	185.893	185.203	184.050	180.385	6.449	175.325	156.912	65.325	50.064	5.609	2.209
322.	188.381	187.774	187.099	185.968	182.347	6.650	177.321	158.921	66.590	51.112	5.787	2.289
323.	190.251	189.663	189.005	187.895	184.320	6.857	179.327	160.943	67.871	52.175	5.970	2.371
324.	192.129	191.560	190.918	189.831	186.302	7.068	181.344	162.979	69.169	53.254	6.158	2.455
325.	194.015	193.465	192.840	191.775	188.294	7.284	183.372	165.028	70.484	54.348	6.351	2.542
326.	195.909	195.378	194.771	193.729	190.295	7.506	185.411	167.091	71.816	55.457	6.548	2.631
327.	197.810	197.299	196.709	195.690	192.306	7.733	187.460	169.167	73.164	56.582	6.750	2.723
328.	199.719	199.227	198.656	197.661	194.327	7.966	189.520	171.257	74.529	57.723	6.957	2.817
329.	201.636	201.164	200.610	199.640	196.357	8.204	191.590	173.360	75.911	58.880	7.169	2.914
330.	203.559	203.108	202.573	201.627	198.397	8.447	193.671	175.476	77.311	60.053	7.387	3.013
331.	205.491	205.061	204.544	203.623	200.446	8.697	195.763	177.606	78.727	61.242	7.609	3.117
332.	207.430	207.021	206.523	205.627	202.505	8.952	197.866	179.749	80.161	62.448	7.837	3.222
333.	209.377	208.989	208.510	207.640	204.573	9.213	199.978	181.905	81.612	63.669	8.070	3.331
334.	211.331	210.964	210.505	209.661	206.650	9.480	202.101	184.075	83.080	64.907	8.309	3.442
335.	213.292	212.947	212.508	211.691	208.737	9.753	204.235	186.258	84.566	66.161	8.553	3.556
336.	215.261	214.938	214.519	213.728	210.833	10.032	206.378	188.454	86.070	67.433	8.803	3.674
337.	217.235	216.936	216.537	215.774	212.938	10.318	208.533	190.663	87.591	68.720	9.059	3.794
338.	219.229	218.942	218.564	217.829	215.053	10.609	210.697	192.885	89.130	70.025	9.320	3.918
339.	221.219	220.956	220.598	219.891	217.177	10.908	212.872	195.121	90.687	71.346	9.587	4.045
340.	223.208	222.977	222.640	221.962	219.309	11.213	215.057	197.369	92.261	72.685	9.861	4.175
341.	225.213	225.005	224.690	224.041	221.452	11.524	217.253	199.631	93.854	74.040	10.140	4.309
342.	227.225	227.041	226.747	226.127	223.603	11.842	219.458	201.905	95.464	75.413	10.426	4.446
343.	229.244	229.084	228.813	228.222	225.763	12.168	221.674	204.193	97.093	76.803	10.718	4.587
344.	231.270	231.135	230.885	230.325	227.932	12.500	223.899	206.494	98.740	78.210	11.017	4.731
345.	233.303	233.193	232.966	232.436	230.110	12.839	226.135	208.808	100.405	79.635	11.322	4.879
346.	235.344	235.258	235.054	234.555	232.298	13.185	228.381	211.134	102.088	81.077	11.633	5.031
347.	237.391	237.331	237.149	236.682	234.494	13.539	230.637	213.474	103.790	82.537	11.952	5.187
348.	239.445	239.411	239.252	238.817	236.699	13.900	232.903	215.826	105.510	84.015	12.277	5.346
349.	241.506	241.498	241.363	240.959	238.913	14.268	235.179	218.191	107.248	85.511	12.609	5.510
350.	243.574	243.592	243.481	243.110	241.135	14.644	237.464	220.570	109.006	87.026	12.948	5.677

Table 5
19 radiosonde sites in SE USA, with VAS-viewed zenith angle

RAOB	Name	Place	$\sec\theta$
1	AMA	Amarillo, Texas	1.33
2	DRT	Del Rio, Texas	1.21
3	SEP	Stephenville, Texas	1.26
4	OKC	Oklahoma City, Oklahoma	1.33
5	BRO	Brownsville, Texas	1.16
6	VCT	Victoria, Texas	1.20
7	GGG	Longview, Texas	1.27
8	LCH	Lake Charles, Louisiana	1.27
9	1M1	North Little Rock, Arkansas	1.32
10	JAN	Jackson, Mississippi	1.28
11	BVE	Boothville, Louisiana	1.23
12	CKL	Centerville, Alabama	1.31
13	BNA	Nashville, Tennessee	1.38
14	AQQ	Apalachicola, Florida	1.26
15	AHN	Athens, Georgia	1.36
16	AYS	Waycross, Georgia	1.31
17	TBW	Tampa Bay, Florida	1.25
18	CHS	Charleston, South Carolina	1.37
19	GSO	Greensboro, North Carolina	1.44

Table 6
Radiosonde temperature profiles at 19 sites

SITE P(MB)	1	2	3	4	5	6	7	8	9	10	11	12	13	14	15	16	17	18	19	MEAN	RMS
0.2	250.0	250.0	250.0	250.0	250.0	250.0	250.0	250.0	250.0	250.0	250.0	250.0	250.0	250.0	250.0	250.0	250.0	250.0	250.0	250.0	0.0
0.3	257.0	257.0	257.0	257.0	257.0	257.0	257.0	257.0	257.0	257.0	257.0	257.0	257.0	257.0	257.0	257.0	257.0	257.0	257.0	257.0	0.0
0.5	265.0	265.0	265.0	265.0	265.0	265.0	265.0	265.0	265.0	265.0	265.0	265.0	265.0	265.0	265.0	265.0	265.0	265.0	265.0	265.0	0.0
0.7	269.0	269.0	269.0	269.0	269.0	269.0	269.0	269.0	269.0	269.0	269.0	269.0	269.0	269.0	269.0	269.0	269.0	269.0	269.0	269.0	0.0
1.0	270.0	270.0	270.0	270.0	270.0	270.0	270.0	270.0	270.0	270.0	270.0	270.0	270.0	270.0	270.0	270.0	270.0	270.0	270.0	270.0	0.0
2.0	260.0	260.0	260.0	260.0	260.0	260.0	260.0	260.0	260.0	260.0	260.0	260.0	260.0	260.0	260.0	260.0	260.0	260.0	260.0	260.0	0.0
3.0	254.0	254.0	254.0	254.0	254.0	254.0	254.0	254.0	254.0	254.0	254.0	254.0	254.0	254.0	254.0	254.0	254.0	254.0	254.0	254.0	0.0
4.0	250.0	250.0	250.0	250.0	250.0	250.0	250.0	250.0	250.0	250.0	250.0	250.0	250.0	250.0	250.0	250.0	250.0	250.0	250.0	250.0	0.0
5.0	246.0	246.0	246.0	246.0	246.0	246.0	246.0	246.0	246.0	246.0	246.0	246.0	246.0	246.0	246.0	246.0	246.0	246.0	246.0	246.0	0.0
6.0	243.0	243.0	243.0	243.0	243.0	243.0	243.0	243.0	227.0	243.0	235.7	227.4	243.0	243.0	243.0	243.0	243.0	243.0	243.0	241.0	5.0
7.0	240.0	232.3	240.0	240.0	240.0	229.2	240.0	240.0	227.8	240.0	236.0	226.9	240.0	240.0	240.0	240.0	240.0	240.0	240.0	237.5	4.6
8.5	237.0	229.9	229.4	226.7	237.0	230.1	226.6	237.0	225.8	227.0	230.3	226.9	237.0	226.8	237.0	227.5	237.0	237.0	237.0	231.8	4.6
10.0	227.3	231.0	229.2	226.1	236.0	231.1	226.6	236.0	225.8	226.5	227.5	226.9	225.0	226.8	236.0	227.0	236.0	236.0	236.0	230.1	4.3
12.5	226.1	229.2	224.6	225.4	231.0	228.3	228.4	232.0	224.4	228.3	227.3	224.9	225.5	228.4	232.0	227.2	232.0	232.0	232.0	228.4	2.7
15.0	225.0	227.5	224.6	224.7	229.5	225.6	226.2	229.0	223.4	227.3	227.0	226.2	224.6	228.2	224.5	227.5	229.0	229.0	229.0	226.7	1.9
17.5	223.9	225.7	224.7	224.0	228.1	224.8	223.9	227.0	224.4	226.4	226.7	227.5	223.4	227.5	223.3	225.7	227.0	227.1	222.3	225.4	1.7
20.0	222.8	224.0	224.9	223.4	226.7	225.2	223.8	226.0	225.4	223.6	226.5	225.4	222.3	226.9	224.6	223.6	226.0	225.6	222.3	224.6	1.4
25.0	219.9	224.1	223.4	222.0	223.9	221.6	222.8	221.7	220.0	225.2	223.9	223.8	221.6	224.7	224.2	221.3	221.0	225.5	220.2	222.7	1.7
30.0	219.9	220.7	220.6	220.6	221.5	220.7	221.9	220.3	218.9	222.8	224.8	219.8	219.1	222.6	222.0	222.1	219.0	220.4	218.2	220.8	1.6
35.0	216.2	219.4	217.5	217.6	218.5	218.2	218.9	218.6	216.5	219.5	221.2	217.4	218.6	219.8	219.2	220.2	217.0	218.2	216.9	218.4	1.3
40.0	213.6	215.0	216.0	214.7	217.1	215.0	215.9	216.1	214.1	214.9	217.6	215.0	216.0	217.1	216.4	214.7	215.0	216.0	215.7	215.6	1.0
50.0	211.6	211.8	211.0	212.0	211.3	207.9	210.0	211.0	212.3	211.5	210.4	210.2	210.9	211.6	210.8	211.1	209.0	215.6	213.2	211.2	1.5
60.0	206.1	206.5	206.8	207.0	207.3	206.3	208.0	205.6	207.4	206.5	209.7	207.6	210.0	208.1	210.4	208.2	205.0	208.8	210.0	207.6	1.5
70.0	203.0	201.9	205.7	205.8	202.9	201.8	205.5	203.9	205.4	205.9	205.3	206.8	209.2	204.7	207.4	205.3	203.0	206.7	209.2	205.2	2.1
85.0	201.4	199.6	201.5	203.3	197.3	197.1	202.4	200.3	205.2	202.0	200.6	203.0	206.0	200.4	203.5	202.4	199.4	204.4	206.5	201.9	2.6
100.0	198.7	200.0	199.4	198.2	199.8	198.1	202.7	200.8	203.9	205.3	201.2	205.2	209.0	200.1	205.1	201.2	198.1	202.2	207.4	201.9	3.2
125.0	202.8	204.8	207.2	206.5	203.1	203.7	204.7	204.6	208.6	204.6	204.0	205.7	209.3	204.1	205.6	204.8	200.3	204.5	209.3	205.2	2.2
150.0	209.7	211.8	207.6	212.2	210.4	209.3	210.8	210.3	209.2	210.6	210.4	210.4	213.6	209.5	210.2	208.6	204.6	210.5	211.3	210.0	1.8
175.0	214.5	214.9	215.3	217.3	214.9	214.9	217.0	215.4	214.1	214.3	216.7	215.2	214.8	234.1	214.5	214.1	210.8	214.6	214.5	215.9	4.5
200.0	218.9	219.6	220.2	221.1	220.7	220.5	216.3	220.5	220.1	218.6	220.6	220.1	219.1	220.5	219.7	219.7	218.7	219.6	217.7	219.5	1.1
250.0	226.7	225.9	225.5	224.0	226.4	225.0	227.0	226.6	226.0	226.0	229.6	226.8	225.1	228.9	224.3	227.0	231.0	226.1	221.2	226.3	2.0
300.0	233.4	234.9	233.4	232.1	235.8	233.0	233.0	233.2	230.8	233.4	234.5	231.7	227.7	235.1	231.7	233.3	239.9	231.8	230.8	233.1	2.4
350.0	242.5	243.2	242.0	240.4	244.0	242.7	241.0	241.3	239.5	241.0	242.2	240.0	237.1	241.7	239.3	241.2	245.3	240.4	238.4	241.2	1.9
400.0	248.8	252.1	250.0	249.1	252.5	250.3	249.3	250.3	248.3	248.6	250.9	247.7	245.8	250.1	246.4	250.4	249.9	249.0	246.0	249.2	1.8
500.0	264.2	264.3	264.2	263.0	266.1	263.2	263.1	263.2	261.0	262.1	263.4	261.5	261.0	262.0	260.5	260.9	262.6	259.9	259.8	262.4	1.6
600.0	274.0	275.1	275.1	273.1	275.4	274.3	272.1	273.0	270.1	271.9	275.0	271.5	268.5	272.8	270.3	271.6	273.5	270.0	269.3	272.4	2.1
700.0	280.7	282.2	282.8	280.7	282.0	282.7	281.3	281.3	281.3	279.1	280.5	277.8	278.9	280.4	277.1	280.2	282.0	280.1	277.7	280.4	1.6
850.0	294.3	294.6	292.2	291.2	291.1	291.3	287.6	286.4	286.6	284.4	284.9	283.8	285.5	286.5	283.5	287.5	283.4	285.3	283.5	287.5	3.6
920.0	298.2	298.1	298.5	296.9	291.3	291.0	292.4	287.7	291.5	290.7	287.5	289.6	291.4	287.9	289.5	286.8	289.5	288.5	288.1	291.3	3.7
1000.0	298.2	302.6	301.5	300.4	296.9	296.6	299.3	293.4	296.5	297.0	293.7	294.2	295.2	290.3	292.1	292.8	293.0	289.9	289.3	295.4	3.8

Table 7
Radiosonde dewpoint profiles at 19 sites

SITE P(MB)	1	2	3	4	5	6	7	8	9	10	11	12	13	14	15	16	17	18	19	MEAN	RMS
0.2	165.0	165.0	165.0	165.0	165.0	165.0	165.0	165.0	165.0	165.0	165.0	165.0	165.0	165.0	165.0	165.0	165.0	165.0	165.0	165.0	0.0
0.3	166.2	166.2	166.2	166.2	166.2	166.2	166.2	166.2	166.2	166.2	166.2	166.2	166.2	166.2	166.2	166.2	166.2	166.2	166.2	166.2	0.0
0.5	167.3	167.3	167.3	167.3	167.3	167.3	167.3	167.3	167.3	167.3	167.3	167.3	167.3	167.3	167.3	167.3	167.3	167.3	167.3	167.3	0.0
0.7	168.8	168.8	168.8	168.8	168.8	168.8	168.8	168.8	168.8	168.8	168.8	168.8	168.8	168.8	168.8	168.8	168.8	168.8	168.8	168.8	0.0
1.0	170.3	170.3	170.3	170.3	170.3	170.3	170.3	170.3	170.3	170.3	170.3	170.3	170.3	170.3	170.3	170.3	170.3	170.3	170.3	170.3	0.0
2.0	175.1	175.1	175.1	175.1	175.1	175.1	175.1	175.1	175.1	175.1	175.1	175.1	175.1	175.1	175.1	175.1	175.1	175.1	175.1	175.1	0.0
3.0	178.0	178.0	178.0	178.0	178.0	178.0	178.0	178.0	178.0	178.0	178.0	178.0	178.0	178.0	178.0	178.0	178.0	178.0	178.0	178.0	0.0
4.0	179.8	179.8	179.8	179.8	179.8	179.8	179.8	179.8	179.8	179.8	179.8	179.8	179.8	179.8	179.8	179.8	179.8	179.8	179.8	179.8	0.0
5.0	180.9	180.9	180.9	180.9	180.9	180.9	180.9	180.9	180.9	180.9	180.9	180.9	180.9	180.9	180.9	180.9	180.9	180.9	180.9	180.9	0.0
6.0	182.3	182.3	182.3	182.3	182.3	182.3	182.3	182.3	182.3	182.3	182.3	182.3	182.3	182.3	182.3	182.3	182.3	182.3	182.3	182.3	0.0
7.0	183.8	183.8	183.8	183.8	183.8	183.8	183.8	183.8	183.8	183.8	183.8	183.8	183.8	183.8	183.8	183.8	183.8	183.8	183.8	183.8	0.0
8.5	185.8	185.8	185.8	185.8	185.8	185.8	185.8	185.8	185.8	185.8	185.8	185.8	185.8	185.8	185.8	185.8	185.8	185.8	185.8	185.8	0.0
10.0	186.7	186.7	186.7	186.7	186.7	186.7	186.7	186.7	186.7	186.7	186.7	186.7	186.7	186.7	186.7	186.7	186.7	186.7	186.7	186.7	0.0
12.5	188.2	188.2	188.2	188.2	188.2	188.2	188.2	188.2	188.2	188.2	188.2	188.2	188.2	188.2	188.2	188.2	188.2	188.2	188.2	188.2	0.0
15.0	188.9	188.9	188.9	188.9	188.9	188.9	188.9	188.9	188.9	188.9	188.9	188.9	188.9	188.9	188.9	188.9	188.9	188.9	188.9	188.9	0.0
17.5	189.8	189.8	189.8	189.8	189.8	189.8	189.8	189.8	189.8	189.8	189.8	189.8	189.8	189.8	189.8	189.8	189.8	189.8	189.8	189.8	0.0
20.0	190.3	190.3	190.3	190.3	190.3	190.3	190.3	190.3	190.3	190.3	190.3	190.3	190.3	190.3	190.3	190.3	190.3	190.3	190.3	190.3	0.0
25.0	190.9	190.9	190.9	190.9	190.9	190.9	190.9	190.9	190.9	190.9	190.9	190.9	190.9	190.9	190.9	190.9	190.9	190.9	190.9	190.9	0.0
30.0	190.8	190.8	190.8	190.8	190.8	190.8	190.8	190.8	190.8	190.8	190.8	190.8	190.8	190.8	190.8	190.8	190.8	190.8	190.8	190.8	0.0
35.0	190.1	190.1	190.1	190.1	190.1	190.1	190.1	190.1	190.1	190.1	190.1	190.1	190.1	190.1	190.1	190.1	190.1	190.1	190.1	190.1	0.0
40.0	189.6	189.6	189.6	189.6	189.6	189.6	189.6	189.6	189.6	189.6	189.6	189.6	189.6	189.6	189.6	189.6	189.6	189.6	189.6	189.6	0.0
50.0	189.2	189.2	189.2	189.2	189.2	189.2	189.2	189.2	189.2	189.2	189.2	189.2	189.2	189.2	189.2	189.2	189.2	189.2	189.2	189.2	0.0
60.0	188.0	188.0	188.0	188.0	188.0	188.0	188.0	188.0	188.0	188.0	188.0	188.0	188.0	188.0	188.0	188.0	188.0	188.0	188.0	188.0	0.0
70.0	188.8	188.8	188.8	188.8	188.8	188.8	188.8	188.8	188.8	188.8	188.8	188.8	188.8	188.8	188.8	188.8	188.8	188.8	188.8	188.8	0.0
85.0	188.3	188.3	188.3	188.3	188.3	188.3	188.3	188.3	188.3	188.3	188.3	188.3	188.3	188.3	188.3	188.3	188.3	188.3	188.3	188.3	0.0
100.0	189.2	189.2	189.2	189.2	189.2	189.2	189.2	189.2	189.2	189.2	189.2	189.2	189.2	189.2	189.2	189.2	189.2	189.2	189.2	189.2	0.0
125.0	190.5	190.5	190.5	190.5	190.5	190.5	190.5	190.5	190.5	190.5	190.5	190.5	190.5	190.5	190.5	190.5	190.5	190.5	190.5	190.5	0.0
150.0	193.3	193.3	193.3	193.3	193.3	193.3	193.3	193.3	193.3	193.3	193.3	193.3	193.3	193.3	193.3	193.3	193.3	193.3	193.3	193.3	0.0
175.0	197.8	197.8	197.8	197.8	197.8	197.8	197.8	197.8	197.8	197.8	197.8	197.8	197.8	197.8	197.8	197.8	197.8	197.8	197.8	197.8	0.0
200.0	203.2	203.2	203.2	203.2	203.2	203.2	203.2	203.2	203.2	203.2	203.2	203.2	203.2	203.2	203.2	203.2	203.2	203.2	203.2	203.2	0.0
250.0	215.0	215.0	215.0	215.0	215.0	215.0	215.0	215.0	215.0	215.0	215.0	215.0	215.0	215.0	215.0	215.0	215.0	215.0	215.0	215.0	0.0
300.0	229.3	223.5	223.1	225.2	205.5	225.2	225.2	203.0	225.2	203.7	204.4	225.2	225.2	205.0	225.2	203.0	229.9	225.2	225.2	218.8	10.1
350.0	236.5	228.0	228.9	232.4	214.0	222.8	211.1	211.4	227.7	211.1	212.3	228.0	230.3	211.7	218.4	211.1	234.7	210.4	228.1	221.5	9.2
400.0	239.9	222.0	233.8	232.5	222.4	220.2	233.8	220.2	235.9	218.6	220.8	234.9	215.7	220.1	237.5	220.4	240.6	218.9	239.0	227.7	8.5
500.0	247.1	234.3	234.2	233.0	236.0	233.2	233.0	233.2	245.1	232.0	233.3	231.5	231.0	231.9	230.5	230.9	232.5	229.8	229.7	233.8	4.5
600.0	254.5	245.1	245.1	243.1	245.4	244.3	242.1	243.0	254.9	241.9	245.0	247.3	259.6	242.8	240.3	241.6	243.5	240.0	239.3	245.2	5.3
700.0	261.9	252.2	252.8	250.7	252.0	252.7	251.3	251.3	262.2	257.8	250.5	259.5	258.1	250.4	258.6	250.2	252.0	250.1	247.7	253.7	4.3
850.0	271.8	264.6	274.1	261.2	261.1	270.2	278.6	269.9	281.1	277.6	270.7	276.4	277.0	256.5	279.2	257.5	280.6	255.3	271.6	270.2	8.3
920.0	270.6	274.0	276.8	266.9	282.1	285.4	281.6	285.5	283.6	279.1	274.0	280.7	278.7	269.4	279.6	270.2	281.9	259.5	278.0	276.8	6.7
1000.0	270.6	280.4	277.1	275.4	288.9	288.1	285.0	288.7	285.8	282.9	286.7	284.9	280.4	283.4	282.3	275.3	284.7	282.1	280.0	282.2	4.8

Table 8
Radiosonde dewpoint depression profiles at 19 sites

SITE P(MB)	1	2	3	4	5	6	7	8	9	10	11	12	13	14	15	16	17	18	19	MEAN	RMS
0.2	85.0	85.0	85.0	85.0	85.0	85.0	85.0	85.0	85.0	85.0	85.0	85.0	85.0	85.0	85.0	85.0	85.0	85.0	85.0	85.0	0.0
0.3	90.8	90.8	90.8	90.8	90.8	90.8	90.8	90.8	90.8	90.8	90.8	90.8	90.8	90.8	90.8	90.8	90.8	90.8	90.8	90.8	0.0
0.5	97.7	97.7	97.7	97.7	97.7	97.7	97.7	97.7	97.7	97.7	97.7	97.7	97.7	97.7	97.7	97.7	97.7	97.7	97.7	97.7	0.0
0.7	100.2	100.2	100.2	100.2	100.2	100.2	100.2	100.2	100.2	100.2	100.2	100.2	100.2	100.2	100.2	100.2	100.2	100.2	100.2	100.2	0.0
1.0	99.7	99.7	99.7	99.7	99.7	99.7	99.7	99.7	99.7	99.7	99.7	99.7	99.7	99.7	99.7	99.7	99.7	99.7	99.7	99.7	0.0
2.0	84.9	84.9	84.9	84.9	84.9	84.9	84.9	84.9	84.9	84.9	84.9	84.9	84.9	84.9	84.9	84.9	84.9	84.9	84.9	84.9	0.0
3.0	76.0	76.0	76.0	76.0	76.0	76.0	76.0	76.0	76.0	76.0	76.0	76.0	76.0	76.0	76.0	76.0	76.0	76.0	76.0	76.0	0.0
4.0	70.2	70.2	70.2	70.2	70.2	70.2	70.2	70.2	70.2	70.2	70.2	70.2	70.2	70.2	70.2	70.2	70.2	70.2	70.2	70.2	0.0
5.0	65.1	65.1	65.1	65.1	65.1	65.1	65.1	65.1	65.1	65.1	65.1	65.1	65.1	65.1	65.1	65.1	65.1	65.1	65.1	65.1	0.0
6.0	60.7	60.7	60.7	60.7	60.7	60.7	60.7	60.7	44.8	60.7	53.4	45.1	60.7	60.7	60.7	60.7	60.7	60.7	60.7	58.7	5.0
7.0	56.2	48.5	56.2	56.2	56.2	45.4	56.2	56.2	44.0	56.2	52.2	43.1	56.2	56.2	56.2	56.2	56.2	56.2	56.2	53.7	4.8
8.5	51.2	44.1	43.6	40.9	51.2	44.3	40.9	51.2	41.0	41.2	44.6	41.1	51.2	41.0	51.2	41.7	51.2	51.2	51.2	46.0	4.6
10.0	40.6	44.3	42.5	39.4	49.3	44.4	39.9	49.3	39.1	39.8	40.9	40.2	38.3	40.1	49.3	40.3	49.3	49.3	49.3	43.5	4.3
12.5	37.9	41.0	38.4	37.2	42.8	40.2	40.2	43.8	36.2	40.1	39.1	36.7	37.3	40.2	43.8	39.1	43.8	43.8	43.8	40.2	2.7
15.0	36.1	38.5	35.7	35.8	40.6	36.7	37.2	40.1	34.5	38.4	38.1	37.3	35.7	39.3	35.6	38.6	40.1	40.1	40.1	37.8	1.9
17.5	34.1	35.9	34.9	34.2	38.3	35.0	34.1	37.2	34.6	36.6	36.9	37.7	33.6	37.7	33.4	35.8	37.2	37.2	32.4	35.6	1.7
20.0	32.5	33.7	34.6	33.1	36.4	34.9	33.5	35.7	35.1	33.3	36.2	35.1	32.0	36.6	34.3	33.3	35.7	35.3	32.0	34.3	1.4
25.0	29.0	33.2	32.5	31.1	33.0	30.7	31.9	30.8	29.1	34.3	33.0	32.9	30.7	33.8	33.3	30.4	30.1	34.6	29.3	31.8	1.7
30.0	29.1	29.9	29.8	29.8	30.7	29.9	31.1	29.5	28.1	32.0	34.0	29.0	28.3	31.8	31.2	31.3	28.3	29.6	27.4	30.0	1.6
35.0	26.1	29.2	27.4	27.5	28.3	28.0	28.8	28.5	26.4	29.4	31.0	27.2	28.5	29.7	29.0	30.1	26.9	28.1	26.8	28.3	1.3
40.0	24.0	25.4	26.4	25.1	27.5	25.4	26.3	26.5	24.5	25.3	28.0	25.4	26.4	27.5	26.8	25.1	25.4	26.4	26.1	26.0	1.0
50.0	22.3	22.5	21.7	22.7	22.0	18.6	20.7	21.7	23.0	22.2	21.1	20.9	21.6	22.3	21.5	21.8	19.8	26.3	23.9	21.9	1.5
60.0	18.1	18.5	18.9	19.1	19.3	18.4	20.1	17.6	19.4	18.6	21.7	19.6	22.0	20.1	22.5	20.2	17.0	20.9	22.0	19.7	1.5
70.0	14.1	13.0	16.8	16.9	14.0	12.9	16.6	15.0	16.5	17.0	16.4	17.9	20.3	15.8	18.5	16.4	14.2	17.8	20.3	16.3	2.1
85.0	13.1	11.3	13.2	15.0	9.0	8.7	14.1	12.0	16.9	13.7	12.3	14.7	17.6	12.0	15.2	14.0	11.0	16.1	18.1	13.6	2.6
100.0	9.4	10.7	10.1	8.9	10.5	8.8	13.4	11.5	14.6	16.0	11.9	15.9	19.7	10.8	15.8	11.9	8.8	12.9	18.1	12.6	3.2
125.0	12.3	14.3	16.7	16.0	12.6	13.2	14.2	14.1	18.1	14.1	13.4	15.2	18.8	13.6	15.0	14.3	9.8	14.0	18.8	14.6	2.2
150.0	16.3	18.4	14.2	18.8	17.0	15.9	17.4	16.9	15.8	17.2	17.0	17.0	20.2	16.1	16.8	15.2	11.2	17.1	17.9	16.7	1.8
175.0	16.7	17.2	17.6	19.6	17.2	17.1	19.3	17.6	16.3	16.5	18.9	17.4	17.1	36.3	16.7	16.3	13.0	16.8	16.7	18.1	4.5
200.0	15.6	16.3	16.9	17.8	17.4	17.2	13.0	17.2	16.8	15.3	17.3	16.8	15.8	16.9	16.4	16.4	15.4	16.3	14.4	16.3	1.1
250.0	11.7	10.9	10.5	9.0	11.4	10.9	12.0	11.6	11.0	11.0	14.6	11.8	10.1	13.9	9.3	12.0	16.0	11.1	6.2	11.3	2.0
300.0	4.0	11.3	10.2	6.9	30.2	7.8	7.8	30.2	5.6	29.7	30.1	6.5	2.5	30.1	6.5	30.3	10.0	6.6	5.6	14.3	10.9
350.0	6.0	15.3	13.1	8.0	30.1	19.9	29.9	29.9	11.8	29.0	30.0	12.0	6.9	30.0	20.9	30.1	10.5	30.0	10.4	19.7	9.4
400.0	8.9	30.0	16.2	16.5	30.0	30.0	15.5	30.0	12.4	29.9	30.0	12.8	30.1	29.9	8.8	30.0	9.3	30.0	6.9	21.4	9.3
500.0	17.1	30.0	30.0	30.0	30.0	30.0	30.0	30.0	15.9	30.0	30.0	30.0	30.0	30.0	30.0	30.0	30.0	30.0	30.0	28.6	4.1
600.0	19.5	30.0	30.0	30.0	30.0	30.0	30.0	30.0	15.2	30.0	30.0	24.2	8.9	30.0	30.0	30.0	30.0	30.0	30.0	27.2	5.9
700.0	18.8	30.0	30.0	30.0	30.0	30.0	30.0	30.0	19.1	21.2	30.0	18.3	20.3	30.0	18.4	30.0	30.0	30.0	30.0	26.7	5.0
850.0	22.5	30.0	18.1	30.0	30.0	21.1	9.0	16.5	5.5	6.8	14.1	7.4	8.5	30.0	4.2	30.0	2.7	30.0	11.9	17.3	10.1
920.0	27.6	23.2	21.7	30.0	9.1	5.7	10.8	2.2	7.9	11.6	13.5	9.0	12.6	18.5	9.9	16.6	7.6	28.9	10.0	14.5	8.0
1000.0	27.6	22.1	24.4	24.9	8.0	8.5	14.3	4.6	10.7	14.1	7.0	9.3	14.7	6.9	9.7	17.5	8.3	7.7	9.3	13.1	6.8

Table 9
VAS T*s observed at 19 sites in SE USA

CASE	CHAN=	1	2	3	4	5	6	7	8	9	10	11	12
1		218.71	214.95	220.27	241.26	278.28	272.65	299.04	304.88	259.13	241.85	239.99	309.37
2		214.77	215.73	221.17	242.55	278.63	274.53	300.13	306.18	264.16	247.05	241.66	309.43
3		214.35	215.80	220.92	241.08	277.89	272.72	297.57	303.03	261.60	246.89	240.42	305.99
4		215.78	215.55	220.41	239.63	276.36	271.20	296.79	303.37	258.04	242.61	239.15	307.33
5		219.43	215.73	221.91	242.67	276.77	273.10	294.89	301.22	271.00	257.83	242.14	306.84
6		218.31	216.82	221.99	242.24	275.74	271.11	292.64	298.71	266.19	250.41	240.59	302 34
7		220.14	216.06	220.48	240.53	273.86	269.31	291.83	297.57	260.66	245.07	239.56	301.04
8		218.58	215.68	220.93	240.89	272.18	267.92	288.31	293.75	262.26	246.67	240.03	297.44
9		219.59	216.87	219.97	239.54	271.82	266.96	289.16	294.60	257.00	241.76	237.10	297.18
10		216.94	215.31	221.14	240.28	272.25	267.58	289.00	294.72	261.80	246.15	238.87	297.27
11		221.32	216.43	221.66	240.89	271.83	267.58	288.44	293.19	264.59	251.88	240.03	295.52
12		214.59	216.08	221.26	239.20	271.49	266.45	288.54	294.31	258.48	245.37	237.97	297.34
13		221.20	216.52	219.75	237.07	269.92	264.67	288.15	293.94	255.47	244.18	235.70	297.32
14		219.32	215.60	221.26	240.46	272.27	266.44	289.67	293.44	267.07	254.06	238.56	294.17
15		216.36	216.61	220.13	238.11	269.15	264.41	285.69	291.43	257.91	244.39	236.79	293.88
16		215.25	216.89	220.96	239.30	271.99	265.57	288.92	293.19	265.19	251.16	237.05	294.11
17		218.81	216.23	221.18	240.82	273.24	267.28	290.10	294.23	264.76	248.57	239.38	295.37
18		219.51	215.66	220.37	238.67	269.86	263.90	286.85	291.14	261.75	247.99	236.49	291.69
19		212.55	214.65	219.88	236.70	268.15	262.22	284.95	289.93	253.74	239.68	234.62	291.40
	STATISTICS												
AVG=		217.55	215.95	220.82	240.10	273.26	268.19	291.09	296.47	261.62	247.03	238.74	299.21
STD DEV=		2.46	0.61	0.65	1.63	3.11	3.41	4.40	4.82	4.24	4.43	1.97	5.78

Table 10
Calculated minus observed VAS ΔT^* at 19 sites

CASE	CHAN=	1	2	3	4	5	6	7	8	9	10	11	12
1		3.23	4.34	3.59	-0.21	-4.37	-1.08	-7.02	-8.32	-1.01	0.00	0.79	-13.84
2		5.34	4.18	4.18	0.87	-0.80	0.71	-2.70	-4.80	4.60	4.90	1.43	-9.45
3		6.00	4.08	3.80	1.30	-1.41	1.17	-2.01	-3.11	4.37	1.97	1.63	-7.22
4		4.65	4.34	3.72	1.41	-0.80	0.96	-1.37	-4.03	7.02	4.18	1.33	-9.71
5		1.34	4.81	4.37	1.56	-1.03	-0.34	-2.56	-5.59	-0.89	-1.13	1.38	-12.23
6		0.80	2.40	2.69	0.42	-0.96	0.76	-1.11	-3.67	1.69	1.70	1.48	-8.14
7		0.47	4.03	4.12	0.97	-0.01	2.22	0.20	-0.76	4.60	4.31	1.30	-4.65
8		2.43	4.82	4.31	1.34	0.38	1.44	0.12	-1.99	6.17	9.01	1.17	-6.43
9		0.25	2.60	3.72	0.34	-0.81	2.29	-1.00	-1.23	1.29	1.46	2.19	-3.66
10		4.12	5.11	3.54	0.81	0.19	2.25	1.10	-0.05	4.88	8.36	1.29	-3.08
11		-0.39	4.22	4.06	1.60	0.99	1.92	0.58	-0.82	3.59	3.92	1.41	-4.23
12		5.68	3.79	2.63	0.89	-0.80	1.52	-0.97	-2.33	2.56	0.26	1.19	-5.92
13		0.64	4.51	4.18	2.05	0.43	2.97	-0.10	-1.09	3.90	0.46	2.52	-5.09
14		1.92	5.64	4.86	1.68	-0.42	1.43	-2.41	-3.77	1.47	1.55	2.33	-5.96
15		5.97	4.58	4.11	1.48	0.34	1.97	0.24	-1.39	2.95	1.03	1.65	-4.50
16		5.47	3.15	3.44	1.61	0.25	2.57	0.22	-1.19	3.15	3.83	2.73	-3.71
17		1.33	3.39	3.93	1.32	-1.75	1.67	-3.09	-3.27	-2.98	-2.50	1.94	-4.84
18		3.25	5.86	4.27	1.51	0.77	2.24	-0.02	-1.83	4.70	3.15	2.32	-4.07
19		10.14	6.76	3.84	1.86	0.55	2.29	0.09	-1.68	6.44	3.53	2.68	-4.62
	STATISTICS												
AVG=		3.30	4.35	3.87	1.20	-0.49	1.52	-1.15	-2.68	3.09	2.63	1.73	-6.39
STD DEV=		2.64	1.04	0.51	0.56	1.19	0.93	1.84	1.98	2.58	2.83	0.56	2.93

Table 11
VAS transmission γ-factor adjustments for 19 sites

CASE \ CHAN=	1	2	3	4	5	6	7	8	9	10	11	12
1	0.67	******	******	0.99	0.78	0.95	******	******	0.95	1.00	1.03	******
2	******	******	1.58	1.04	0.96	1.03	0.45	******	1.29	1.26	1.05	******
3	******	******	******	1.06	0.93	1.05	0.63	******	1.27	1.10	1.06	******
4	******	******	******	1.06	0.96	1.04	0.71	******	1.41	1.21	1.05	******
5	0.87	******	1.59	1.07	0.96	1.02	0.69	******	0.94	0.94	1.06	******
6	0.92	******	1.26	1.02	0.96	1.06	0.91	******	1.12	1.08	1.06	******
7	0.95	******	******	1.04	1.00	1.10	1.03	0.67	1.32	1.24	1.05	******
8	0.75	******	******	1.06	1.04	1.10	1.18	0.53	1.55	1.66	1.05	******
9	0.97	******	******	1.02	0.95	1.11	0.85	0.57	1.08	1.09	1.09	******
10	******	******	******	1.04	1.01	1.11	1.20	0.99	1.45	1.62	1.05	******
11	1.04	******	******	1.08	1.08	1.12	1.33	1.25	1.31	1.26	1.06	******
12	******	******	1.39	1.04	0.95	1.07	0.83	******	1.18	1.01	1.05	******
13	0.92	******	******	1.10	1.02	1.14	0.98	0.51	1.29	1.03	1.12	******
14	0.78	******	******	1.08	0.90	1.02	******	******	1.11	1.09	1.10	******
15	******	******	******	1.07	1.02	1.10	1.05	******	1.21	1.06	1.08	******
16	******	******	******	1.07	0.94	1.07	******	******	1.24	1.24	1.12	******
17	0.88	******	1.53	1.06	0.89	1.09	0.44	******	0.83	0.88	1.08	******
18	0.69	******	******	1.07	1.05	1.11	0.94	******	1.34	1.17	1.11	******
19	******	******	******	1.10	1.03	1.12	1.02	******	1.43	1.19	1.14	******
STATISTICS												
SUCCESSES=	11	0	5	19	19	19	16	6	19	19	19	0
AVG=	0.86	******	1.47	1.06	0.97	1.07	0.89	0.75	1.23	1.16	1.07	******
STD DEV=	0.11	******	0.13	0.03	0.07	0.05	0.25	0.27	0.18	0.20	0.03	******

Table 12
Observed and retrieved precipitable water at 3 sites

Above Pressure Level	Precipitable Water (gm/cm^2)					
	Amarillo, Texas		Jackson, Mississippi		Tampa Bay, Florida	
	RAOB	VAS	RAOB	VAS	RAOB	VAS
850 mb	0.93	0.48	0.50	0.42	0.51	0.36
920 mb	1.19	0.77	0.81	0.79	0.83	0.64
1000 mb	–	–	1.40	1.49	1.30	1.19